

Miocene magmatism in the Bodie Hills volcanic field, California and Nevada: A long-lived eruptive center in the southern segment of the ancestral Cascades arc

David A. John^{1,*}, Edward A. du Bray², Richard J. Blakely¹, Robert J. Fleck¹, Peter G. Vikre³, Stephen E. Box⁴, and Barry C. Moring¹

¹U.S. Geological Survey, 345 Middlefield Road, Menlo Park, California 94025, USA

²U.S. Geological Survey, MS 973, Federal Center, Denver, Colorado 80225, USA

³U.S. Geological Survey, University of Nevada, Reno, Nevada 89557, USA

⁴U.S. Geological Survey, 904 West Riverside Avenue, Spokane, Washington 99201, USA

ABSTRACT

The Middle to Late Miocene Bodie Hills volcanic field is a >700 km², long-lived (~9 Ma) but episodic eruptive center in the southern segment of the ancestral Cascades arc north of Mono Lake (California, U.S.). It consists of ~20 major eruptive units, including 4 trachyandesite stratovolcanoes emplaced along the margins of the field, and numerous, more centrally located silicic trachyandesite to rhyolite flow dome complexes. Bodie Hills volcanism was episodic with two peak periods of eruptive activity: an early period ca. 14.7–12.9 Ma that mostly formed trachyandesite stratovolcanoes and a later period between ca. 9.2 and 8.0 Ma dominated by large trachyandesite-dacite dome fields. A final period of small silicic dome emplacement occurred ca. 6 Ma. Aeromagnetic and gravity data suggest that many of the Miocene volcanoes have shallow plutonic roots that extend to depths ≥1–2 km below the surface, and much of the Bodie Hills may be underlain by low-density plutons presumably related to Miocene volcanism.

Compositions of Bodie Hills volcanic rocks vary from ~50 to 78 wt% SiO₂, although rocks with <55 wt% SiO₂ are rare. They form a high-K calc-alkaline series with pronounced negative Ti-P-Nb-Ta anomalies and high Ba/Nb, Ba/Ta, and La/Nb typical of subduction-related continental margin arcs. Most Bodie Hills rocks are porphyritic, commonly containing 15–35 vol% phenocrysts of plagioclase, pyroxene, and hornblende ± biotite. The oldest eruptive units have the most mafic compositions, but volcanic rocks oscillated between mafic and intermediate to

felsic compositions through time. Following a 2 Ma hiatus in volcanism, postsubduction rocks of the ca. 3.6–0.1 Ma, bimodal, high-K Aurora volcanic field erupted unconformably onto rocks of the Miocene Bodie Hills volcanic field.

At the latitude of the Bodie Hills, subduction of the Farallon plate is inferred to have ended ca. 10 Ma, evolving to a transform plate margin. However, volcanism in the region continued until 8 Ma without an apparent change in rock composition or style of eruption. Equidimensional, polygenetic volcanoes and the absence of dike swarms suggest a low differential horizontal stress regime throughout the lifespan of the Bodie Hills volcanic field. However, kinematic data for veins and faults in mining districts suggest a change in the stress field from transtensional to extensional approximately coincident with the inferred cessation of subduction.

Numerous hydrothermal systems were operative in the Bodie Hills during the Miocene. Several large systems caused alteration of volcaniclastic rocks in areas as large as 30 km², but these altered rocks are mostly devoid of economic mineral concentrations. More structurally focused hydrothermal systems formed large epithermal Au-Ag vein deposits in the Bodie and Aurora mining districts. Economically important hydrothermal systems are temporally related to intermediate to silicic composition domes.

Rock types, major and trace element compositions, petrographic characteristics, and volcanic features of the Bodie Hills volcanic field are similar to those of other large Miocene volcanic fields in the southern segment of the ancestral Cascade arc. Relative to other parts of the ancestral arc, especially

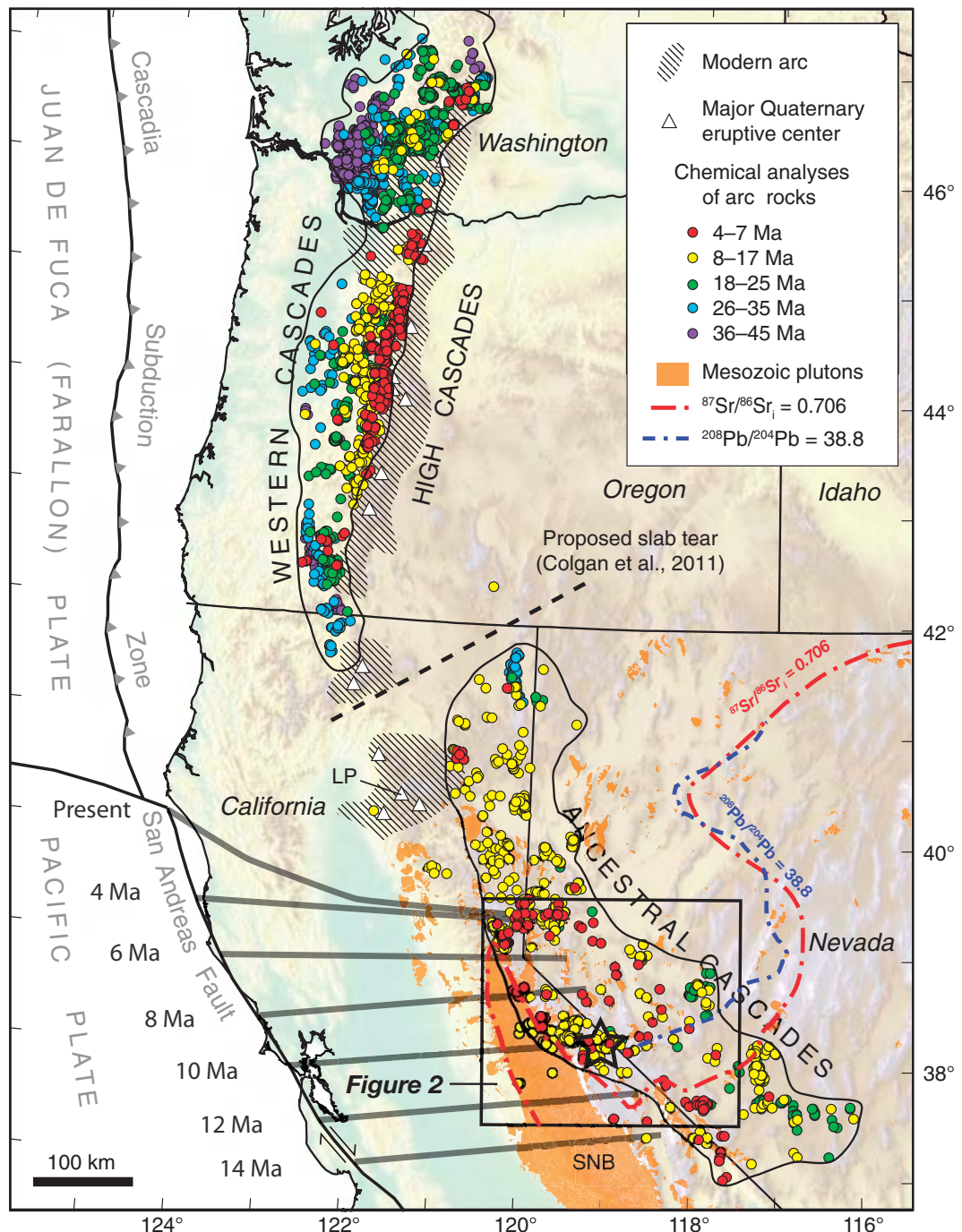
north of Lake Tahoe in northeastern California, the scarcity of mafic rocks, relatively K-rich calc-alkaline compositions, and abundance of composite dome fields in the Bodie Hills may reflect thicker crust beneath the southern ancestral arc segment. Thicker crust may have inhibited direct ascent and eruption of mafic, mantle-derived magma, instead stalling its ascent in the lower or middle crust, thereby promoting differentiation to silicic compositions and development of porphyritic textures characteristic of the southern ancestral arc segment.

INTRODUCTION

From Eocene through Miocene time, subduction of the Farallon plate beneath western North America sustained magmatism associated with the well-characterized ancestral (Western) Cascades arc segment in Washington, Oregon, and northernmost California, which was slightly west of the modern Cascades arc (Fig. 1; Atwater, 1970; McBirney, 1978; Priest, 1990; Smith, 1993; Sherrod and Smith, 2000; du Bray et al., 2006; du Bray and John, 2011). A swath of Oligocene to Pliocene volcanic rocks in eastern California and western Nevada (Fig. 1) has often been interpreted as the southern extension of this ancestral arc magmatism (e.g., Noble, 1972; Christiansen and Yeats, 1992; Dickinson, 1997, 2006; Putirka and Busby, 2007; Cousens et al., 2008, 2011; Busby et al., 2008; Busby and Putirka, 2009; du Bray et al., 2009; Hagan et al., 2009; Vikre and Henry, 2011; Colgan et al., 2011; C.J. Busby, 2011, written commun.). The southern and eastern extent of the ancestral Cascades arc is debated, however, and Glazner and Farmer (2008) questioned the existence of an ancestral arc south of the southern terminus of the modern Cascades arc at Lassen Peak in

*E-mail: djohn@usgs.gov

Figure 1. Map of the western United States showing the inferred extent of ancestral and modern Cascades magmatic arcs in Washington, Oregon, California, and Nevada (modified from du Bray et al., 2009; Colgan et al., 2011). Star shows location of the Bodie Hills. Sample locations of ancestral Cascade arc rocks from geochemical databases of du Bray et al. (2006, 2009). Heavy gray lines show the southern edge of subducting Farallon plate at the time specified (Atwater and Stock, 1998). Red dashed line is the initial $^{87}\text{Sr}/^{86}\text{Sr} = 0.706$ isopleth for Mesozoic plutonic rocks in California (Kistler, 1990) and Nevada (Tosdal et al., 2000). Blue dashed line is the $^{208}\text{Pb}/^{204}\text{Pb} = 38.8$ isopleth (Tosdal et al., 2000). Outcrops of Mesozoic granitic rocks are from Ludington et al. (2005). Black box outlines area of Figure 2. LP—Lassen Peak; SNB—Sierra Nevada batholith.



northern California (Fig. 1). Rocks interpreted as constituents of the southern ancestral Cascades arc segment are part of a diverse suite of Cenozoic volcanic rocks erupted across the Basin and Range Province and related to multiple tectonic processes (Cousens et al., 2008, 2011; du Bray et al., 2009; Henry et al., 2009; Colgan et al., 2011), including a major pulse of mid-Tertiary magmatism probably related to delamination and/or foundering of the shallowly east-dipping Farallon slab (e.g., Armstrong and

Ward, 1991; Best et al., 1989; Humphreys, 1995; Dickinson, 2006).

Recent studies of the southern ancestral Cascades arc segment have focused on Neogene volcanic rocks in the central Sierra Nevada between Sonora Pass and Lake Tahoe (Putirka and Busby, 2007, 2009; Busby et al., 2008; Cousens et al., 2008, 2011; C.J. Busby, 2011, written commun.) and in the Warner Range in northeasternmost California (Colgan et al., 2011). With the exception of a geologic

map and brief summary of part of the Miocene Virginia City volcanic center (Fig. 2; Hudson et al., 2009), few detailed studies of Miocene–Pliocene, possibly ancestral arc-related, volcanic fields in the western Basin and Range east of the central Sierra Nevada have been completed.

In the central Sierra Nevada, recent studies of late Cenozoic tectonics and magmatism suggest the formation ca. 12 Ma of a Sierra Nevada microplate between the San Andreas fault to the

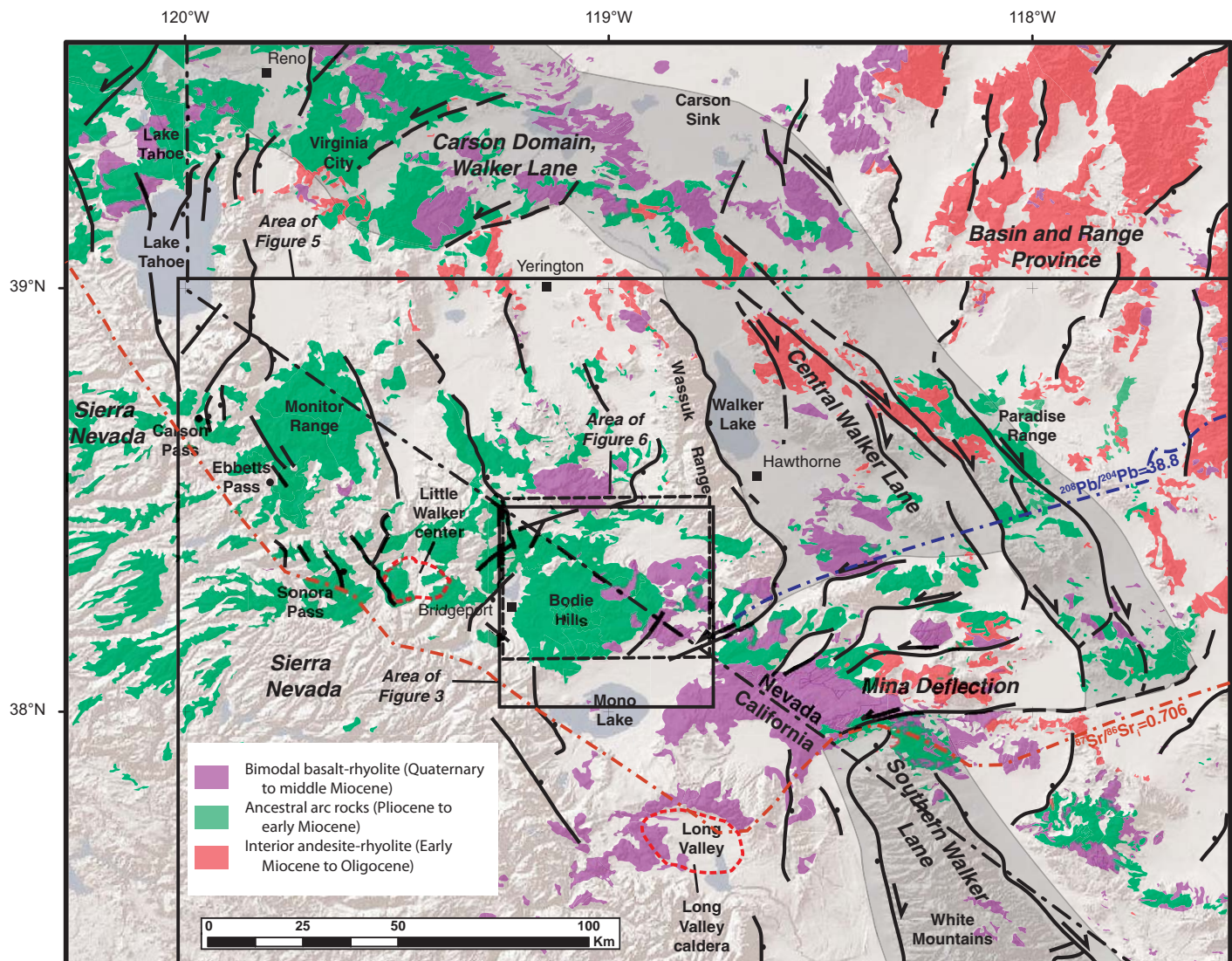


Figure 2. Map showing regional setting of the Bodie Hills in the context of Cenozoic volcanic rocks in the eastern Sierra Nevada and western Basin and Range, major faults, and major volcanic fields and/or eruptive centers inferred to represent the ancestral Cascades arc. Mina deflection and segments of the Walker Lane are from Faulds and Henry (2008). Red dashed line is the initial $^{87}\text{Sr}/^{86}\text{Sr} = 0.706$ isopleth for Mesozoic plutonic rocks in California (Kistler, 1990) and Nevada (Tosdal et al., 2000). Blue dashed line is the $^{208}\text{Pb}/^{204}\text{Pb} = 38.8$ isopleth for Mesozoic plutonic rocks in Nevada (Tosdal et al., 2000). Cenozoic volcanic rock units are generally classified according to volcanic assemblages of Christiansen and Yeats (1992), Ludington et al. (1996), and John (2001). Arrows show sense of lateral displacement on strike-slip faults. Black boxes outline areas of Figures 3 and 5; dashed box outlines area of Figure 6.

west and the Walker Lane to the east (Putirka and Busby, 2007; Busby et al., 2008; Busby and Putirka, 2009, 2010). These studies relate the 11–9 Ma eruption of voluminous high-K magma in the Little Walker center–Sonora Pass area (Fig. 2) to transtensional faulting related to microplate formation. The above-cited authors suggested that the Little Walker center and other large arc-related volcanic centers may have been localized at releasing transtensional stepovers on strike-slip faults.

The Bodie Hills are in the western part of the Basin and Range Province, 20 km east of the Little Walker center and the central Sierra Nevada (Fig. 2). They are mostly underlain by the >700 km² Bodie Hills volcanic field, which formed between ca. 14.7 and 5.5 Ma (Figs. 3 and 4). Numerous hydrothermal systems were active during Miocene magmatism and formed several large mineral deposits and extensive alteration zones. The Bodie Hills are coincident with the eastward protrusion of a broad gravity

low that is characteristic of the Sierra Nevada batholith (Eaton et al., 1978; Fig. 5). Northwest- and northeast-trending gravity gradients define the eastern contact of plutonic rocks with higher density pre-Tertiary basement rocks. The northeast-trending gravity gradient is parallel to several mapped post-11 Ma faults in the Bodie Hills (Fig. 3), but both the faults and the gravity lineaments may be structures inherited from the underlying rifted Proterozoic continental margin. The eastern and southeastern parts of the

Bodie Hills volcanic field

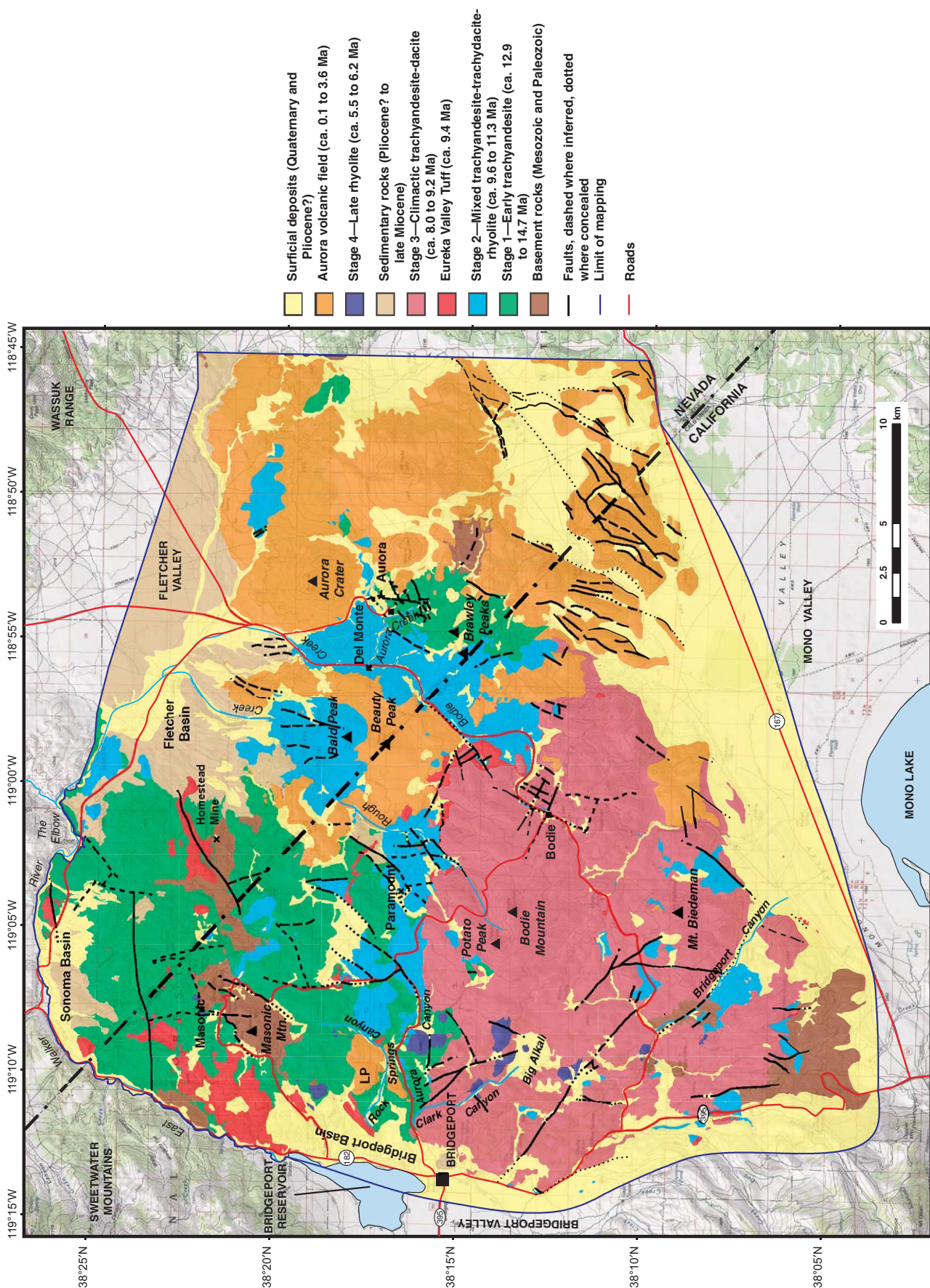


Figure 3. Generalized geologic map of Bodie Hills volcanic field showing four stages of Miocene magmatic activity: the Eureka Valley Tuff, Miocene–Pliocene(?) sedimentary rocks, and the Pliocene–Pleistocene Aurora volcanic field. LP—Locomotive Point.

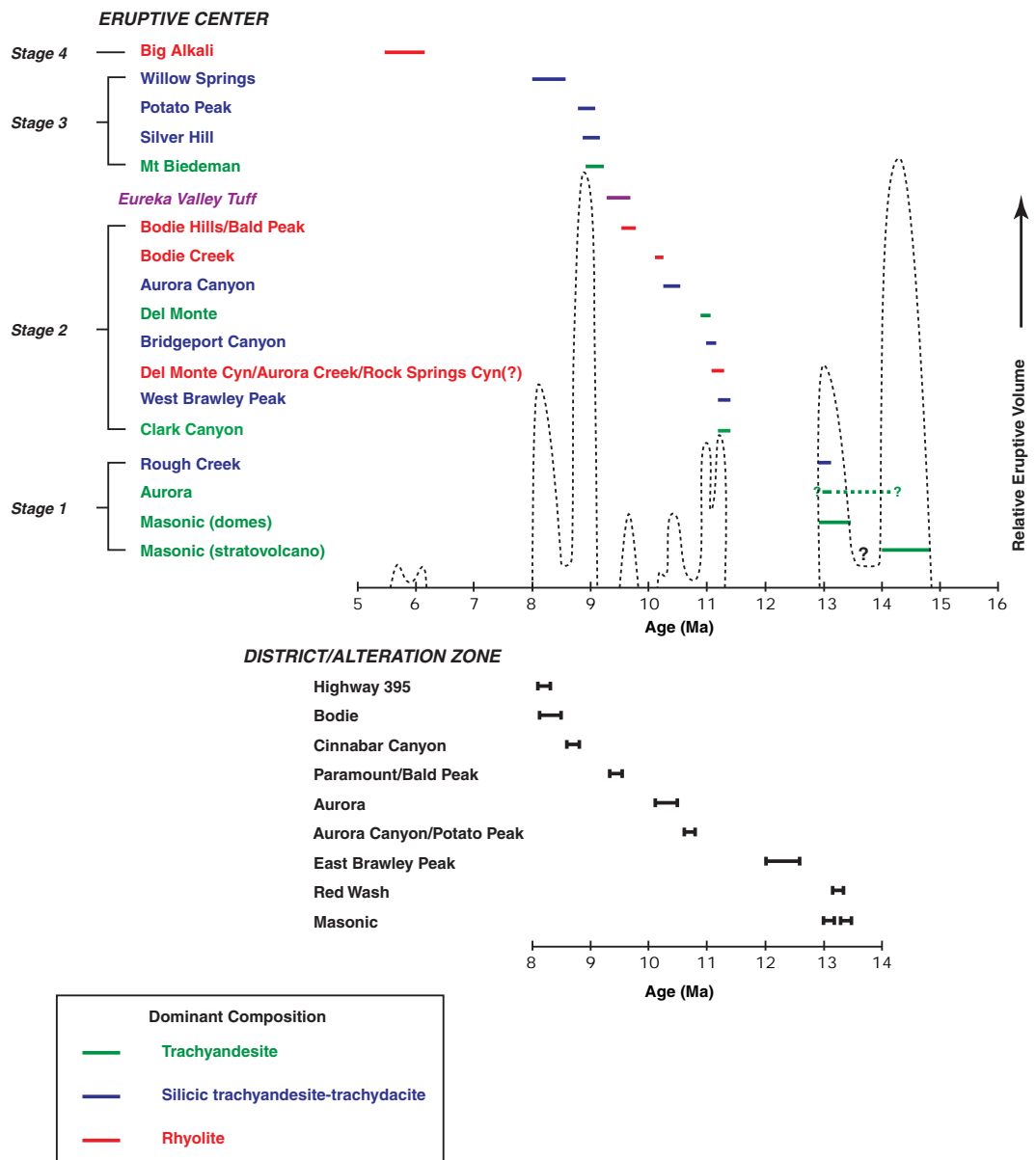


Figure 4. Age-event diagrams showing major Miocene eruptive units classified by bulk composition (upper figure) and major Miocene hydrothermal systems (lower figure). Age ranges are based mostly on new $^{40}\text{Ar}/^{39}\text{Ar}$ dates (Table 2). Hydrothermal systems are summarized in Table 5 and their locations are shown in Figure 16. Dashed lines in upper figure show relative volume of eruptive products inferred from preserved area and thickness of major eruptive units. Cyn—canyon.

Bodie Hills volcanic field are overlain by post-subduction rocks of the Pliocene to late Pleistocene Aurora volcanic field (Fig. 3; Lange et al., 1993; Lange and Carmichael, 1996).

In this paper we describe the spatial, temporal, and geochemical evolution of the Bodie Hills volcanic field and its associated hydrothermal systems and compare it to several other large volcanic fields in the southern segment of the ancestral Cascades arc. The geochemical data are interpreted only in reconnaissance fashion, because the detailed petrogenesis of these rocks is the subject of our ongoing research. New and existing gravity data help define the location and size of silicic intrusions beneath the Bodie Hills, and high-resolution aeromagnetic data indicate the lateral extent of volcanic rocks from various

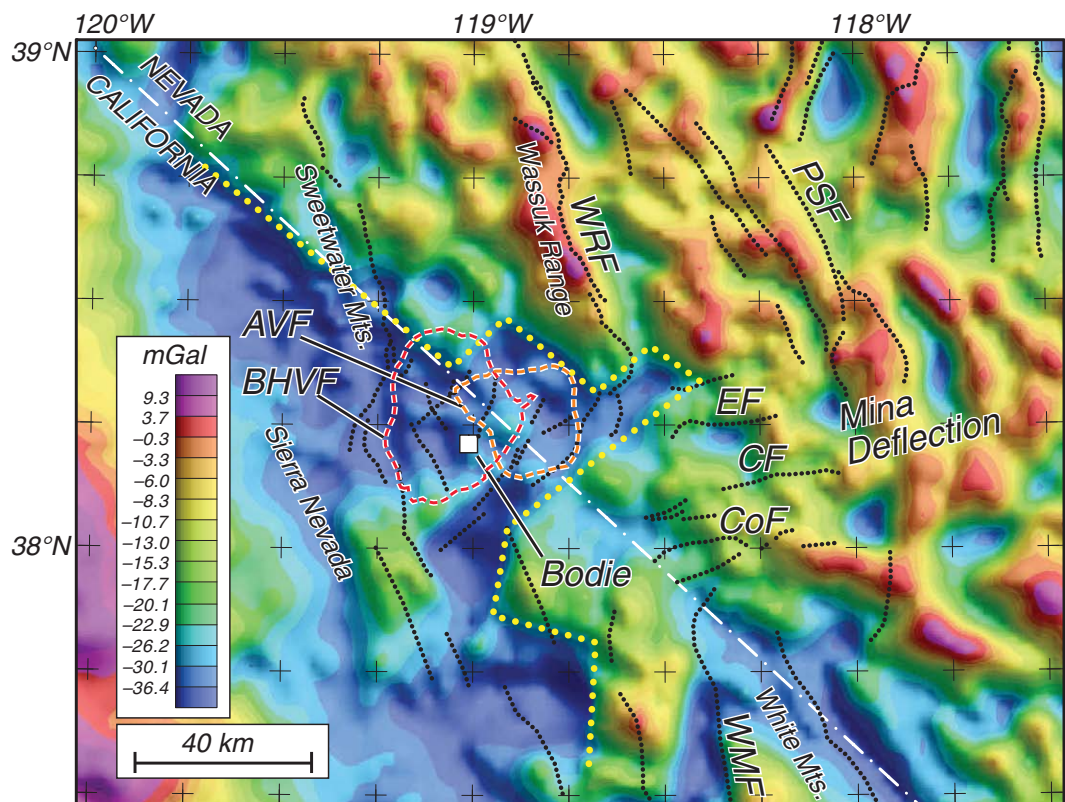
eruptive episodes during Bodie Hills volcanism. We compare the tectonic controls on Miocene magma emplacement in the Bodie Hills to those inferred for other parts of the southern ancestral arc. We also compare subduction-related ancestral arc rocks of the Bodie Hills volcanic field to the postsubduction Aurora volcanic field.

PREVIOUS STUDIES

Previous geologic studies of the Bodie Hills focused on mineral deposits in the Bodie, Aurora, and Masonic mining districts (e.g., Hill, 1915; Chesterman et al., 1986; Herrera et al., 1991, 1993; Silberman and Chesterman, 1991; Osborne, 1991; Breit, 2000; Vikre and Henry, 2011), volcanic units in the Bodie 15' quadrangle

(Chesterman, 1968; Chesterman and Gray, 1975), late Cenozoic development of the Mono Basin (Gilbert et al., 1968; Al-Rawi, 1969), and the postsubduction Pliocene–Pleistocene Aurora volcanic field (Lange et al., 1993; Lange and Carmichael, 1996). Several studies have used gravity and magnetic data to interpret regional-scale Basin and Range geology and tectonism in the area surrounding the Bodie Hills (e.g., Eaton et al., 1978; Blakely and Jachens, 1991; Saltus and Jachens, 1995). More detailed geophysical examinations of the Bodie Hills (e.g., Kleinhapl et al., 1975; Smailbegovic, 2002; Rockwell, 2010) have focused on geophysical expression of mineral deposits. Available geologic maps of the Bodie Hills are at a scale of 1:250,000 or smaller (Stewart et al., 1982).

Figure 5. Isostatic residual gravity anomalies of east-central California and west-central Nevada. Black dotted lines are selected faults from Gutierrez et al. (2010), Crafford (2007), and Faulds and Henry (2008). Yellow dotted line indicates eastward limit of gravity low discussed in text. White square is the location of Bodie. Red and orange dashed lines show outlines of Bodie Hills (BHVF) and Aurora (AVF) volcanic fields, respectively, as shown in Figure 3. WRF—Wassuk Range frontal fault; PSF—Petrified Spring fault; EF—Excellor fault; CF—Cady fault; CoF—Coaldale fault; WMF—White Mountain fault.



NEW GEOLOGIC, GEOCHEMICAL, AND GEOPHYSICAL DATA AND METHODOLOGY

We present a new 1:50,000-scale geologic map of the Bodie Hills volcanic field that combines new mapping, based on modern volcanologic concepts, with significant modification of other geologic maps, including those of Johnson (1951), Stanford Geological Survey (1961), Al-Rawi (1969), Chesterman and Gray (1975), Kleinhampel et al. (1975), Dohrenwend (1981, 1982), Dohrenwend and Brem (1982), Chesterman et al. (1986), M.L. Silberman (2000, written commun.), and Smailbegovic (2002).

Our geologic and tectonic interpretations are supported by new and existing gravity and airborne magnetic measurements of the Bodie Hills and surrounding areas. We acquired 207 new gravity measurements (Supplemental Table 1¹) at key locations along all accessible roads and tracks in the Bodie Hills. These raw measurements were reduced to gravity

anomalies using standard methods established by the U.S. Geological Survey. Specifically, raw gravity measurements were corrected for latitude, Earth tides, elevation (free-air correction), and terrain effects (Bouguer correction). The resulting complete Bouguer anomaly values were then merged with existing Bouguer gravity values from the larger region. The merged database was corrected for deep crustal masses that isostatically support topographic loads in order to obtain the isostatic residual gravity anomaly (Fig. 6A; Simpson et al., 1986).

Our magnetic interpretations are based on a high-resolution aeromagnetic survey (U.S. Geological Survey, 2001) acquired in 1999 (by Sander Geophysics Ltd. working under contract to the U.S. Geological Survey). Measurements were made using a fixed-wing aircraft along flight lines spaced 150 m apart and at an altitude of 150 m above ground (or as near to the ground as safely possible). Total-field measurements were reduced to total-field anomaly values (Fig. 6B) by subtraction of the International Geomagnetic Reference Field appropriate for the date of the survey.

New chemical and petrographic data were obtained for all Bodie Hills volcanic field rocks. Representative samples of all units were col-

lected throughout their respective geographic distributions. Whole-rock chemical analyses for ~313 unaltered samples were performed by SGS Minerals (under contract to the U.S. Geological Survey). Major oxide abundances were determined by wavelength dispersive X-ray fluorescence spectrometry. All plots and references in the text involving major element oxides refer to abundances recalculated to 100%, volatile free. Trace element abundances were determined by a combination of inductively coupled plasma–atomic emission and inductively coupled plasma–mass spectrometry. (For analytical methods, see Taggart, 2002; also see http://minerals.cr.usgs.gov/projects/analytical_chem/references.html.) Previously published analyses (principally major oxides) of an additional 79 samples compiled from the literature (du Bray et al., 2009) are included in the syntheses described here. All chemical data are presented in Supplemental Table 2². Standard petrographic microscope techniques were employed to identify

¹Supplemental Table 1. PDF file of numerous additional data plots, tabular data, and ancillary text in support of this paper. If you are viewing the PDF of this paper or reading it offline, please visit <http://dx.doi.org/10.1130/GES00674.S1> or the full-text article on www.gsapubs.org to view Supplemental Table 1.

²Supplemental Table 2. Excel file of chemical analyses of Cenozoic volcanic rocks in the Bodie Hills, California and Nevada. If you are viewing the PDF of this paper or reading it offline, please visit <http://dx.doi.org/10.1130/GES00674.S2> or the full-text article on www.gsapubs.org to view Supplemental Table 2.

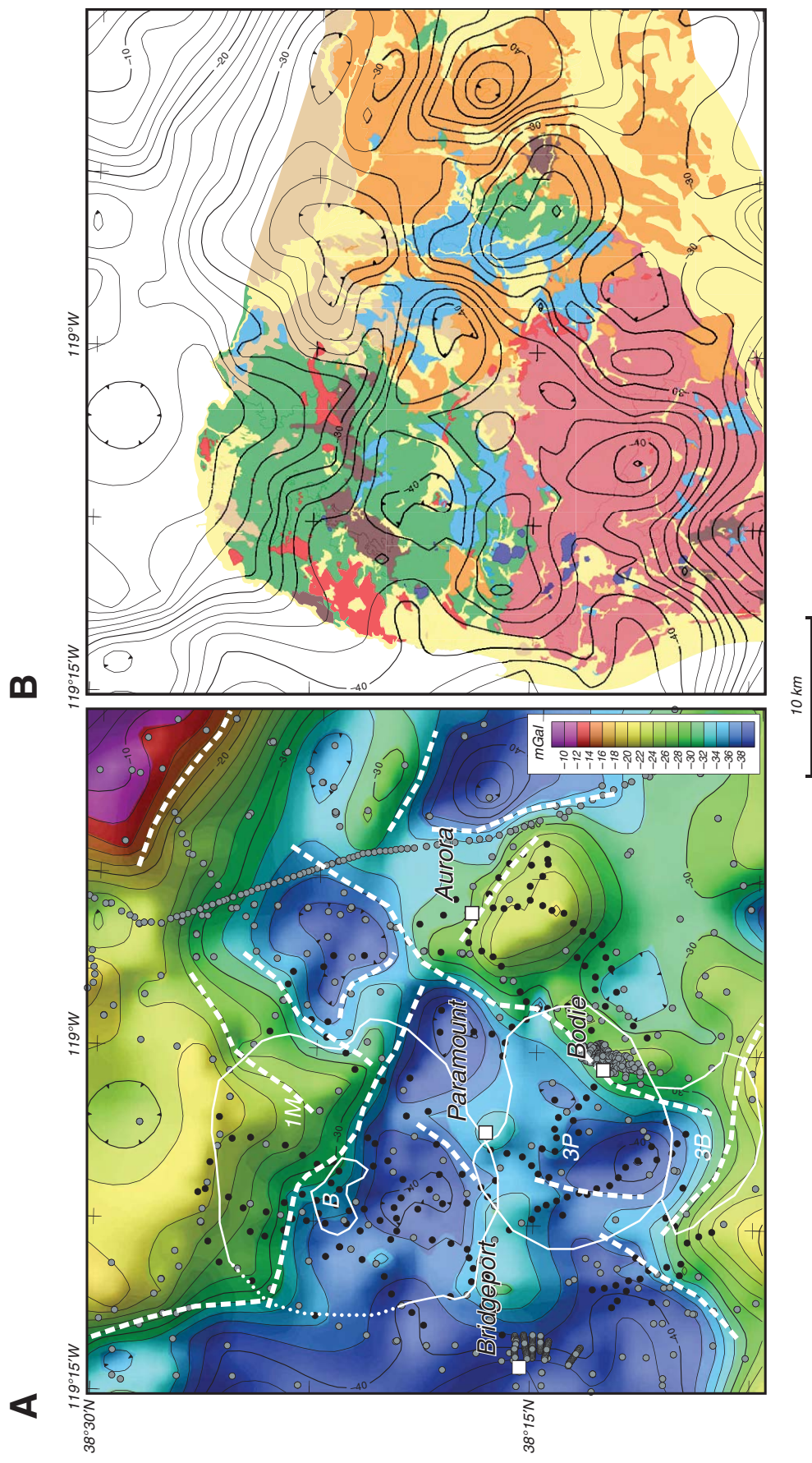


Figure 6 (*on this and following page*). (A) Isostatic residual gravity anomalies of the Bodie Hills. Black circles indicate location of new gravity stations acquired as part of this study; gray circles are other publicly available gravity stations. Bold dashed white lines are linear density contrasts interpreted from gravity anomalies and discussed in text. White polygonal lines are interpreted magnetic sources from Figure 8 (discussed in text). 1M—Masonic volcanic rocks; 3P—Potato Peak volcanic rocks; 3B—pre-Tertiary basement. (B) Isostatic gravity contours on generalized geologic map of Figure 3. Contour interval is 2 mGal. See Figure 3 for description of geologic units.

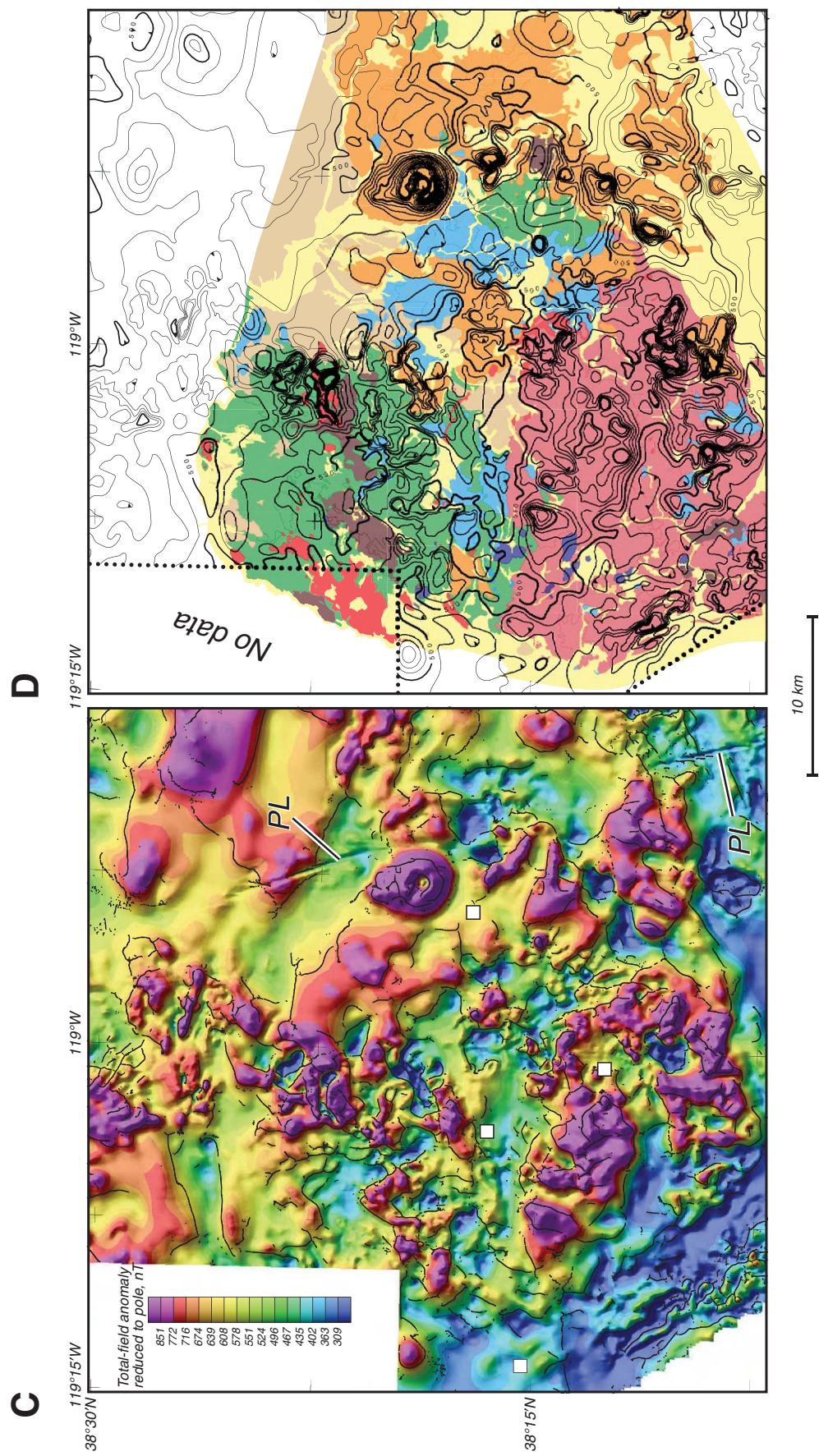


Figure 6 (*continued*). (C) Airborne magnetic anomalies (U.S. Geological Survey, 2001). Small black dots are magnetic contacts determined automatically from magnetic data (Phillips et al., 2007). Anomalies have been reduced to the pole (Blakely, 1995), a process that reduces anomaly skewness caused by nonvertical magnetization and ambient magnetic field. Color contour interval is established by an equal-area histogram algorithm. PL indicates a linear anomaly caused by a powerline. (D) Aeromagnetic contours on generalized geologic map of Figure 3. Contour interval is 100 nT.

phenocryst minerals and their relative abundances, as well as other diagnostic petrographic criteria in ~450 samples of Bodie Hills volcanic field rocks. These petrographic observations were synthesized by a host rock unit and were used in map unit identification during geologic mapping.

New $^{40}\text{Ar}/^{39}\text{Ar}$ age determinations ($n = 101$) on mineral separates provide temporal constraints on volcanic and hydrothermal activity. Volcanic rocks were dated using separates of one or more phenocryst minerals (plagioclase, sanidine, biotite); hydrothermal alteration was dated using separates of alunite or adularia. Where practical, multiple minerals from individual samples were prepared to confirm results. Samples collected for $^{40}\text{Ar}/^{39}\text{Ar}$ analysis were crushed and sieved to sizes appropriate for mineral separation of each sample. Samples were irradiated in the U.S. Geological Survey TRIGA Reactor Facility in Denver, Colorado; irradiation times were between 10 and 16 h. Plagioclase, biotite, and alunite $^{40}\text{Ar}/^{39}\text{Ar}$ ages were obtained by incremental-heating analysis, i.e., sequential extraction of the argon from the sample at progressively higher temperatures until the sample was fused. Incremental-heating analyses utilized a low-blank, tantalum and molybdenum, resistance-heated furnace, commonly releasing all Ar in 8–15 temperature-controlled heating increments. Ages from incremental-heating experiments were determined by an evaluation of the $^{40}\text{Ar}/^{39}\text{Ar}$ age spectrum and isochron diagrams of the data. Many of the ages are defined by an $^{40}\text{Ar}/^{39}\text{Ar}$ plateau, defined as the weighted mean age of contiguous gas fractions representing >50% of the ^{39}Ar released for which no difference can be detected between the ages of any two fractions at the 95% level of confidence (Fleck et al., 1977). Where no plateau is defined, either the $^{40}\text{Ar}/^{39}\text{Ar}$ isochron age or the integrated age of all increments was adopted.

Sanidine ages were obtained by laser-fusion analysis, in which grains are fused with a CO_2 laser in a single heating step. Single grains or several grains are used in each analysis, depending on the grain size. The reported age for laser-fusion analyses represents the weighted mean of six or more replicate analyses, with the inverse variance of propagated, within-run (i.e., internal) errors used as the weighting factors (Taylor, 1982). Sanidine from the Taylor Creek Rhyolite (TCR-2) was used for calculation of the neutron flux in all irradiations. Ages are reported relative to an age of 28.02 Ma for the Fish Canyon Tuff sanidine standard (Renne et al., 1998). Decay and abundance constants are those recommended by Steiger and Jäger (1977).

REGIONAL GEOLOGIC AND GEOPHYSICAL SETTING OF THE BODIE HILLS

The Bodie Hills straddle an ~40 × 30 km area along the California-Nevada border and rise to an elevation of 3112 m at Potato Peak, ~1100–1400 m above Bridgeport and Fletcher Valleys, Mono Basin, and the East Walker River (Fig. 3). Approximately 8 km west of the Bodie Hills, the central Sierra Nevada rises nearly 2000 m above Bridgeport Valley and Mono Basin. The Bodie Hills are in a complex tectonic domain near the west edge of the Walker Lane and at the northwest limit of the Mina deflection (Fig. 2; Stewart, 1988; Faulds and Henry, 2008). The Walker Lane is a broad, northwest-striking zone of right-lateral shear that accommodates ~20% of the right-lateral motion between the Pacific and North America plates (Oldow, 2003; Faulds and Henry, 2008). The Mina deflection is a 60 km right step in the Walker Lane (Stewart, 1988; Oldow, 1992; Faulds and Henry, 2008), in which slip is transferred across an ~80-km-wide complex array of northwest-striking right-lateral faults, northeast-striking normal faults, and east- to east-northeast-striking left-lateral faults (Oldow, 1992; Wesnousky, 2005). The Bodie Hills are at the northwest corner of the Mina deflection, where east-striking left-lateral faults rotate into northeast-striking normal faults. Slip transfer in the Mina deflection apparently began after ca. 11 Ma (Faulds and Henry, 2008) and may have followed the east-northeast-trending Neoproterozoic continental margin, generally considered to correspond to the initial $^{87}\text{Sr}/^{86}\text{Sr}$ (Sr_i) = 0.706 and/or $^{208}\text{Pb}/^{204}\text{Pb}$ = 38.8 isopleths in Mesozoic granitic plutons (Fig. 2; Kistler and Peterman, 1978; Stewart, 1988; Tosdal et al., 2000).

Miocene igneous rocks in the Bodie Hills were erupted onto pre-Tertiary basement, discontinuously exposed throughout the Bodie Hills (Fig. 3). Pre-Tertiary rocks (shown as undifferentiated basement rocks in Fig. 3) consist of (1) early Paleozoic hornfelsed argillite, sandstone, chert, and pebble conglomerate; (2) Triassic(?) metamorphosed sandstone, siltstone, chert, tuff, and pillow basalt; (3) Mesozoic metaandesite, metatuff, and metavolcaniclastic rocks; and (4) Late Cretaceous (98–95 Ma K-Ar ages) granitic rocks that are part of the Sierra Nevada batholith (Chesterman and Gray, 1975; Stewart et al., 1982; Robinson and Kistler, 1986). Three of the plutons exposed in northwest and southwest parts of the Bodie Hills have Sr_i values that range from 0.7053 to 0.7059 (Robinson and Kistler, 1986). Granitic rocks crop out around the margins of the Bodie Hills, whereas metavolcanic rocks are exposed in the northern

and east parts and metasedimentary rocks occur in the southwestern and northern parts.

The Bodie Hills area likely was a topographic high during the early and mid Tertiary. Tertiary sedimentary and volcanic rocks are not exposed beneath the Miocene volcanic rocks. Paleosols developed on pre-Tertiary basement rocks are preserved locally, notably near the Homestead Mine in the northeast part of the Bodie Hills (Fig. 3). Unlike other areas in the western Great Basin, early to middle Tertiary, west-draining paleochannels apparently did not cross the 40 km north-south extent of the Bodie Hills (Henry, 2008; Busby and Putirka, 2009; Henry and Faulds, 2010).

The Bodie Hills volcanic field consists principally of four eroded trachyandesite stratovolcanoes emplaced on its north, east, and southwest margins and large silicic trachyandesite, trachydacite, and rhyolite dome fields that form the core of the volcanic field (Figs. 3 and 7; Table 1). This volcanic field covers >700 km², was active from ca. 14.7 to 5.5 Ma, and includes both synsubduction and postsubduction magmatism. Early volcanic units were erupted during subjacent subduction of the Farallon plate prior to migration of the Mendocino triple junction north of the latitude of the Bodie Hills. Subduction beneath the Bodie Hills is inferred to have ceased ca. 10 Ma (Atwater and Stock, 1998). New $^{40}\text{Ar}/^{39}\text{Ar}$ age (Table 2) and petrographic data (Table 3) are critical in defining the evolution of the Bodie Hills volcanic field.

Miocene volcanic rocks in the Bodie Hills are locally interbedded with, and overlain by, poorly consolidated Late Miocene and possible Pliocene conglomerate, sandstone, and siltstone. These sedimentary deposits form extensive pediment surfaces along the margins of the Bodie Hills and extend under Quaternary surficial deposits in Bridgeport Valley to the west and Fletcher Valley to the east (Fig. 3). Sedimentary rocks on the north and east sides of the Bodie Hills constitute the southern part of the Coal Valley Formation, which was deposited in a Late Miocene basin that extends ~50 km north of the Bodie Hills (Gilbert and Reynolds, 1973).

The eastern and southeastern parts of the Bodie Hills volcanic field are unconformably overlain by Pliocene to late Pleistocene (ca. 3.9–0.1 Ma) volcanic rocks (Fig. 3; Gilbert et al., 1968; Al-Rawi, 1969; Chesterman and Gray, 1975; Kleinhampl et al., 1975; Lange et al., 1993). These postsubduction rocks erupted in an extensional tectonic setting and are broadly characterized as bimodal. The less silicic component includes rocks spanning a broad range in composition, from trachybasalt to trachydacite, whereas the silicic component comprises only high-silica rhyolite.

Stage 1: Early Trachyandesite (ca. 14.7–12.9 Ma)

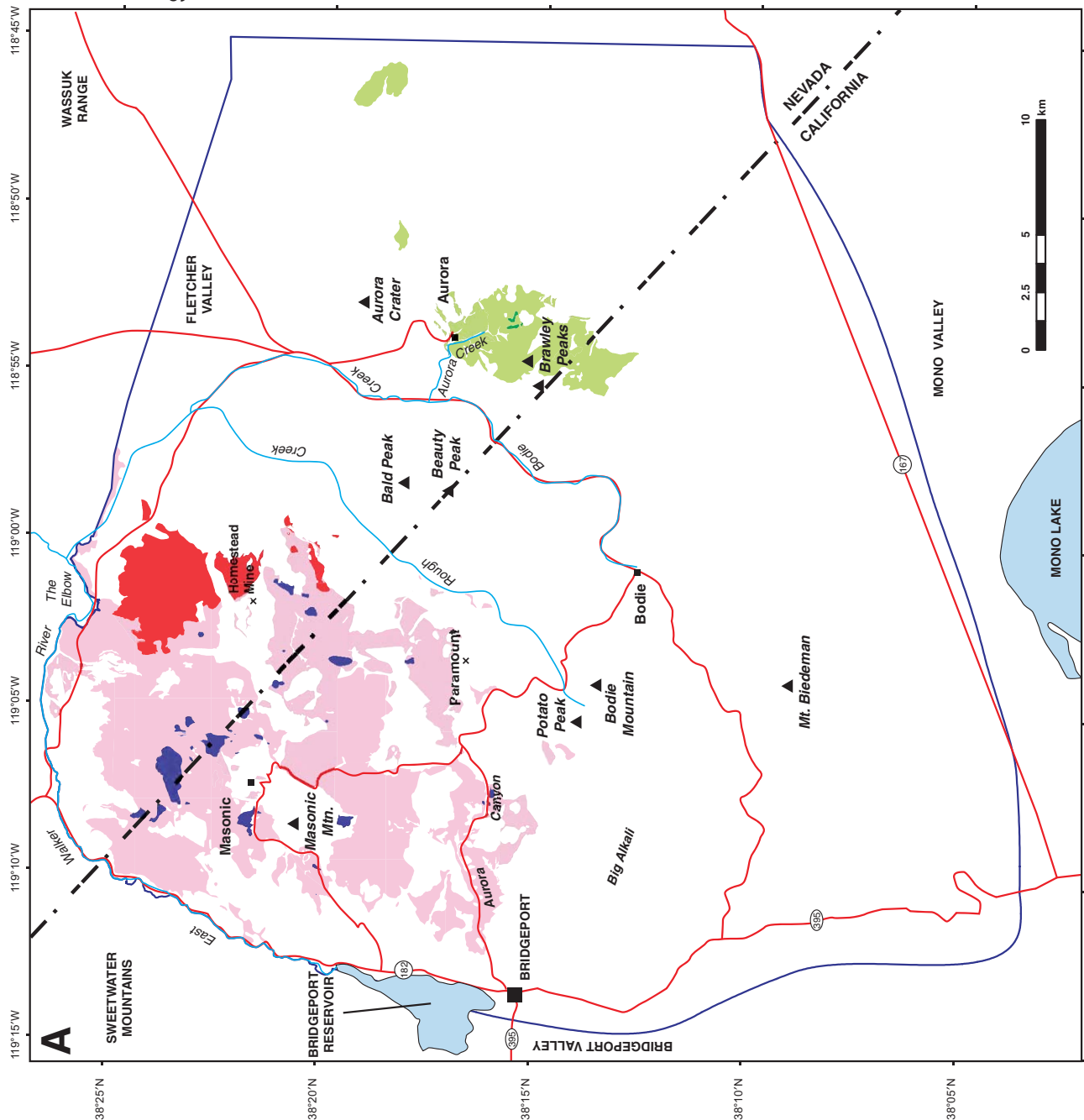


Figure 7 (on this and following four pages). Maps showing time-space-composition evolution of major magmatic units in the Bodie Hills volcanic field and Miocene sedimentary rocks and the Eureka Valley Tuff. Magmatic units summarized in Table 1. (A) Stage 1: Early trachyandesite volcanism. (B) Stage 2: Mixed trachyandesite, trachydacite, and rhyolite. (C) Stage 3: Climactic trachyandesite-dacite volcanism. (D) Stage 4: Late rhyolite volcanism. (E) Eureka Valley Tuff and sedimentary rocks. The Eureka Valley Tuff is inferred to have erupted from the Little Walker center ~20 km west of the Bodie Hills (Fig. 2) and flowed in paleochannels carved around and across the eruptive centers formed during stage 1 and 2 volcanism.

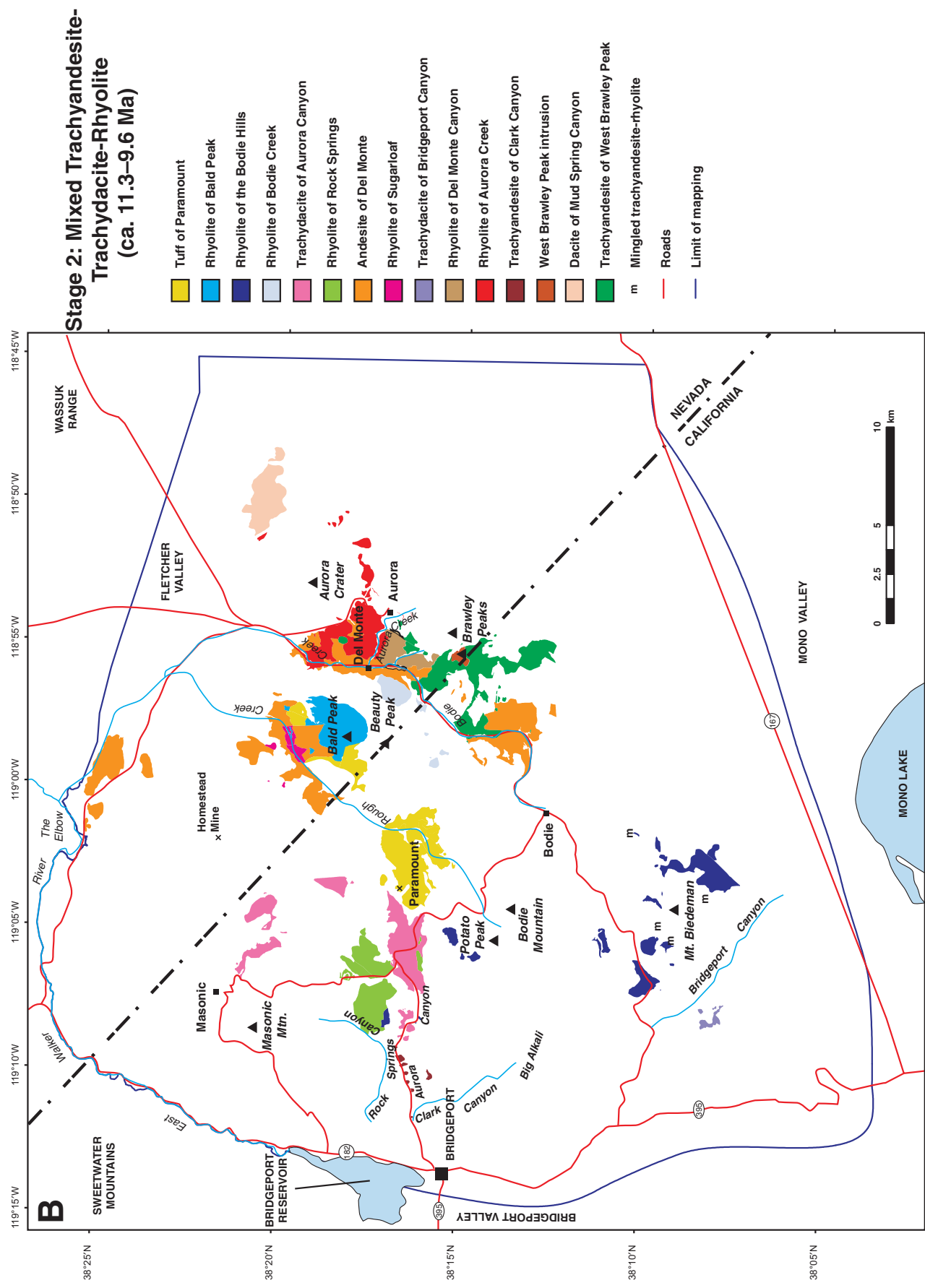


Figure 7 (continued).

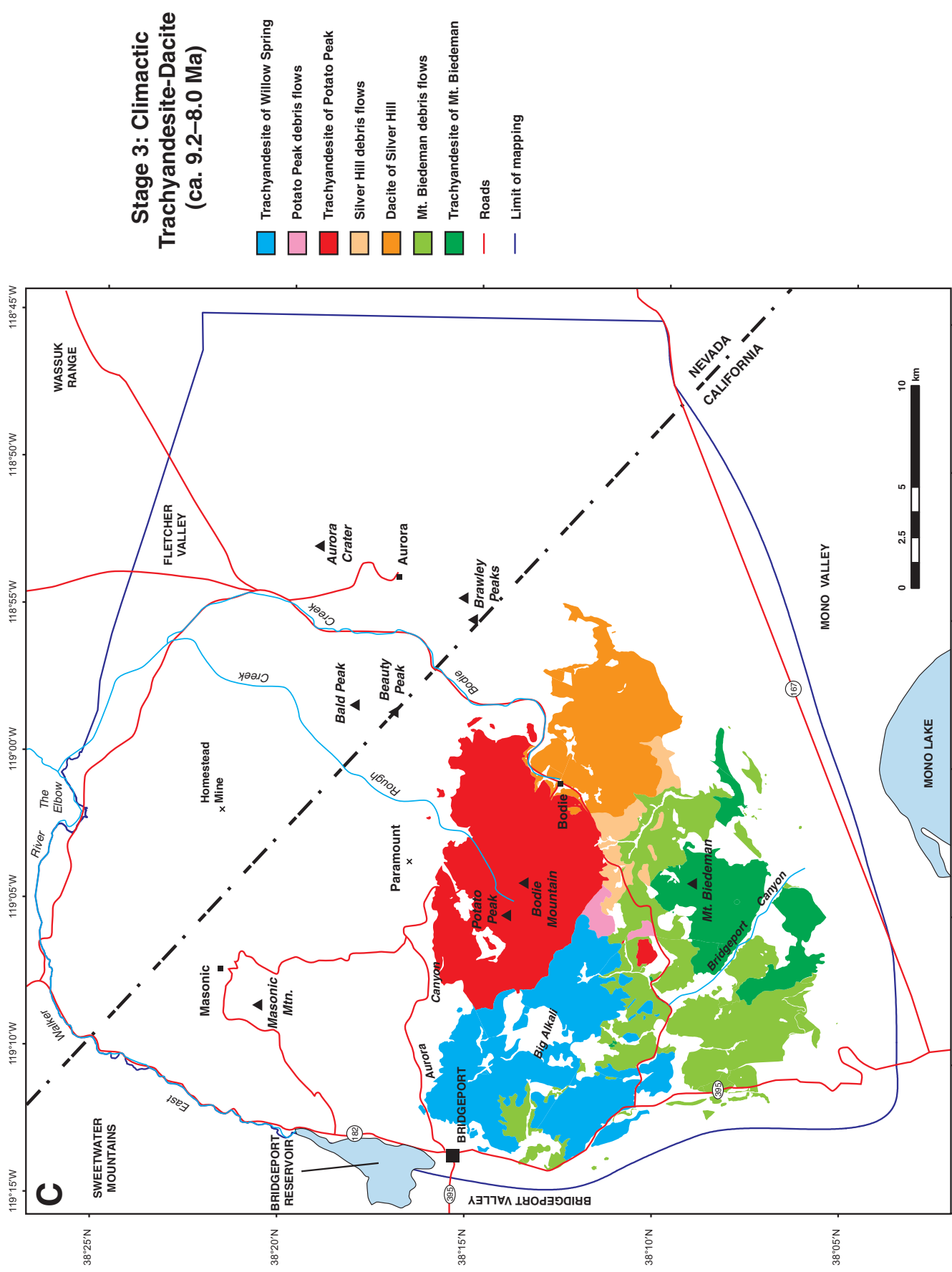


Figure 7 (continued).

Stage 4: Late Rhyolite Domes (ca. 6.2–5.5 Ma)

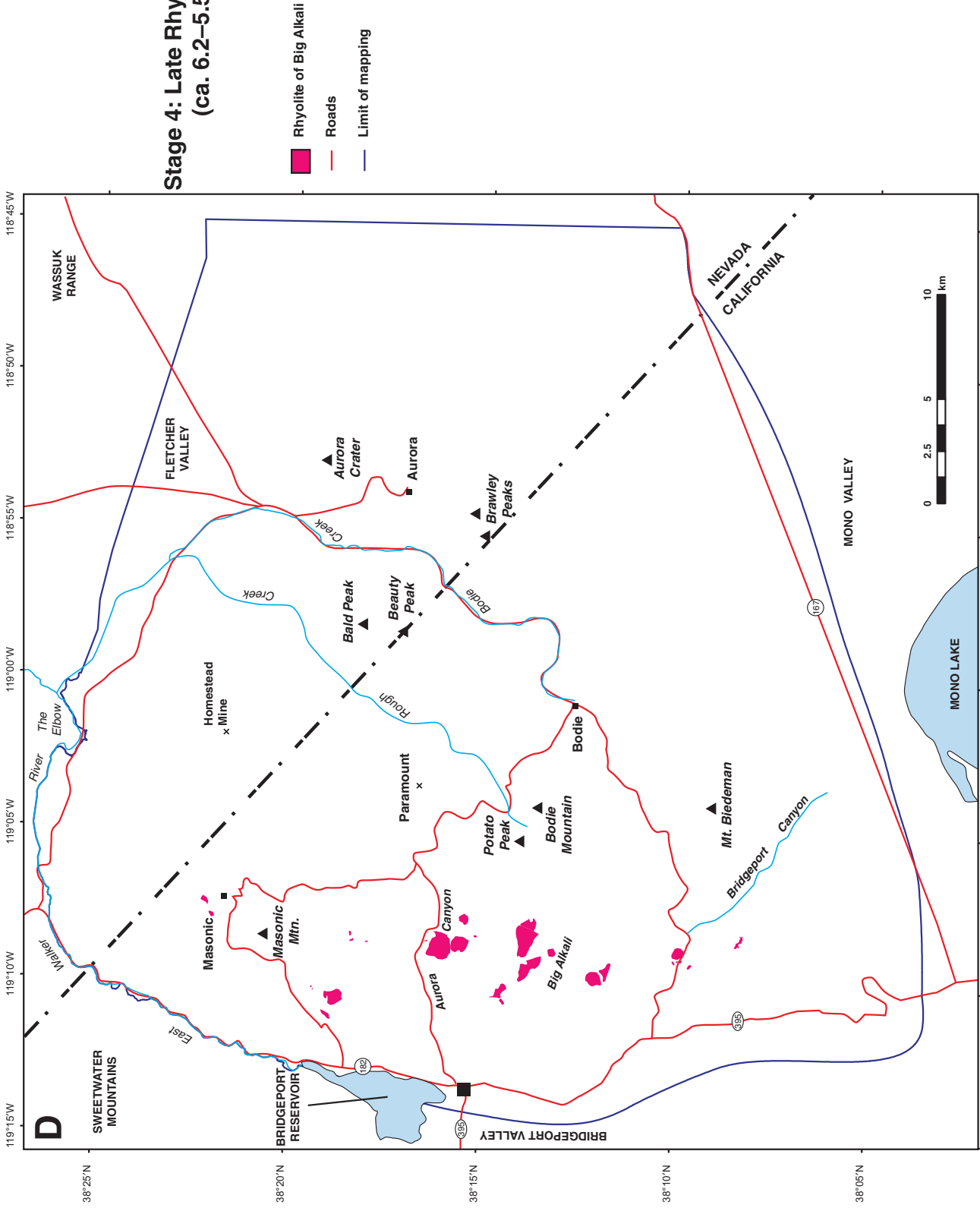


Figure 7 (*continued*).

Bodie Hills volcanic field

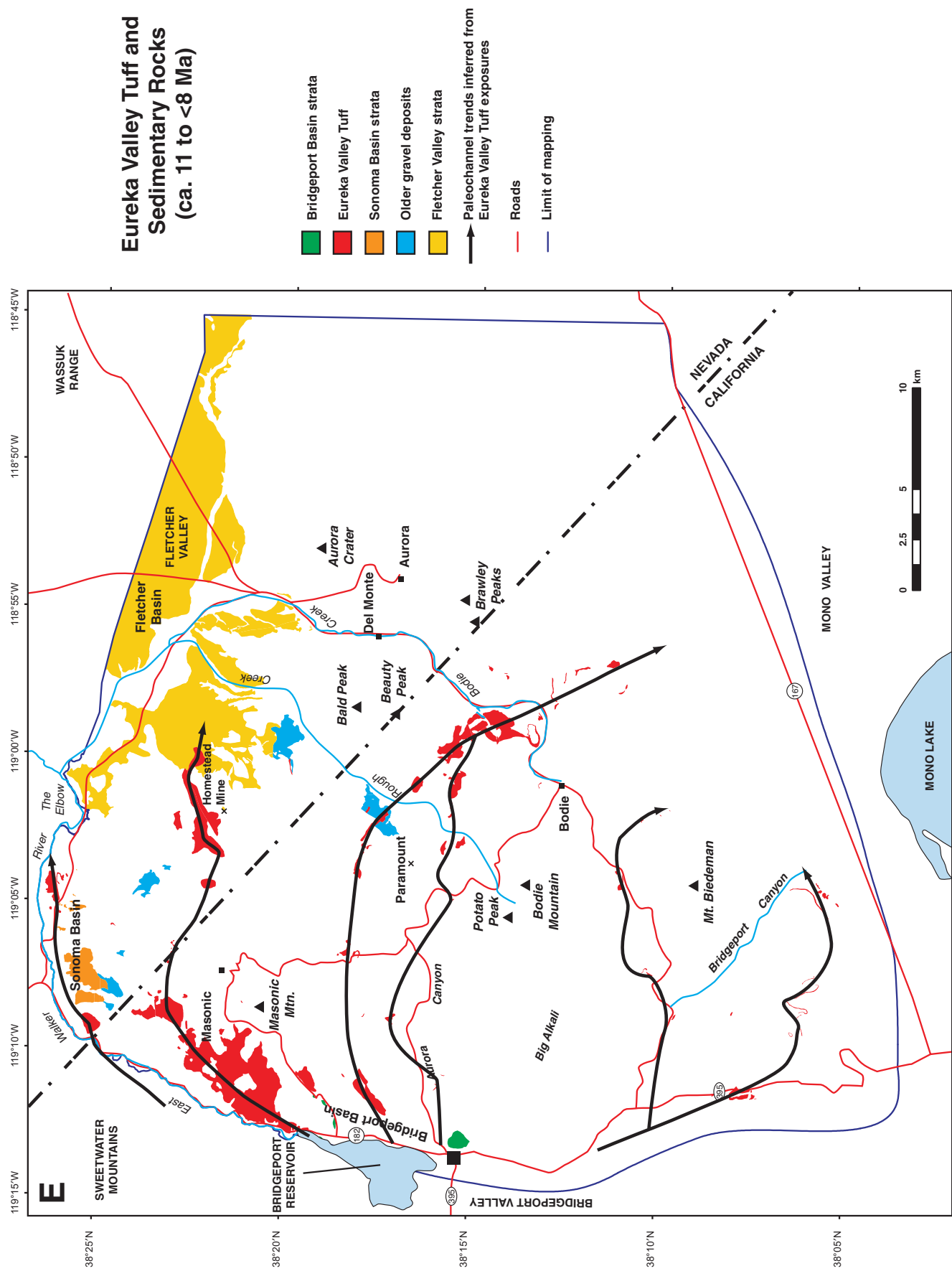


Figure 7 (*continued*).

TABLE 1. CHARACTERISTIC FEATURES OF MAJOR ERUPTIVE UNITS IN THE BODIE HILLS VOLCANIC FIELD

Eruptive center	Volcanic landform	Eruptive products	Composition	Area and dimensions
1: Early trachyandesite volcanism				
Masonic	Stratovolcano	Lava flows, debris flows, volcaniclastic sedimentary rocks, plugs and domes, minor block and ash flows	Trachyandesite and basaltic trachyandesite; with minor basaltic andesite and dacite	200 km ² ; circular, ~16 km diameter
Aurora	Stratovolcano(?)	Lava flows, debris flows, block and ash flows, small shallow intrusions, minor volcaniclastic sedimentary rocks	Trachyandesite with minor andesite	>25 km ² ; 2-4 × 8 km but largely covered by younger rocks
Rough Creek	Domes	Flow domes, carapace breccias, and minor block and ash flows	Trachydacite and trachyandesite	>20 km ² , largest mass ~4 × 4 km, extensive cover by younger deposits
2: Mixed trachyandesite-trachydacite-rhyolite volcanism				
West Brawley Peak	Stratovolcano	Central plug, lava flows and breccias	Trachyandesite, andesite, and trachydacite	>20 km ² ; semicircle ~7 km in diameter with flow lobe extending 3 km farther north; southwest part covered by younger rocks
Clark Canyon	Intrusions	Small plugs, lava flow	Trachyandesite	<1 km ²
Aurora Creek rhyolite	Domes	Flow domes, carapace breccias, lava flows, and lithic-rich tuffs	Rhyolite	10 km ² ; L-shaped, 4 km, north-south, 5 km east-west, ~1 km wide
Del Monte Canyon rhyolite	Domes	Lava flows and pyroclastic rocks	Rhyolite	3 km ² ; ~1 × 3 km
Rock Springs Canyon	Domes	Flow domes	Rhyolite	7 km ² ; two lobes, 1.5 × 2.5 km and 2 × 2 km
Trachydacite of Bridgeport Canyon	Domes	Lava flows and domes	Trachydacite	<1 km ²
Del Monte	Unknown	Lava flows, flow breccias, debris flows, volcaniclastic sedimentary rocks	Basaltic trachyandesite, trachyandesite, and trachydacite	>25 km ² ; four main masses separated by younger rocks
Aurora Canyon	Domes	Flow domes, carapace breccias, and minor block and ash flows	Trachydacite and trachyandesite	10 km ² , largest body ~1 × 5 km
Bodie Creek	Domes	Domes and lava flows	Rhyolite	2.5 km ² ; 4 small domes, largest ~1 × 1.5 km
Bodie Hills	Domes	Flow domes and minor pyroclastic rocks	Rhyolite and minor dacite	~8 km ² ; largest body ~2 × 2 km; extensive cover by younger rocks
Bald Peak–Paramount	Domes	Flow domes and carapace breccia (Bald Peak), lithic-rich tuff and volcaniclastic sedimentary rocks (Paramount basin)	Rhyolite	Bald Peak: 11 km ² ; main dome ~2.5 × 4 km; Paramount basin: ~20 km ² , 2-3 × 8 km; extensive younger cover
3: Climactic trachyandesite-dacite volcanism				
Mt. Biederman	Stratovolcano	Lava flows, debris flows, intrusions, and minor block and ash flows	Trachyandesite and basaltic trachyandesite with minor basalt and dacite	~100 km ² ; circular volcano ~5 km in diameter with debris aprons extending 3 to 15 km farther outward
Silver Hill	Domes	Flow domes, carapace breccias, block and ash flows, debris flows, volcaniclastic sedimentary rocks	Dacite, trachydacite, andesite, and trachyandesite	>50 km ² ; ~7 × 7 km; extensive younger cover
Potato Peak	Domes	Flow domes, lava flows and flow breccias, block and ash flows, debris flows	Trachydacite and trachyandesite	100 km ² ; 3–8 × 14 km with ~3 × 6 km debris flow apron on south side
Willow Springs	Domes	Flow domes, lava flows	Trachydacite and trachyandesite	90 km ² ; ~9 × 10 km
4: Late rhyolite volcanism				
Big Alkali	Domes	Flow domes, minor air-fall tuff	Rhyolite, dacite, and trachydacite	~6 km ² ; largest body circular ~1 km in diameter

(continued)

Bodie Hills volcanic field

TABLE 1. CHARACTERISTIC FEATURES OF MAJOR ERUPTIVE UNITS IN THE BODIE HILLS VOLCANIC FIELD (*continued*)

Eruptive center	Age (Ma)*	Notable features
1: Early trachyandesite volcanism		
Masonic	14.7–14.1 (main lava flows and debris flows); 13.4–12.9 (late domes)	East-west-trending horst of Mesozoic rocks bifurcates unit; debris flows and volcaniclastic rocks more abundant near margins of unit's distribution; late domes concentrated on north side of Masonic Mountain and include trachyandesite of Lakeview
Aurora	13.1 (Ar-Ar); 15.7 to 13.9 (K-Ar)	Hydrothermally altered in most places
Rough Creek	12.94	Abundantly and coarsely porphyritic, northwest-elongated flow domes; unconformably overlie hydrothermally altered Masonic center rocks
2: Mixed trachyandesite-trachydacite-rhyolite volcanism		
West Brawley Peak	11.3	Outward-dipping lava flows and flow breccias on south, west, and north sides of plug forming West Brawley Peak; buttress unconformity with hydrothermally altered Aurora center rocks forming East Brawley Peak
Clark Canyon	11.3	Series of east-northeast-aligned plugs
Aurora Creek rhyolite	11.18	Nearly aphyric, sparse phenocrysts
Del Monte Canyon rhyolite	11.2–11.1	North-dipping sequence of coarsely porphyritic lava flows and underlying lithic tuffs that flowed down Del Monte Canyon
Rock Springs Canyon	<14 and >10.5 Ma	Two east-west-elongated elliptical lobes of nearly aphyric rhyolite; local zones of black obsidian
Trachydacite of Bridgeport Canyon	11.08	Small domes and lava flows erupted onto Paleozoic basement rocks
Del Monte	11.0	Northern and central masses: lava flows, flow breccias, debris flows, and possible vent in Rough Creek. Southern masses: interbedded lava flows, debris flows, sedimentary rocks; unit filled paleotopography (ancestral Bodie Creek)
Aurora Canyon	ca. 10.45–10.25	Abundantly porphyritic flow domes form semicircular outcrop pattern
Bodie Creek	10.16	Erosional domes largely covered by Pliocene-Pleistocene lava flows
Bodie Hills	9.9–9.6	Porphyritic rhyolite domes partly surround Mount Biedeman stratovolcano and extend 15 km to northwest; includes several outcrops of rhyolite with mingled hornblende andesite blobs
Bald Peak–Paramount	9.7	North-northeast-elongated, nearly aphyric rhyolite domes surrounded by cogenetic lithic tuffs and volcaniclastic sedimentary rocks mostly deposited in shallow northeast-elongated basin to southwest of domes
3: Climactic trachyandesite-dacite volcanism		
Mt. Biedeman	ca. 9.2–8.9 (Ar-Ar); 9.8–9.5 (K-Ar)	Central intrusion forming Mount Biedeman surrounded by outward-dipping lava flows and more distal debris flows and volcaniclastic sedimentary rocks; includes minor(?) older rocks of the unmapped Rancheria center
Silver Hill	9.1–8.9	Host rock for Bodie Au-Ag deposits
Potato Peak	9.0–8.8	Thick sequences of lava flows with rubby flow tops and fronts forming prominent flow lobes on west, north, and east sides; flow-banded intrusions exposed on south side
Willow Springs	8.6–8.0	Coarsely porphyritic lava flows and flow domes
4: Late rhyolite volcanism		
Big Alkali	6.2–5.4	North-south-trending series of glassy, spongy, locally flow banded domes

*New Ar-Ar ages (see Table 2) unless otherwise noted.

TABLE 2. $^{40}\text{Ar}/^{39}\text{Ar}$ GEOCHRONOLOGY OF THE BODIE HILLS VOLCANIC FIELD

Sample	Longitude*	Latitude*	Rock type	Method	Mineral dated	Age†	Error (1σ)	MSWD	Notes
Trachyandesite of Masonic									
09-BA-7	-119.0873	38.3379	Trachyandesite lava	IH	Plagioclase	14.674	0.025	0.98	
088-22B	-119.0780	38.3794	Trachyandesite lava	IH	Plagioclase	14.07	0.08	4.9	
088-23F	-119.1170	38.3107	Trachyandesite lava	IH	Plagioclase	14.193	0.038	0.33	
08-BA-62	-119.0494	38.3201	Trachyandesite lava	IH	Plagioclase	14.13	0.031	0.26	
098-12B	-119.1814	38.3876	Trachyandesite lava	IH	Plagioclase	14.715	0.025	0.046	
098-12D	-119.1194	38.4000	Trachyandesite lava	IH	Plagioclase	14.590	0.02		
098-12F	-119.1142	38.3754	Trachyandesite lava	IH	Hornblende	14.094	0.017	0.7	
10-BA-15	-119.1157	38.3413	Pyroxene trachyandesite lava	IH	Plagioclase	14.140	0.017	0.78	
098-12E	-119.1240	38.3914	Trachyandesite dome	IH	Plagioclase	13.441	0.026	0.47	Late dome; locally altered
07-BA-38	-119.1450	38.3605	Trachyandesite dome	IH	Plagioclase	12.93	0.03	0.66	Lakeview Spring dome; post-alteration
Trachydacite of Rough Creek									
10-BA-6	-119.0247	38.3338	Porphyritic trachydacite flow	IH	Plagioclase	12.945	0.02	0.39	
Tuff of Jack Springs									
09-BA-23	-119.1749	38.1285	Porphyritic rhyolite ignimbrite	LF	Sanidine	12.044	0.016	0.107	Distally derived rhyolite ignimbrite
098-11A	-119.1695	38.1224	Porphyritic rhyolite ignimbrite	LF	Sanidine	12.069	0.015	0.044	Distally derived rhyolite ignimbrite
Trachyandesite of West Brawley Peak									
077-7G	-118.9667	38.2344	Porphyritic trachyandesite lava	IH	Plagioclase	11.32	0.03	1.02	
Trachyandesite of Clark Canyon									
09-BA-43	-119.1683	38.2636	Porphyritic andesite lava	IH	Plagioclase	11.27	0.11	4.6	
098-13D	-119.1606	38.2766	Porphyritic andesite plug	IH	Plagioclase	11.341	0.017	1.5	
Rhyolite of Del Monte Canyon									
077-9C	-118.9304	38.2766	Porphyritic rhyolite flow	LF	Sanidine	11.19	0.02	0.56	
077-9C	-118.9304	38.2766	Porphyritic rhyolite flow	IH	Plagioclase	11.26	0.14	6.3	
077-9D	-118.9280	38.2856	Porphyritic rhyolite flow	LF	Sanidine	11.14	0.02	0.96	
077-9D	-118.9280	38.2856	Porphyritic rhyolite flow	IH	Plagioclase	11.20	0.03	1.4	
Rhyolite of Aurora Creek									
10-BA-20	-118.9113	38.3168	Sparingly porphyritic rhyolite	IH	Plagioclase	11.177	0.013	0.66	Flow dome
10-BA-21	-118.8974	38.3032	Porphyritic rhyolite	LF	Sanidine	11.181	0.02	0.365	Flow dome
Dacite intrusions									
09-BA-35	-119.0464	38.2905	Porphyritic dacite plug	IH	Biotite	11.269	0.034	2.74	Intrusion into Masonic center debris flows
077-8B	-119.0562	38.2833	Porphyritic dacite plug	LF	Sanidine	11.16	0.03	0.84	Intrusion into Masonic center debris flows
Trachydacite of Bridgeport Canyon									
09SB020A	-119.1328	38.1323	Porphyritic trachydacite lava	IH	Plagioclase	11.080	0.019	0.9	
Andesite of Rancheria									
098-11B	-119.1713	38.1245	Andesite lava	IH	Plagioclase	11.067	0.022	1.7	Lava flow overlying tuff of Jack Springs and shown as part of Mount Biedeman center
Fletcher Valley sedimentary rocks									
08SB032	-118.9558	38.3456	Reworked air-fall tuff in sedimentary sequence	IH	Plagioclase	11.08	0.04	NA	
Trachyandesite of Del Monte									
077-9E	-118.9100	38.3191	Pyroxene andesite flow	IH	Plagioclase	10.95	0.03	0.59	
08SB-38	-118.9738	38.4083	Porphyritic trachydacite flow	IH	Biotite	10.98	0.05	3.60	
Trachydacite of Aurora Canyon									
077-8C	-119.0778	38.2715	Porphyritic trachydacite	LF	Sanidine	10.45	0.01	0.15	Flow dome
077-8C	-119.0778	38.2715	Porphyritic trachydacite	IH	Plagioclase	10.43	0.03	0.21	Flow dome
077-8C	-119.0778	38.2715	Porphyritic trachydacite	IH	Biotite	10.47	0.04	4.1	Flow dome
088-21A	-119.1396	38.2736	Porphyritic trachydacite	IH	Plagioclase	10.358	0.025	0.74	Flow dome
088-23A	-119.1002	38.2785	Porphyritic trachydacite	IH	Biotite	10.58	0.03	1.16	Flow dome; probable recoil
088-23A	-119.1002	38.2785	Porphyritic trachydacite	IH	Plagioclase	10.27	0.11	NA	Flow dome
088-23B	-119.0991	38.2783	Porphyritic trachydacite	IH	Biotite	10.54	0.05	2.26	Flow dome; probable recoil
088-23B	-119.0991	38.2783	Porphyritic trachydacite	IH	Plagioclase	10.31	0.02	0.78	Flow dome
088-23D	-119.1021	38.2811	Porphyritic trachydacite	IH	Biotite	10.46	0.032	2.07	Flow dome; probable recoil
088-23D	-119.1021	38.2811	Porphyritic trachydacite	IH	Plagioclase	10.265	0.05	0.66	Flow dome
088-25A	-119.0908	38.2732	Porphyritic trachydacite	IH	Plagioclase	10.43	0.03	NA	Flow dome
Rhyolite of Bodie Creek									
077-9B	-118.9506	38.2697	Sparingly porphyritic rhyolite	LF	Sanidine	10.16	0.03	0.355	Flow dome
Rhyolite of Bodie Hills									
09-BA-20	-119.0474	38.1566	Porphyritic rhyolite	LF	Sanidine	9.609	0.013	0.192	Flow dome
077-7D	-119.0998	38.1672	Porphyritic rhyolite	IH	Sanidine	9.86	0.01	0.54	Flow dome
077-7D	-119.0998	38.1672	Porphyritic rhyolite	LF	Plagioclase	9.86	0.03	0.47	Flow dome
088-21C	-119.0838	38.2513	Porphyritic rhyolite	LF	Sanidine	9.776	0.006	NA	Flow dome
088-21C	-119.0838	38.2513	Porphyritic rhyolite	IH	Biotite	9.824	0.046	0.49	Flow dome

(continued)

Bodie Hills volcanic field

TABLE 2. $^{40}\text{Ar}/^{39}\text{Ar}$ GEOCHRONOLOGY OF THE BODIE HILLS VOLCANIC FIELD (continued)

Sample	Longitude*	Latitude*	Rock type	Method	Mineral dated	Age†	Error (1 σ)	MSWD	Notes
<u>Rhyolite of Bodie Hills (continued)</u>									
088-21C	-119.0838	38.2513	Porphyritic rhyolite	LF	Plagioclase	9.806	0.019	0.668	Flow dome
088-21C	-119.0838	38.2513	Porphyritic rhyolite	IH	Plagioclase	9.740	0.023	1.02	Flow dome
088-21C	-119.0838	38.2513	Porphyritic rhyolite	IH	Biotite	9.776	0.017	0.95	Flow dome
08-BA-50	-119.0966	38.2482	Porphyritic rhyolite	LF	Sanidine	9.757	0.013	0.551	Flow dome
098-10B	-119.0838	38.2514	Porphyritic rhyolite	LF	Sanidine	9.771	0.003	5.12	Flow dome
098-13B	-119.1322	38.2680	Porphyritic rhyolite	LF	Sanidine	9.813	0.027	2.37	Flow dome
09-BA-47	-119.1382	38.2841	Porphyritic rhyolite	LF	Sanidine	9.877	0.013	0.152	Flow dome
<u>Rhyolite of Bald Peak</u>									
08-BA-65	-118.9506	38.2697	Glassy, nearly aphyric rhyolite	LF	Sanidine	9.69	0.013	0.616	Margin of flow dome
<u>Eureka Valley Tuff</u>									
09-BA-49	-119.0475	38.2639	Trachydacite ignimbrite	IH	Biotite	9.267	0.019	0.218	Upper member(?)
077-9A	-118.9744	38.2209	Glassy trachydacite ignimbrite	IH	Biotite	9.40	0.02	1.69	Upper member(?)
077-9A	-118.9744	38.2209	Glassy trachydacite ignimbrite	IH	Plagioclase	9.38	0.03	1.8	Upper member(?)
098-12A	-119.1992	38.3592	Lithic biotite trachydacite ignimbrite	IH	Plagioclase	9.45	0.03	NA	Maximum age (excess argon)
<u>Trachyandesite of Mt. Biederman</u>									
09SB015A	-119.1484	38.1231	Porphyritic trachyandesite lava	IH	Plagioclase	8.895	0.06	NA	
098-11E	-119.1584	38.1110	Hornblende andesite lava	IH	Plagioclase	9.019	0.028	0.75	
09-BA-22	-119.1797	38.1430	Pyroxene andesite flow	IH	Plagioclase	9.00	0.10	0.94	
<u>Dacite of Silver Hill</u>									
09-BA-26	-118.9834	38.1893	Block and ash flow	IH	Biotite	9.132	0.02	1.76	
077-7F	-118.9780	38.1732	Dacite	IH	Plagioclase	8.93	0.03	1.17	Late intrusion(?) into trachyandesite of Potato Peak
077-6F	-119.0085	38.1881	Hornblende dacite dome	IH	Plagioclase	9.09	0.03	0.69	Sugarloaf dome
08-BA-66	-119.0568	38.1863	Block and ash flow	IH	Plagioclase	9.07	0.024	0.76	
<u>Trachyandesite of Potato Peak</u>									
088-21B	-119.0750	38.2642	Porphyritic trachyandesite flow	IH	Plagioclase	8.84	0.13		Maximum age (excess argon)
088-21D	-119.0921	38.2433	Porphyritic trachyandesite flow	IH	Plagioclase	8.81	0.07	NA	
088-21E	-119.0858	38.2346	Porphyritic trachyandesite flow	IH	Plagioclase	8.86	0.05	0.23	
088-24C	-119.1121	38.2479	Porphyritic trachyandesite flow	IH	Plagioclase	8.996	0.025	1.2	
088-24D	-119.1038	38.2268	Porphyritic trachyandesite flow	IH	Plagioclase	9.09	0.04	NA	
088-24E	-119.1019	38.2181	Porphyritic trachyandesite flow	IH	Plagioclase	8.93	0.03	1.04	Total gas age; recoil
08-BA-68	-119.0684	38.1932	Porphyritic trachyandesite flow	IH	Plagioclase	8.99	0.02	0.067	
098-10C	-119.0920	38.2492	Porphyritic trachyandesite flow	IH	Plagioclase	8.982	0.023	0.68	
098-13C	-119.0922	38.2507	Porphyritic trachyandesite flow	IH	Plagioclase	8.998	0.021	1.4	
08-BA-61	-119.1017	38.2077	Block and ash flow	IH	Plagioclase	8.93	0.7	0.22	
<u>Trachyandesite of Willow Springs</u>									
077-7A	-119.1948	38.1786	Porphyritic trachyandesite	IH	Biotite	8.00	0.04	1.69	
077-7A	-119.1948	38.1786	Porphyritic trachyandesite	IH	Plagioclase	8.05	0.02	1.8	
077-7B	-119.1524	38.1918	Porphyritic trachyandesite	IH	Biotite	8.12	0.03	0.13	
077-7B	-119.1524	38.1918	Porphyritic trachyandesite	IH	Hornblende	8.07	0.02	0.44	
077-7B	-119.1524	38.1918	Porphyritic trachyandesite	IH	Plagioclase	8.09	0.03	NA	
088-24B	-119.1412	38.2550	Porphyritic trachyandesite	IH	Plagioclase	8.575	0.022	0.28	
088-24F	-119.0898	38.2018	Porphyritic trachyandesite	IH	Plagioclase	8.15	0.02	0.34	
<u>Rhyolite of Big Alkali</u>									
09-BA-42	-119.1489	38.2700	Rhyolite dome	IH	Biotite	5.455	0.026	0.41	
077-7C	-119.1583	38.1968	Dacite dome	IH	Plagioclase	5.48	0.02	0.73	
088-24A	-119.1395	38.2528	Porphyritic dacite dome	IH	Plagioclase	6.201	0.026	1.4	
098-13A	-119.1279	38.2575	Dacite dome	IH	Plagioclase	6.173	0.028	0.19	
<u>Hydrothermal alteration minerals</u>									
39509-3K	-119.2275	38.2079	Quartz-alunite alteration	IH	Alunite	8.169	0.013	1.4	Highway 395 alteration zone
077-6A	-119.0037	38.2149	Quartz vein	LF	Adularia	8.29	0.02	1.41	Standard Hill, Bodie
CC09-9D2	-119.1705	38.1987	Quartz-alunite alteration	IH	Alunite	8.68	0.02	1.3	Cinnabar Canyon
CC09-9D1	-119.1705	38.1987	Quartz-alunite alteration	IH	Alunite	8.82	0.29	0.68	Cinnabar Canyon
08-BA-46	-119.1039	38.2443	Quartz-alunite alteration	IH	Alunite	10.83	0.06	NA	Alta Plano mine, Potato Peak
PP09-10A1	-119.1384	38.2531	Quartz-alunite alteration	IH	Alunite	10.866	0.064	NA	Aurora Canyon alteration zone
AUR10-3	-118.8992	38.2375	Quartz-alunite alteration	IH	Alunite	11.954	0.016	0.48	East Brawley Peak alteration zone
088-22A	-119.1073	38.3673	Quartz-alunite alteration	IH	Alunite	13.018	0.06	1.01	Maybellie mine, Masonic
07-BA-40	-119.1161	38.3655	Quartz-alunite alteration	IH	Alunite	13.02	0.05	0.47	Pittsburgh-Liberty mine, Masonic; dump sample
MAS07-3	-119.1268	38.3597	Quartz-alunite alteration	IH	Alunite	13.26	0.05	0.32	Sarita mine, Masonic; dump sample
MAS10-55	-119.1026	38.4142	Quartz-alunite alteration	IH	Alunite	13.27	0.02	0.132	Red Wash alteration zone
MAS09-1	-119.1327	38.3578	Quartz-alunite alteration	IH	Alunite	13.32	0.14	NA	Red Rock mine area, Masonic
RW08-1	-119.1241	38.4112	Quartz-alunite alteration	IH	Alunite	13.338	0.035	0.72	Red Wash alteration zone
MAS09-1A	-119.1382	38.3585	Quartz-alunite alteration	IH	Alunite	13.37	0.11	6.9	Red Rock mine area, Masonic
MAS07-1A	-119.1483	38.3499	Quartz-alunite alteration	IH	Alunite	13.39	0.07	0.45	Chemung mine, Masonic

Note: IH—incremental heating; LF—laser fusion; NA—not applicable, total gas age; MSWD—mean square of weighted deviates.

*NAD27 (1927 North American Datum) coordinates.

†Relative to Fish Canyon Tuff sanidine = 28.02 Ma.

TABLE 3. SUMMARY OF PETROGRAPHIC CHARACTERISTICS FOR ROCKS OF THE BODIE HILLS VOLCANIC FIELD

Unit	Abundances							Total crystals	Color index	Maximum phenocryst size (mm)						Accessory minerals	
	Qz	Afs	Pl	Hbl	Bt	Pyx	OI	Opq		Qz	Afs	Pl	Hbl	Bt	Pyx		
Masonic	22	4	TR	3	TR	2	31	9	3.0	2.0	1.5	1.5	1.0	0.3	Ap		
Masonic domes	15	4	TR	4	TR	2	25	10	4.0	2.5	1.5	2.5	1.0	0.3	Ap		
Aurora	17	3		TR		1	21	4	2.5	2.0		1.5		0.3	(Ap)		
Rough Creek	TR	11	6	2	TR	TR	1	20	9	1.0	6.0	2.5	2.5	1.0	0.3	Ap, Zrn	
Clark Canyon		17	4	2	2		2	27	10		3.0	3.0	1.5	2.0	0.5	Ap	
West Brawley Peak	TR	11	5	2	2	TR	1	21	10	1.0	6.0	2.0	2.5	1.0	1.0	0.2	
Aurora Creek	TR	1	4	TR	TR	TR	1	6	1	2.0	1.5	2.0	2.5	1.0	1.0	(Ap, Ti)	
Del Monte Canyon	3	1	10	2	2	1	1	20	6	2.5	2.0	3.5	2.0	2.0		0.2	
Rock Springs Canyon		TR	TR	TR	TR		TR	TR	TR	0.5	0.5	0.5	0.2		0.1	(Zrn)	
Bridgeport Canyon		15	TR		1		1	17	2		6.0	0.5		2.0		0.5	Ap
Del Monte		17	2	3	2	TR	1	25	8		4.5	1.5	1.5	2.5	0.5	0.5	Ap
Aurora Canyon		14	4	2	1		1	22	8		4.5	1.5	1.5	2.5		0.3	Ap (Zrn)
Bodie Creek	4	2	5	TR	2		1	14	3	2.5	3.0	2.5	1.0	0.5		0.2	Ti (Ap, Zrn)
Bodie Hills	3	3	6	1	2		1	16	4	2.0	3.0	2.0	1.0	1.5		0.3	Ap, Ti, Zrn,
Bald Peak		TR	TR	TR	TR	TR	TR	TR	TR	1.0	1.5	1.5	0.5	0.5	0.5	0.4	—
Mount Biedeman		21	4	TR	3	TR	2	30	9		2.5	2.5	1.5	2.0	1.5	0.3	Ap
Silver Hill	TR	TR	14	6	2		1	23	9	1.0	2.0	3.0	2.0	1.5		0.3	Ap, Zrn (Ti)
Potato Peak		12	4	2			1	19	7		3.5	2.0	1.5			0.2	Ap (Zrn)
Willow Springs	TR	13	4	2	2	TR	1	22	9	0.5	4.5	2.0	1.5	2.0	1.0	0.2	Ap (Zrn)
Big Alkali	TR	TR	16	2	3		1	22	6	1.0	1.5	2.0	1.5	1.0		0.2	Ap, Ti (Zrn)

Note: Mineral abundances are microscopic estimates in volume percent relative to total rock. TR—trace. Qz—quartz; Afs—alkali feldspar; Pl—plagioclase; Hbl—hornblende; Bt—biotite; Pyx, pyroxene; OI—olivine; Opq—opaque Fe-Ti oxides. Maximum phenocrysts sizes, except opaque Fe-Ti oxides, rounded to the nearest 0.5 mm. Accessory minerals (less commonly observed minerals in parentheses): Aln—allanite; Ap—apatite; Ti—titanite; Zrn—zircon.

The Bodie Hills are within a rhomboid-shaped isostatic residual gravity anomaly that protrudes from the broad Sierra Nevada gravity low to the west (Fig. 6A). Isostatic residual gravity anomalies include free-air, Bouguer, and isostatic corrections (Simpson et al., 1986), so in principle, isostatic residual anomalies reflect density contrasts in the middle and upper crust and should not include significant topographic effects. The rhomboid-shaped isostatic residual gravity anomaly therefore suggests that the Bodie Hills is underlain by relatively low density crust. Most likely, this crust corresponds either to Mesozoic granitic rocks that cause the Sierra Nevada gravity anomaly (Fig. 5), or to Miocene intrusive rocks related to the Bodie Hills volcanic field. Gravity gradients within the rhomboid-shaped gravity low may reflect mid- to shallow-crustal structures that focused emplacement of intrusive bodies beneath the Bodie Hills. These structures are now completely concealed beneath Miocene and younger rocks, although several faults mapped in the Bodie Hills have similar orientations.

In contrast to the gravity anomalies, magnetic anomalies in the Bodie Hills (Fig. 6C) have high amplitudes and short wavelengths typical of unaltered volcanic rocks. Some magnetic anomalies are clearly related to individual volcanic edifices, notably Aurora Crater, Aurora Peak, West Brawley Peak, and Potato Peak. The negative magnetic anomaly directly over Aurora Peak indicates that this volcanic edifice formed mostly or entirely during a period of reversed magnetic polarity. Both andesitic (e.g., Aurora Peak) and dacitic

(e.g., Potato Peak) rocks are significantly magnetic. We use filtered versions of the magnetic anomaly map to infer the lateral extent of specific volcanic units.

MIocene MAGMATISM OF THE BODIE HILLS VOLCANIC FIELD

Magmatic activity in the Bodie Hills volcanic field spanned ~9 Ma, from ca. 14.7 to 5.5 Ma (Fig. 4; Table 2). Volcanic rocks erupted during this period are exposed over ~700 km² and may underlie a much larger area now covered by younger rocks and surficial deposits. The Bodie Hills volcanic field consists of at least 20 separate eruptive centers that include large trachyandesite stratovolcanoes and trachydacite flow dome complexes and small exogenous rhyolite intrusions (Table 1). These eruptive centers can be divided into four stages on the basis of age, composition, and eruptive rate (Figs. 3, 4, and 7): (1) early trachyandesite volcanism (ca. 14.7–12.9 Ma), (2) mixed trachyandesite-trachydacite-rhyolite volcanism (ca. 11.3–9.6 Ma), (3) climactic trachydacite volcanism (ca. 9.2–8.0 Ma), and (4) late rhyolite volcanism (ca. 6.2–5.5 Ma). Clastic sedimentary rocks were deposited around eruptive center margins during much of the Miocene volcanic activity, and the ca. 9.4 Ma Eureka Valley Tuff, which is inferred to have erupted from the Little Walker center ~20 km west of the Bodie Hills (Fig. 2), flowed in paleochannels carved around and across the eruptive centers and separates stages 2 and 3. Major eruptive episodes, their associated volcanic deposits, and the evolution of the Bodie

Hills volcanic field are described in the following sections.

To investigate magnetic anomalies caused by volcanic rocks in the Bodie Hills area, we used a matched filtering method to emphasize magnetic anomalies originating from volcanic depths. Matched filters exploit the fact that magnetic sources at different depths produce anomalies with different spectral properties (Syberg, 1972). In addition, volcanic rocks are typically more magnetic than overlying, younger sedimentary deposits and underlying pre-Tertiary basement and Tertiary intrusive rocks. The method assumes that crust is composed of horizontal layers with distinct magnetic properties, then estimates the depth to each layer by application of a best-fitting algorithm applied to the power spectrum of magnetic anomalies (Phillips, 2007). Best-fit layers (Fig. 8) were identified at depths of 0.2 and 1.9 km below the observation surface, the former presumably corresponding to Bodie Hills volcanic rocks, and the latter representing sub-volcanic lithologies, possibly shallow intrusive rocks with varying magnetic properties. With depths thus determined, matched filters were then designed and applied to observed magnetic anomalies to accentuate anomalies originating from those depths. Thus, the two maps in Figure 8 show magnetic anomalies filtered in order to enhance sources at 0.2 and 1.9 km depth, which we refer to as shallow-source and deep-source magnetic anomalies, respectively. Shallow-source anomalies (Fig. 8B) show distinct ovoid patterns that we interpret in terms of the four Bodie Hills volcanic field stages, as described in the following.

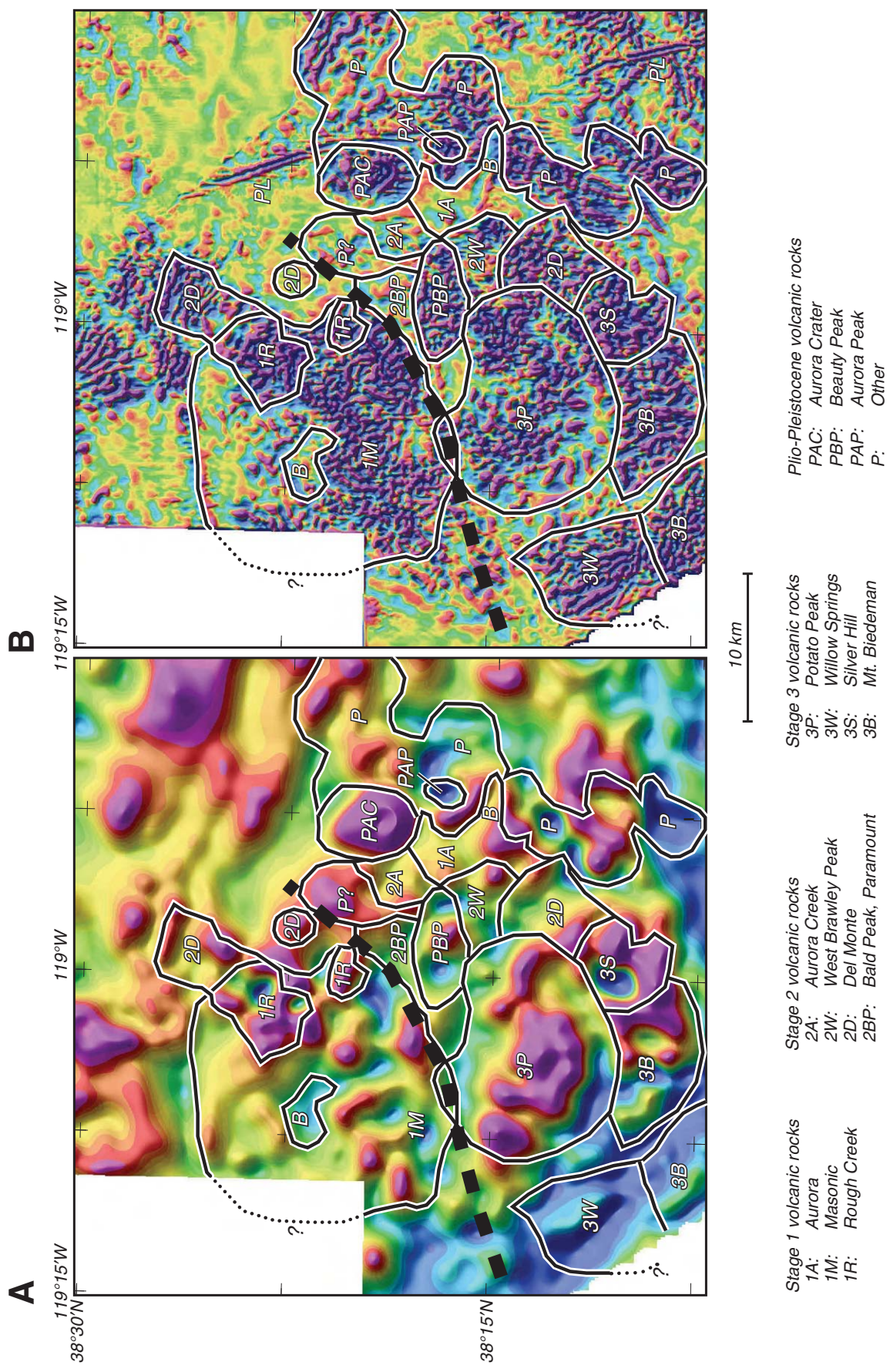


Figure 8. Filtered versions of the airborne magnetic data (U.S. Geological Survey, 2001). Filters were designed based on the spectral content of magnetic anomalies (Syberg, 1972; Phillips, 2007). (A) Magnetic anomalies filtered to emphasize deep (1.9 km depth) magnetic sources, presumably dominated by sources beneath the volcanic edifice. (B) Magnetic anomalies filtered in order to emphasize shallow (0.2 km depth) magnetic sources, which we interpret to represent Miocene and younger volcanic rocks. Black lines delineate the extent of volcanoes and their related rocks, interpreted from filtered magnetic anomalies and discussed in the text. See legend for identification of volcanic units. Bold black dashed line is geological and geophysical lineament discussed in text.

**Stage 1: Early Trachyandesite Volcanism:
The Masonic and Aurora Eruptive Centers
and the Rough Creek Dome Field
(ca. 14.7–12.9 Ma)**

Miocene magmatic activity in the Bodie Hills began ca. 14.7 Ma and was initially focused in the north and east, where relatively mafic rocks of the Masonic and Aurora centers were erupted onto Mesozoic basement rocks (Figs. 3 and 7A). Both centers likely formed stratovolcanoes that are now deeply eroded and partly covered by younger rocks and sediments. The hydrothermally altered northeast part of the Masonic center was intruded and overlain by trachydacites of Rough Creek dome field at the end of this stage.

Masonic Volcanic Center

The Masonic volcanic center in the northwestern part of the Bodie Hills forms the largest volcanic feature in the area. It spans ~16 km in diameter and covers ~200 km². A discontinuous, roughly circular pattern of magnetic anomalies (1M in Fig. 8B) surrounding the Masonic center suggests that its lateral extent may include a somewhat larger area, ~270 km². This volcanic center is bifurcated by a 1–2.5- km-wide, east-northeast-trending zone of Mesozoic basement rocks that underlie Masonic Mountain and areas east to the Homestead Mine (Figs. 7A and 9A).

The Masonic center is composed of thick sequences of trachyandesitic lava flows and volcaniclastic rocks, and small plugs and domes. The volcaniclastic rocks are mostly coarse debris flows (Fig. 9J) and include less abundant sedimentary rocks and minor block and ash deposits. Lava flows are more abundant near Masonic Mountain, whereas volcaniclastic rocks dominate more distal exposures. Small plugs and larger domes are common locally (Fig. 9E), notably the Lakeview porphyry on the north side of Masonic Mountain. Volcaniclastic rocks of the Masonic center generally dip northward on the north side of Masonic Mountain and southward on its south side, consistent with a vent location near the present Masonic Mountain (Fig. 9A).

Most Masonic lava flows and intrusive rocks are porphyritic, contain fine- to medium-grained phenocrysts of plagioclase and clinopyroxene ± hornblende (Table 3), and are composed of trachyandesite and basaltic trachyandesite (Fig. 10). Most late Masonic domes on the north side of Masonic Mountain are abundantly and coarsely porphyritic. Plagioclase $^{40}\text{Ar}/^{39}\text{Ar}$ ages from 8 lava flows throughout the volcano range from ca. 14.7 to 14.1 Ma, whereas two domes that intrude the lava flows and volcaniclastic rocks on the

north side of Masonic Mountain yield younger ages of ca. 13.4 and 12.9 Ma (Table 2).

Coarse, locally derived debris flows and interbedded volcaniclastic sedimentary rocks are most abundant on the north and south sides of the Masonic center, suggesting that it formed a stratovolcano with the greatest topographic relief near Masonic Mountain. Field relationships and radiometric dates suggest formation of the main volcano between ca. 14.7 and 14 Ma, followed by significant erosion and faulting along northeast- and north-striking faults that channelized hydrothermal fluids and

later juxtaposed unaltered Mesozoic basement rocks at Masonic Mountain against hydrothermally altered Masonic center rocks. Extensive hydrothermal alteration on the north side of the volcano between ca. 13.4 and 13.0 Ma likely is related to 13.4–12.9 Ma porphyritic trachyandesite dome emplacement.

Within the northern part of the Masonic center a subdued magnetic anomaly (1M in Fig. 8B) may be attributed to a thickened section of weakly magnetic debris flows and volcaniclastic sedimentary rocks and/or pervasive hydrothermal alteration.

→

Figure 9 (on following three pages). Photographs of volcanoes, volcanic features, and rocks in the Bodie Hills volcanic field. (A) Panorama looking northeast at the southeast part of Masonic stratovolcano, which consists mostly of interbedded trachyandesite lava flows and debris flows that dip gently south or southeast. Light colored rocks forming Masonic Mountain are Cretaceous granite, which have been uplifted relative to the Masonic rocks along a northeast-striking fault near the base of Masonic Mountain. Field of view across the Masonic volcano is ~6 km. Rocks in the foreground are trachyandesite lava flows from the Potato Peak dome field. (B) Panorama looking south of West Brawley Peak volcano, which consists of a trachyandesite plug that forms West Brawley Peak and trachyandesite lava flows that dip away from it. Photo is about 4 km across. (C) Panorama looking north at a large dome of trachydacite of Rough Creek overlain by Eureka Valley Tuff (EVT), which flowed in a paleochannel that passes behind the Rough Creek dome. Dome is ~2 km wide. (D) Panorama looking south at the north side of the Potato Peak dome complex showing a series of onlapping trachyandesite lava flows with pronounced rubbly, brecciated flow fronts. Photo is about 5 km across. (E) Small, columnar-jointed trachyandesite(?) plug intruding debris flows in the eastern part of Masonic stratovolcano. Plug is about 150 m wide. (F) Flow ramp in trachyandesite lava flow of West Brawley Peak volcano. Flow traveled from left to right in photo. Note person (circled) for scale. (G) View looking north from Mount Biedeman toward Potato Peak (PP). Mount Biedeman is underlain by a platy-jointed trachyandesite intrusion that probably filled a vent for the Mount Biedeman stratovolcano. The south side of the Potato Peak massif is composed of massive, flow-banded trachyandesite of Potato Peak that probably is mostly intrusive. The low area between Mount Biedeman and Potato Peak is underlain mostly by coarse debris flows derived from the two centers. Skyline is about 10 km wide. (H) View looking south at Bald Peak. Bald Peak forms a circular rhyolite dome ~1 km in diameter with lava flows and bedded tuffs (white rocks in foreground) that extend outward from the dome on its east, north, and west sides. (I) View of the east side of Potato Peak, a small volcanic neck, surrounded by outward-dipping lava flows of trachyandesite of Potato Peak that have prominent flow fronts (cf. D). I is about 1.5 km wide. (J) Glassy, flow-banded, platy-jointed rhyolite dome of Big Alkali intruding early Paleozoic argillites (Pz) at the mouth of Cinnabar Canyon. Base of photo is about 100 m wide. (K) Debris flow in the Masonic stratovolcano consisting of blocks of trachyandesite of Masonic as much as 3 m in maximum dimension in an unsorted cobble to sand matrix. Hammer handle is ~55 cm long. (L) Well-bedded air-fall tuff and lithic tuff underlying the rhyolite of Del Monte Canyon. Hammer handle is ~55 cm long. (M) Silicified, monolithic, clast-supported carapace breccia in dacite of Silver Hill on the northeast side of Bodie Bluff. Hammer handle is ~55 cm long. (N) Glassy, prismatically jointed, coarsely porphyritic trachyandesite of Potato Peak from the summit of Potato Peak. Hammer handle is ~55 cm long. (O) Block and ash flow in the trachyandesite of Potato Peak. Rock is composed of homogeneous blocks of porphyritic trachyandesite in matrix of white ash. Hammer handle is ~45 cm long. (P) Comingled magma near Mount Biedeman. Rock consists of rounded and locally flattened, partly disaggregated hornblende pyroxene trachyandesite in matrix of quartz-rich rhyolite of Bodie Hills. Mingled magmas are exposed in at least four localities surrounding Mount Biedeman (Fig. 7B). Magnet is 12 cm long.

Bodie Hills volcanic field

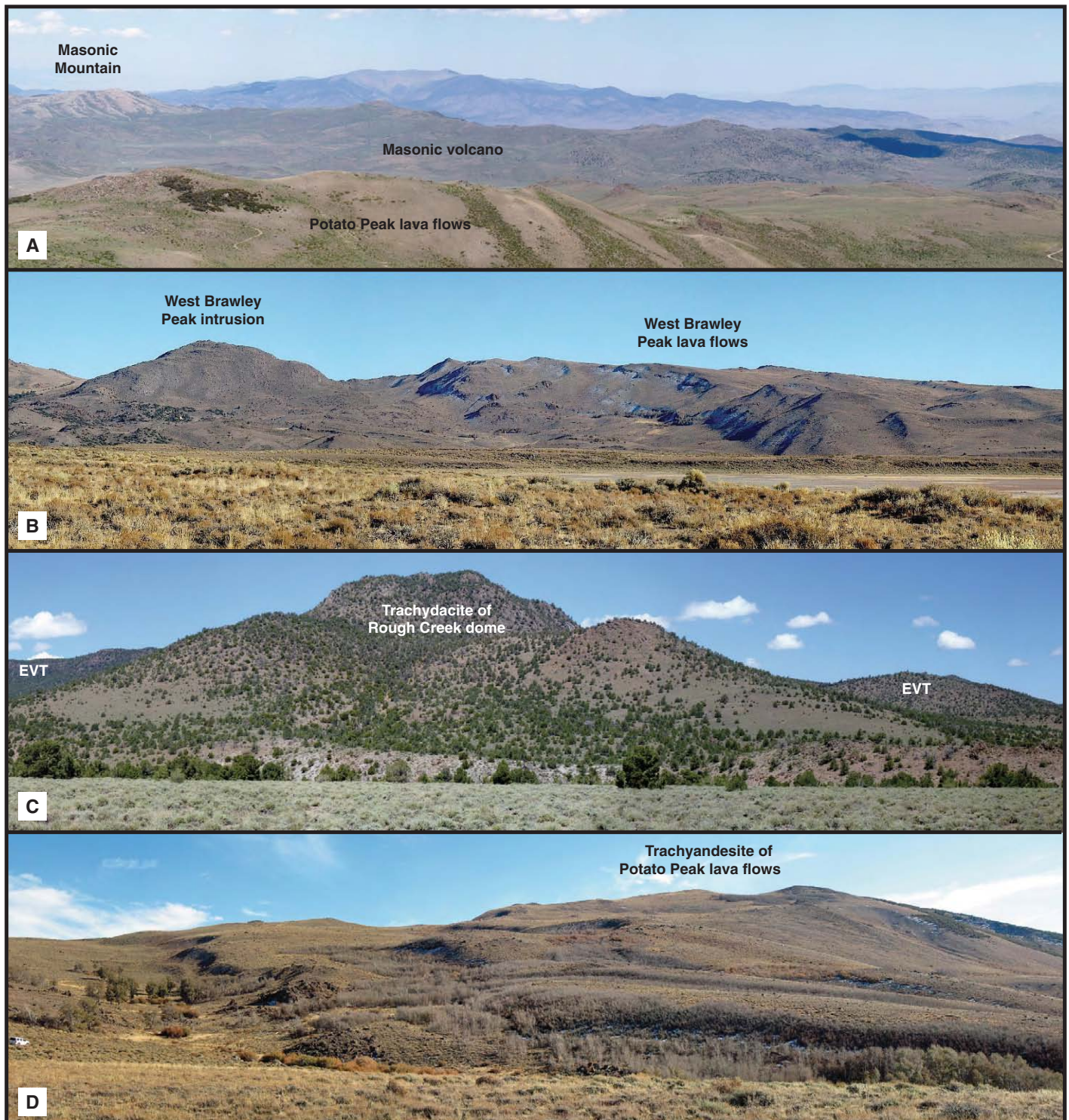


Figure 9.

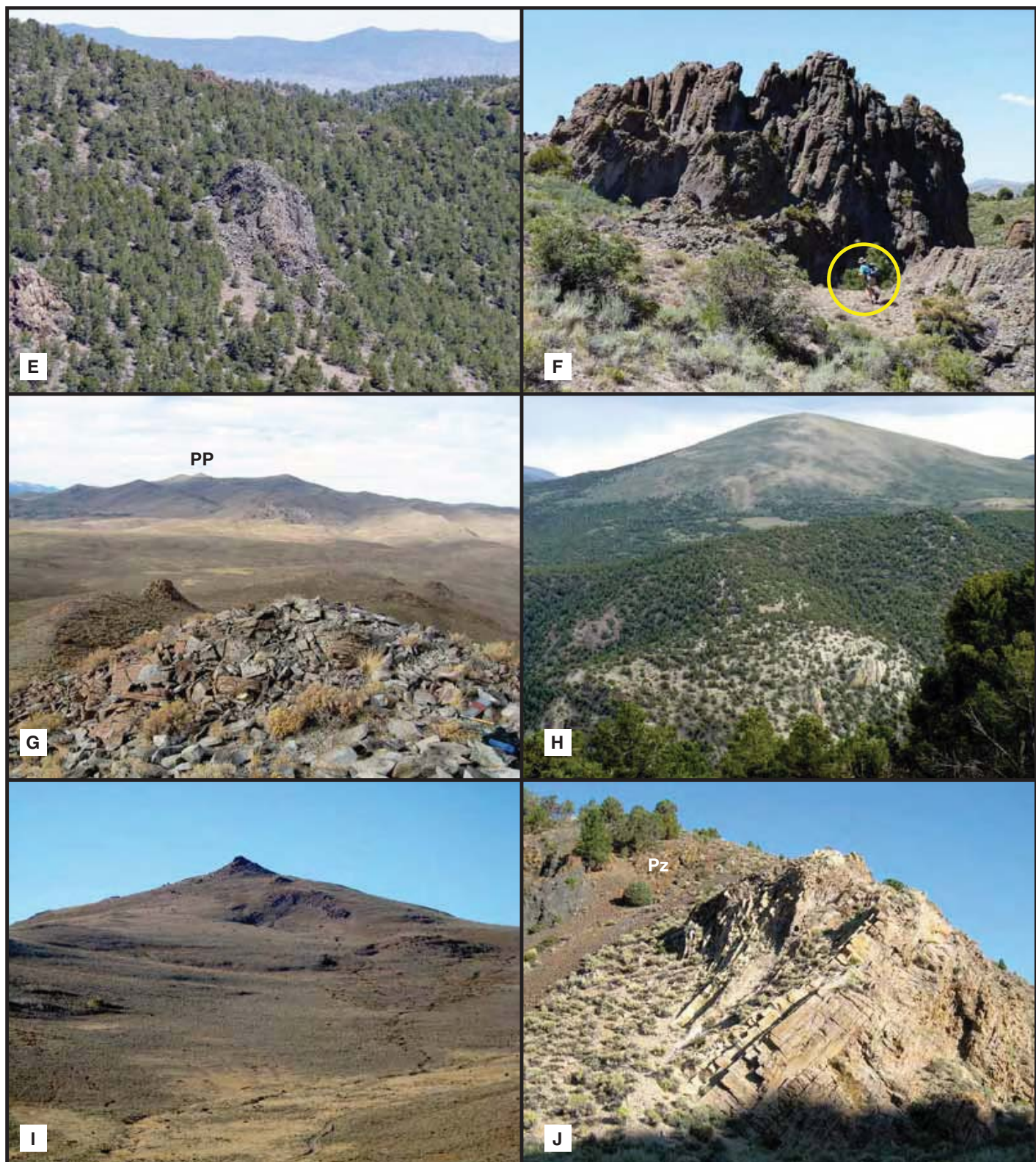


Figure 9 (continued).

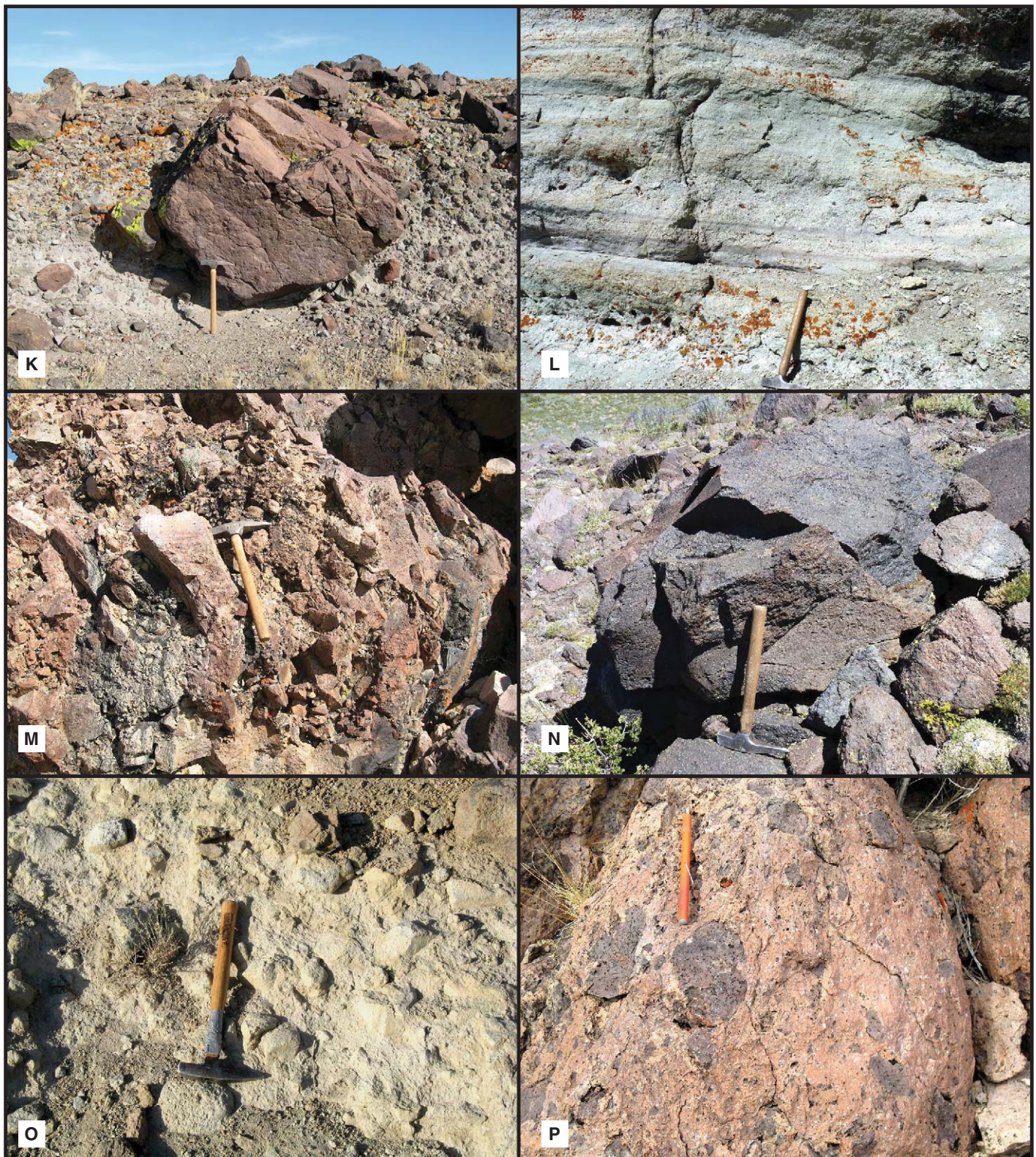


Figure 9 (continued).

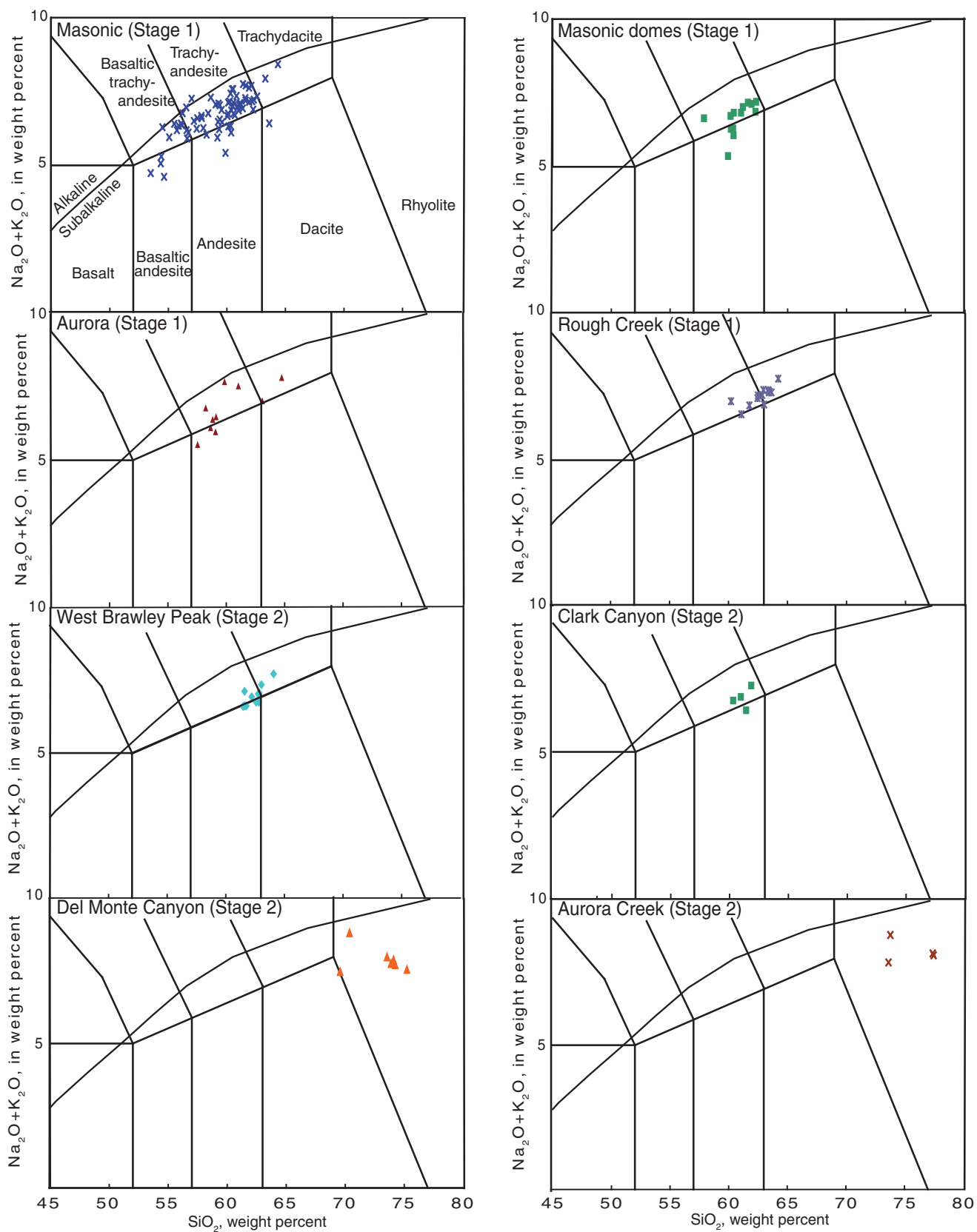


Figure 10 (on this and following two pages). Total alkali-silica variation diagram showing compositions of rocks of Bodie Hills volcanic field by unit. Diagrams are arranged from oldest to youngest unit (Tables 1 and 2). Field boundaries are from Le Bas et al. (1986). Alkaline-subalkaline boundary is from Irvine and Baragar (1971).

Bodie Hills volcanic field

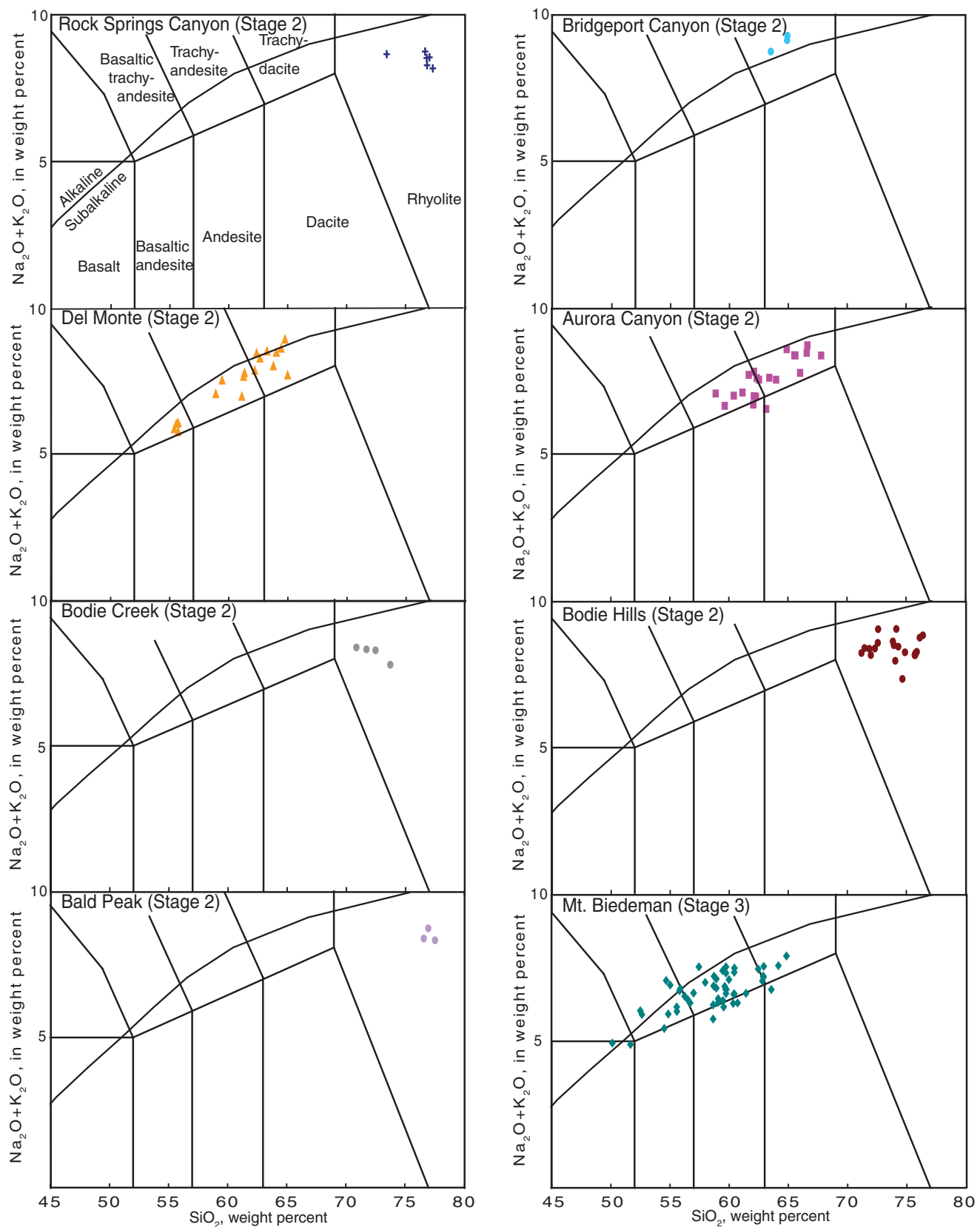


Figure 10 (continued).

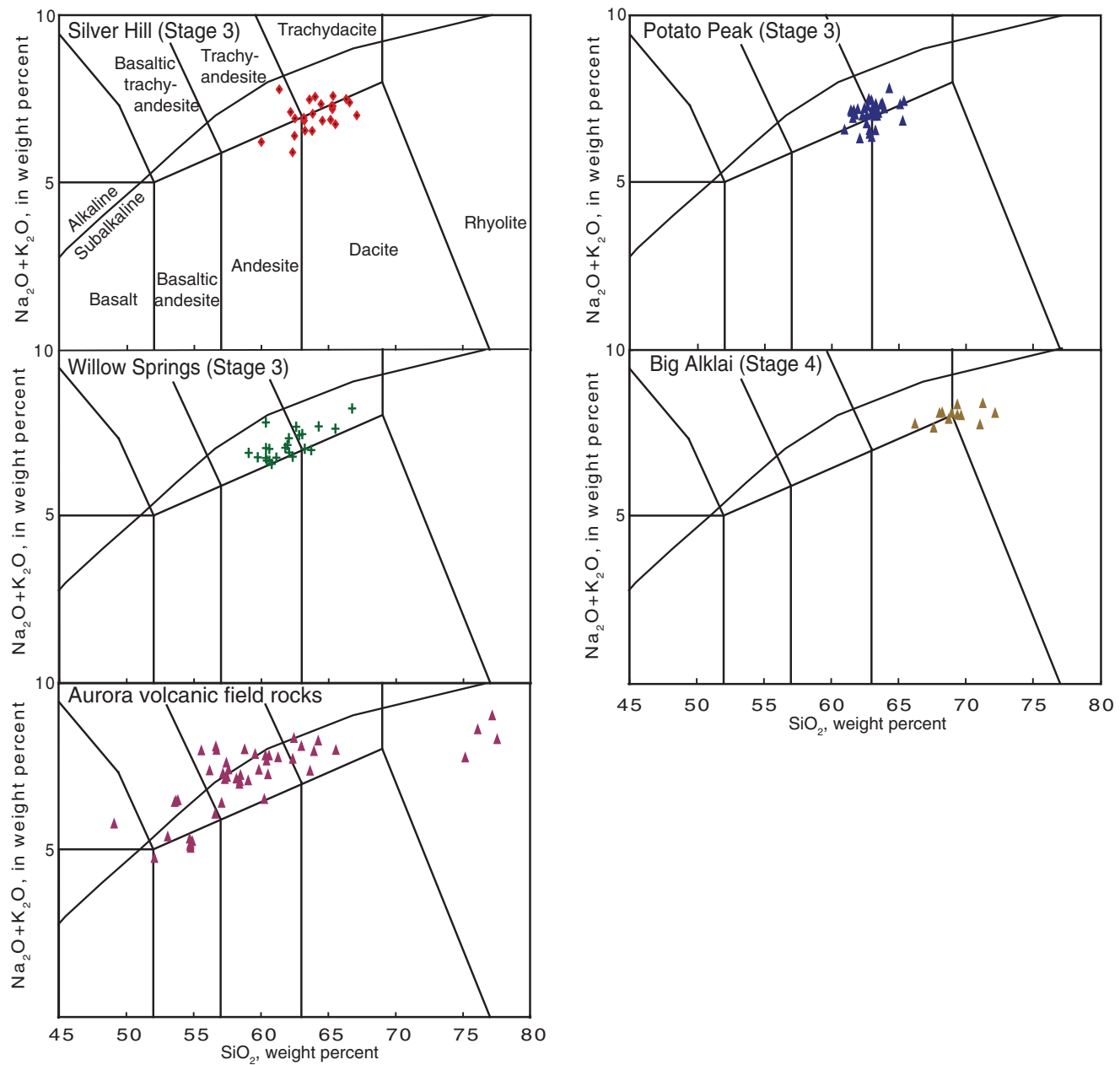


Figure 10 (continued).

Aurora Volcanic Center

The Aurora volcanic center (Fig. 7A) forms the easternmost exposed Miocene volcanic center in the Bodie Hills and includes the primary host rocks for epithermal gold-silver vein deposits in the Aurora district. The Aurora center consists of lava flows, tuff breccia, debris flows, shallow intrusions, and minor volcaniclastic rocks. Most of these rocks are porphyritic and contain 1–5 mm phenocrysts of plagioclase and hornblende ± clinopyroxene (Table 3). The size of horn-

blende phenocrysts is highly variable; some are as long as 3 cm. Most analyzed rocks at Aurora are composed of trachyandesite, although nearly pervasive hydrothermal alteration now obscures primary magmatic composition of most rocks. Hydrothermal alteration also has hindered dating these rocks; hornblende from two lava flows yielded identical $^{40}\text{Ar}/^{39}\text{Ar}$ ages of 13.05 Ma (L. Snee, 2002, written commun.), although 3 published K-Ar ages range from 15.8 to 13.9 Ma (Silberman and McKee, 1972). Shallow-source magnetic

anomalies (1A in Fig. 8B) are subdued over exposures of the Aurora center, probably reflecting pervasive hydrothermal alteration of these rocks.

The presence of abundant debris flows interbedded with lava flows and interspersed with numerous small intrusions suggests that the Aurora center also may have formed a stratovolcano. Younger volcanic rocks, including extensive Pliocene–Pleistocene lava flows, probably cover much of the Aurora center, concealing its full extent.

Rough Creek Trachydacite Domes

The trachydacite of Rough Creek consists of coarsely porphyritic biotite-hornblende-plagioclase trachydacite and trachyandesite flow domes and minor pyroclastic deposits in the northeast corner of the Bodie Hills. Exposed domes occupy an area covering 20 km² that extends 7 km from Cow Camp Creek north to near the Elbow on the East Walker River (Fig. 7A). The lateral extent of the trachydacite of Rough Creek is well expressed by shallow-source magnetic anomalies (2R in Fig. 8B). The trachydacite of Rough Creek is ca. 12.95 Ma (Table 2) and overlies hydrothermally altered Masonic center rocks south of the Elbow and along Red Wash Creek.

Stage 2: Mixed Trachyandesite-Trachydacite-Rhyolite Volcanism (ca. 11.3–9.6 Ma)

Volcanism resumed ca. 11.3 Ma in the Bodie Hills after an apparent hiatus of ~1.5 Ma, shifting to diverse and mostly more silicic compositions that erupted along margins of the earlier centers (Figs. 3 and 7B). Volcanic rocks and eruptive centers formed during this period include (1) the trachyandesitic West Brawley Peak volcano, (2) rhyolite flow domes in Bodie and Aurora Creeks, in Del Monte Canyon, in Rock Springs Canyon, at Bald Peak, and across the west side of the Bodie Hills, (3) trachyandesite and trachydacite flow domes in Aurora and Bridgeport Canyons, and (4) trachyandesite and basaltic trachyandesite lava flows and breccias along the northeast side and in the southwest corner of the Bodie Hills. The small Paramount basin (Fig. 7B) also formed near the end of this period of volcanism and was partly filled with detritus from the Bald Peak dome. Volcanic rocks of stage 2 produce variable magnetic anomaly patterns (2A, 2W, 2D in Fig. 8).

West Brawley Peak Volcano

The 11.3 Ma West Brawley Peak volcano is a small composite cone on the southwest margin of the Aurora center (Fig. 7B). A plug of vertically flow-banded trachyandesite, apparently a feeder to flows, forms West Brawley Peak. This plug is surrounded on its south, west and north sides by thick sequences of outward-dipping lava flows (Figs. 9B, 9H). Resistant ledges of quartz-alunite altered Aurora andesite form the east flank of the volcano. A small but pronounced positive magnetic anomaly (Fig. 6B) directly over the trachyandesite plug suggests that these rocks are normally magnetized. Most rocks associated with the West Brawley Peak volcano are coarsely porphyritic trachydacite and trachyandesite lavas (Fig. 10) containing abundant

tabular plagioclase phenocrysts as long 2 cm and less abundant phenocrysts of hornblende, biotite, and minor clinopyroxene (Table 3).

Trachyandesite of Clark Canyon

The 11.3 Ma trachyandesite of Clark Canyon forms seven small plugs and a lava flow of moderately porphyritic hornblende-clinopyroxene-plagioclase andesite that intrude and overlie hydrothermally altered Masonic center debris flows on the southwest side of Aurora Canyon (Fig. 7B). The plugs are aligned in an east-northeast orientation.

Trachyandesite of Rancheria

A small volcanic center is inferred in the area adjacent to and east of U.S. 395, along the western margin of the trachyandesite of Mount Biedeman (Fig. 7C). In this area, coarse debris flows and less abundant lava flows of pyroxene-hornblende trachyandesite and basaltic trachyandesite locally overlie pre-Tertiary basement rocks, apparently are interleaved with the distally sourced, ca. 12 Ma tuff of Jack Springs, and underlie the ca. 9.4 Ma Eureka Valley Tuff. Chesterman and Gray (1975) identified these rocks as the Rancheria Tuff Breccia. A ⁴⁰Ar/³⁹Ar age of 11.07 Ma (Table 2) contrasts with somewhat older K-Ar ages of 13.8 and 11.6 Ma (Kleinhampl et al., 1975). These rocks are laterally continuous with, and compositionally and petrographically similar to, rocks erupted from the ca. 9.2–8.9 Ma Mount Biedeman stratovolcano (Fig. 10; Table 3; see following stage 3 discussion). Given their lack of diagnostic petrographic and geochemical features, distinguishing older Rancheria rocks from those of the Mount Biedeman volcanic center has not been possible. Consequently, the Rancheria rocks are provisionally included with those associated with the Mount Biedeman center (Fig. 7C).

Rhyolite Domes in Bodie and Aurora Creeks and Del Monte Canyon

Rhyolite flow domes and associated pyroclastic rocks crop out across the north end of the Aurora mining district, in Aurora and Bodie Creeks, and in Del Monte Canyon (Fig. 7B). We divided these rhyolitic rocks into three units, the rhyolites of Aurora Creek, Del Monte Canyon, and Bodie Creek, on the basis of their ages, petrographic characteristics, and geographic distribution.

The 11.2 Ma rhyolite of Aurora Creek forms a series of flow domes and related pyroclastic rocks on the north side of the Aurora mining district (Fig. 7B). Much of this rhyolite is hydrothermally altered; locally, it hosts epithermal gold-silver vein deposits in the Aurora district.

Endogenous domes and lava flows are mostly flow banded and sparsely porphyritic, containing phenocrysts of quartz, sanidine, plagioclase, and biotite (Table 3). Lithic-rich tuffs mantle the margins of domes.

The 11.2–11.1 Ma rhyolite of Del Monte Canyon consists of lava flows and associated pyroclastic deposits that overlie lava flows of the trachyandesite of West Brawley Peak on the north side of West Brawley Peak and in Del Monte Canyon. This coarsely porphyritic rhyolite contains plagioclase, hornblende, biotite, and minor sanidine and rounded quartz phenocrysts (Table 3). Well-bedded, lithic-rich rhyolite tuffs locally underlie the lava flows (Fig. 9L).

The 10.2 Ma rhyolite of Bodie Creek forms several small flow domes that intrude and overlie the andesite of Del Monte Canyon on the north side of Bodie Creek southwest and east of Beauty Peak (Fig. 7B). These rhyolites are largely covered by lava flows erupted from the Pliocene Beauty Peak volcano. The Bodie Creek rhyolites contain moderate amounts of fine- to medium-grained biotite, plagioclase, sanidine, and quartz phenocrysts (Table 3).

Trachydacite of Bridgeport Canyon

The 11.1 Ma trachydacite of Bridgeport Canyon forms small domes and lava flows of coarsely porphyritic, plagioclase-rich rock that were emplaced on Paleozoic basement rocks in Bridgeport Canyon and were overlain by debris flows related to the Mount Biedeman center. These lavas are notably K rich, and compositionally and petrographically resemble the Table Mountain Latite erupted from the Little Walker center and from near Sonora Pass, but they are ~1 Ma older (Putirka and Busby, 2007; C.J. Busby, 2011, written commun.).

Trachyandesite of Del Monte

The trachyandesite of Del Monte is a heterogeneous sequence of lava flows, flow breccias, debris flows, and lesser volcaniclastic sedimentary rocks that crop out discontinuously for ~13 km on the east side of the Bodie Hills volcanic field. There are four principal exposures: in upper and lower Bodie Creek, in Rough Creek, and near the Elbow (Fig. 7B). The northern three exposures are composed mostly of lava flows, flow breccias, and coarse, relatively homogeneous andesite debris flows, whereas the southwestern exposure also contains debris flows with more heterogeneous clast compositions and abundant interbedded volcaniclastic sedimentary rocks. The ⁴⁰Ar/³⁹Ar ages of lava flows from near the Elbow and near the mouth of Bodie Creek are nearly identical, ca. 11.0 Ma (Table 2). The distribution, lithologic characteristics, and a pronounced aeromagnetic high east

of Homestead Mine (2D in Fig. 8A) suggest multiple sources, including near the north end of the West Brawley Peak volcano, in Rough Creek, and beneath Miocene sedimentary rocks east of the Homestead Mine.

Rock Springs Canyon Rhyolite Domes

The rhyolite of Rock Springs Canyon forms two domes straddling the crest of the central Bodie Hills (Fig. 7B). The two bulbous lobes intrude rocks of the Masonic center and are overlain by the trachydacite of Aurora Canyon, the rhyolite of the Bodie Hills, and the Eureka Valley Tuff. The rhyolite is commonly flow banded and nearly aphyric. Zones of black obsidian are present locally; elsewhere the rhyolite is completely devitrified. The rhyolite of Rock Springs has not been directly dated; stratigraphic relations suggest that it was emplaced ca. 11 Ma.

Aurora Canyon Trachydacite Domes

The 10.6–10.3 Ma trachydacite of Aurora Canyon forms a series of flow domes that discontinuously outline a semicircle ~12 km in diameter extending counterclockwise from Aurora Canyon to the east side of Masonic Mountain (Fig. 7B). This unit is composed of trachydacite and trachyandesite that contain 15%–30% phenocrysts of plagioclase, hornblende, biotite, and minor clinopyroxene in a glassy groundmass (Table 3). Coarse block and ash deposits and carapace breccias are preserved locally along the margins of some domes.

Bodie Hills Rhyolite Domes

The 9.9–9.6 Ma rhyolite of the Bodie Hills forms a northwest-trending series of porphyritic exogenous domes on the west side of the Bodie Hills that are discontinuously exposed for ~20 km from just north of Mono Lake to near Rock Springs Canyon (Fig. 7B). The largest domes are on the northwest and southeast periphery of Mount Biedeman and on the north side of Potato Peak. These rhyolites generally contain 15%–20% phenocrysts of plagioclase, sanidine, quartz, biotite, and hornblende (Table 3). Carapace breccias on domes are common; external to domes the flows commonly have coarse basal breccias. Quartz-rich rhyolite comingled with abundant hornblende andesite blobs form several distinctive outcrops around Mount Biedeman (Figs. 7B and 9P).

Bald Peak Rhyolite Dome, Tuff of Paramount, and the Paramount Basin

Bald Peak (Figs. 7B and 9H) is a prominent ca. 9.7 Ma rhyolite flow dome exposed in the east-central part of the Bodie Hills, where it is draped by Pliocene andesite lava flows erupted from the Beauty Peak shield volcano. The

Bald Peak dome is flanked on its west, north, and east sides by the tuff of Paramount, rhyolite tuffs and volcaniclastic deposits that likely erupted from the Bald Peak dome and fill the shallow, northeast-elongated Paramount basin to the southwest. The rhyolite of Bald Peak is nearly aphyric, containing only trace amounts of sanidine, plagioclase, and biotite phenocrysts (Table 3). The tuff of Paramount varies from an unwelded pumice-rich, nearly aphyric tuff similar in appearance to the rhyolite of Bald Peak to lithic-rich tuff with abundant clasts of porphyritic dacite and andesite and nearly aphyric rhyolite. Sandstone and conglomerate are interbedded in the tuff of Paramount; their abundances increase from Bald Peak southwest to near Paramount. Silica sinter is widespread in the upper parts of the sedimentary rock sequence (Fig. 11E), and most of the tuff and related sedimentary rocks are pervasively hydrothermally altered. Unaltered ca. 9.4 Ma Eureka Valley Tuff commonly overlies hydrothermally altered tuff and sedimentary rocks.

Shallow-source magnetic anomalies over the Bald Peak rhyolite dome and Paramount basin (2BP in Fig. 8B) contrast markedly with neighboring anomalies likely associated with rocks of the Masonic volcanic center (1M in Fig. 8B) and Pliocene Beauty Peak volcano (PPB in Fig. 8B). The subdued nature of Bald Peak magnetic anomalies is consistent with extensive hydrothermal alteration of Paramount basin sediments and the high-silica rhyolite (nonmagnetic) composition of the Bald Peak dome. Deep-source magnetic anomalies (Fig. 8A), as discussed in the following, suggest that rhyolite of Bald Peak may underlie Pliocene andesite flows northwest of Beauty Peak.

Eureka Valley Tuff

The ca. 9.4 Ma Eureka Valley Tuff is a K-rich trachydacitic ash-flow tuff erupted from the Little Walker center ~20 km northwest of the Bodie Hills (Fig. 2; Noble et al., 1974; Priest, 1979). It flowed across the Bodie Hills through Miocene paleochannels and forms an important regional stratigraphic and structural marker in the area (Fig. 7E). The Eureka Valley Tuff is composed of three members, the Tollhouse Flat, By-Day, and Upper Members, distinguished by their phenocryst assemblages and paleomagnetic properties (Noble et al., 1974; King et al., 2007; Pluhar et al., 2009). Based on abundant biotite phenocrysts, the Tollhouse Flat Member seems to be the most widely exposed member in the Bodie Hills, although all three members are exposed on the west side of the Bodie Hills near Bridgeport reservoir, and more than one member is pres-

ent in major paleochannels within the Bodie Hills. Two samples of the Upper(?)Member collected in the center of the Bodie Hills yielded $^{40}\text{Ar}/^{39}\text{Ar}$ ages of 9.27–9.40 Ma and a third sample collected just north of Bridgeport Reservoir yielded a maximum age of 9.45 Ma (Table 2). These ages are similar to preferred $^{40}\text{Ar}/^{39}\text{Ar}$ ages for the Upper and By-Day Members reported by Pluhar et al. (2009).

In most exposures in the Bodie Hills, the Eureka Valley Tuff is a black to dark brown, densely welded vitrophyre with strongly flattened pumice blocks as long as 30 cm. Within major channels, compaction foliation is mostly subhorizontal, but in smaller channels and in isolated exposures, foliation commonly has variable but locally steep dips where the tuff banked against and conformed to channel walls. In the Bodie Hills, the Eureka Valley Tuff is locally underlain by poorly exposed, coarse conglomerates that contain well-rounded cobbles, including granitic rocks likely sourced beyond the Bodie Hills (Fig. 7E).

Stage 3: Climactic Trachyandesite-Dacite Volcanism (ca. 9.2–8.0 Ma)

Miocene magmatic activity climaxed with formation of the trachyandesitic Mount Biedeman stratovolcano in the southwest part of the Bodie Hills and emplacement of three large silicic trachyandesite to dacite flow dome complexes, the Silver Hill, Potato Peak, and Willow Springs, between ca. 9.2 and 8 Ma (Fig. 7C). Each dome complex is composed of numerous domes, lava flows, and related pyroclastic rocks and debris flows that form the core and highest parts of the Bodie Hills; together these rocks are exposed over >240 km².

Mount Biedeman Stratovolcano

The Mount Biedeman eruptive center is an eroded trachyandesite stratovolcano centered on Mount Biedeman (Fig. 7B). Mount Biedeman is composed of a platy jointed trachyandesite intrusion that probably filled a major vent (Fig. 9G). Extrusive rocks of the Mount Biedeman volcano consist of an inner zone ~5 km in diameter dominantly composed of lava flows and an outer zone dominantly composed of debris flows. Debris flow deposits associated with the Mount Biedeman volcano are asymmetrically distributed around the central intrusion; they extend ~15 km to the northwest and 8–10 km to the west and southwest, but only ~6 km to the south and east; the north side is mostly covered by deposits from the Potato Peak center. Distal deposits to the northwest are notably more distinctly sorted and bedded than in more proximal deposits.

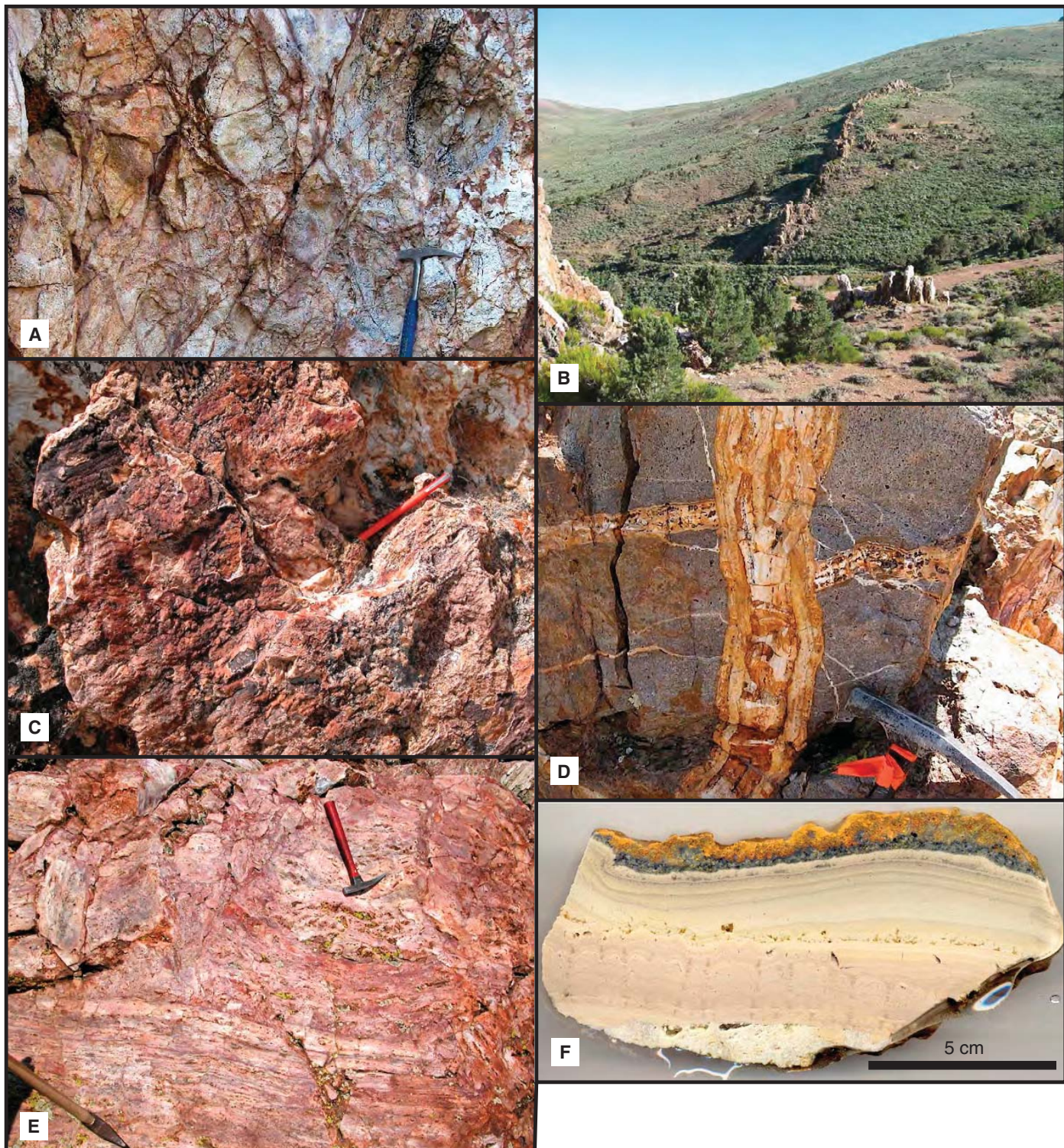


Figure 11. Photographs showing features of Miocene hydrothermal systems in the Bodie Hills. (A) Conjugate set of steep N10°E and N60°E, vuggy hematite seams and hairline quartz veins with right-slip and left-slip offsets, respectively, in altered andesite at the Maybelle mine in the Masonic district. Hammer handle is 42 cm long. (B) View looking south at north-south to N15°E trending Esmeralda vein in the Aurora district. Quartz-carbonate vein is as much as 20 m wide. (C) Surface of the Esmeralda vein showing moderately dipping slickensides that indicate right-oblique slip. Magnet is 12 cm long. (D) Small banded quartz vein filling normal fault in Bodie district. Hammer head is 20 cm long. (E) Brecciated sinter at Paramount. Angular blocks of sinter are recemented by hematite-rich quartz. Hammer is ~34 cm long. (F) Intricately banded hydrothermal sediments from the Sarita mine, Masonic district. White to beige layers composed of chalcedony are overlain by dark gray layer of enargite (Cu-As sulfide) covered with open-space filling Fe-oxides that probably replace pyrite.

Most Mount Biedeman rocks are trachyandesite or basaltic trachyandesite (Fig. 10) that contain 15%–40% phenocrysts of plagioclase, clinopyroxene, and hornblende (Table 3). The $^{40}\text{Ar}/^{39}\text{Ar}$ ages for lava flows in the west part of the volcano are 9.2–8.9 Ma (Table 2; L. Snee, 2001, written commun.), somewhat younger than the published 9.5–9.8 Ma K-Ar ages for andesite lava flows near Mount Biedeman (Silberman and Chesterman, 1972).

The Mount Biedeman eruptive center is well expressed by shallow-source magnetic anomalies (3B in Fig. 8B). The lateral extent of this magnetic pattern agrees closely with mapped exposures of trachyandesite lava flows, intrusions, and debris flows. Deep-source magnetic anomalies (Fig. 8A) exhibit high amplitudes over the eastern parts of the Mount Biedeman eruptive center, possibly indicative of underlying mafic intrusive rocks and suggesting that the source of Mount Biedeman volcanism is east of the present landform of Mount Biedeman. Two mapped areas of Mount Biedeman volcanic rocks are separated by a region of subdued shallow-source magnetic anomalies (Fig. 8B) coincident with exposures of pre-Tertiary metasedimentary rocks presumed to have low magnetization. Deep-source magnetic anomalies (Fig. 8A) are subdued over the western area of Mount Biedeman volcanic rocks, possibly reflecting basement rocks at shallow depth concealed by only a thin cover of Mount Biedeman debris flows.

Dacite of Silver Hill

The 9.1–8.9 Ma dacite of Silver Hill, the easternmost and oldest of the three dome complexes, is composed of numerous small domes with associated carapace breccias, block and ash flows, debris flows, and volcaniclastic sedimentary rocks that are exposed across >50 km² and host large epithermal gold-silver vein deposits in the Bodie Mining District (Figs. 7C, 9M, and 11D). Most Silver Hill rocks are characterized by fairly abundant hornblende phenocrysts (Table 3). Rock compositions include andesite, dacite, trachyandesite, and trachydacite (Fig. 10). The dacite of Silver Hill is well expressed in shallow-source magnetic anomalies (3S in Fig. 8B). A pronounced magnetic low in deep-source magnetic anomalies (3S in Fig. 8B) within the Silver Hill magnetic anomaly pattern may indicate a concealed, reversely magnetized dome or intrusion.

Trachyandesite of Potato Peak

The 9.0–8.8 Ma trachyandesite of Potato Peak forms an 80 km² complex of lava flows and domes that rises more than 600 m above the western and southern parts of the Bodie Hills (Fig. 7C). This complex consists of dozens of lava flows that form prominent flow lobes 300–

1000 m wide and several hundred meters thick (Fig. 9D). These lobes, composed of numerous flows that emanated from the crest of the Bodie Hills, flowed east, north, and west down the flanks of Potato Peak and locally lap onto the dacite of Silver Hill. Potato Peak is a small plug that likely marks a vent for some of the flows (Fig. 9I). Rubbly breccias form the tops and toes of many flows (Fig. 9D). The southern end of the flow dome complex is topographically steep and exposes steeply flow-banded intrusive rocks and less abundant lava flows (Fig. 9G). Debris flow deposits that contain coarse (several meter) blocks of Potato Peak lava are abundant in the low areas between the steep south side of the complex and Mount Biedeman. Rocks of the Potato Peak complex are coarsely porphyritic and contain abundant phenocrysts of plagioclase and lesser hornblende and biotite (Table 3; Fig. 9N). Rock compositions are andesite, dacite, trachyandesite, and trachydacite (Fig. 10). The most profound magnetic anomaly in the Bodie Hills is coincident with the trachyandesite of Potato Peak (Fig. 6A), and the lateral extent of these rocks is well expressed in shallow-source magnetic anomalies (3P in Fig. 6A). A high-amplitude, deep-source magnetic anomaly forms the center of the shallow-source magnetic pattern, possibly indicative of mafic intrusions related to Potato Peak volcanism.

Trachyandesite of Willow Springs

The 8.6–8.0 Ma trachyandesite of Willow Springs, the westernmost and youngest of the three stage 3 flow-dome complexes, is exposed over ~90 km² in the western part of the Bodie Hills (Fig. 7C). It is composed of numerous thick lava flows and flow domes mostly emplaced onto hydrothermally altered rocks of the Masonic and Mount Biedeman centers and locally onto Paleozoic basement rocks. These flows also abut the steep western flanks of the Potato Peak center. Willow Springs rocks are coarsely porphyritic and contain abundant phenocrysts of plagioclase, biotite, hornblende, and clinopyroxene (Table 3). Most Willow Springs rocks are trachyandesites and trachydacites and are compositionally similar to Silver Hill and Potato Peak rocks (Fig. 10). The negative sense of magnetic anomalies over Willow Springs rocks (Fig. 8A) suggests that they are reversely magnetized, as also observed with fluxgate-magnetometer measurements of specific outcrops (Chesterman and Gray, 1975).

Stage 4: Late Rhyolite Volcanism: Big Alkali Domes (ca. 6.2–5.5 Ma)

Miocene magmatic activity resumed following an ~2 Ma hiatus with emplacement of the small 6.2–5.5 Ma rhyolite to trachydacite domes

of the Big Alkali center that mostly intrude the Willow Springs and Masonic volcanic centers in the western Bodie Hills (Fig. 7D). Most outcrops form a narrow north-trending alignment of domes ~20 km long and centered on Big Alkali; two isolated domes crop out 6 km farther north on the north side of Masonic Mountain. Most of these rocks are flow banded, glassy, and contain moderate abundances of plagioclase, biotite, and hornblende, and minor quartz and sanidine phenocrysts (Table 3; Fig. 9J). They range in composition from silicic trachydacite to rhyolite (Fig. 10).

Miocene and Pliocene(?) Sedimentary Rocks

Sequences of sandstone, conglomerate, and lacustrine(?) shale underlie low-relief basins on the northeastern (Fletcher basin strata), northwestern (Sonoma basin strata), and western (Bridgeport basin strata) flanks of the Bodie Hills (Figs. 3 and 7E).

Fletcher Basin Strata

Exposures of Fletcher basin strata include at least 200 m of braided stream deposits, with north-easterly paleocurrent directions, that contain well-rounded volcanic clasts with local interbedded felsic tephras. Dips of as much as 20° are common, and the host basin appears to be bounded on the north by an east-northeast-striking normal fault. Near the junction of Rough Creek with the East Walker River, Fletcher basin strata are overlain by the trachyandesite of Del Monte and by the Eureka Valley Tuff; an interbedded tephra from this section collected ~8 km east-southeast of the Elbow yielded a biotite K-Ar age of 11.7 ± 0.5 Ma (Gilbert and Reynolds, 1973). In Rough Creek canyon both north and northeast of Bald Peak, Fletcher basin strata appear to overlie the trachyandesite of Del Monte. A fallout tuff interbedded in this section yielded a plagioclase $^{40}\text{Ar}/^{39}\text{Ar}$ age of 11.07 Ma (Table 2).

Sonoma Basin Strata

Sonoma basin strata are exposed in the vicinity of lower Sonoma and Masonic Creeks near their junctions with East Walker River; they consist of alternating fine lacustrine strata and coarse fluvial strata that are dominated by volcanic clasts, include rare interbedded tuffs, and have northwesterly paleocurrent directions. Close to their faulted northern margin, the strata dip as much as 20° north and are interbedded with angular sedimentary breccias composed of Mesozoic metasedimentary rocks, which suggests active faulting during basin filling. These strata overlie the trachyandesite of Masonic and locally the Eureka Valley Tuff, but their minimum age is uncertain.

Bridgeport Basin Strata

Bridgeport basin strata are exposed in only a few places, notably just east of Bridgeport, but they are presumed to underlie all or most of the wide, flat Bridgeport Valley. Near Bridgeport, a section of braided stream deposits with northerly paleocurrent directions is >70 m thick and contains rounded granitic and lesser volcanic clasts. The strata dip 20° to the west and are underlain by the trachyandesite of Willow Springs. To the north along the Masonic Road, trough cross-bedded volcanic clast conglomerate and interbedded white lacustrine(?) shale are exposed in roadcuts; these deposits dip gently to the west and overlie the Eureka Valley Tuff. Bridgeport basin strata are thus younger than 8.0 Ma, but their minimum age is uncertain.

PLIOCENE–PLEISTOCENE BIMODAL VOLCANISM (ca. 3.9–0.1 MA)

Pliocene to late Pleistocene postsubduction volcanic rocks of the Aurora volcanic field unconformably overlie the Miocene Bodie Hills volcanic field on the east and southeast sides of the Bodie Hills (Fig. 3; Gilbert et al., 1968; Al-Rawi, 1969; Lange et al., 1993; Lange and Carmichael, 1996). The Aurora volcanic field covers ~325 km² and is composed of high-K and shoshonitic lavas having diverse silica contents. The ages of these lavas range from 3.6 to 0.1 Ma (Lange et al., 1993).

Rocks of the Aurora volcanic field have compositions that include trachybasalt through trachydacite and high-silica rhyolite (~48–76 wt% SiO₂), but no rocks with SiO₂ contents between 65% and 75% (Fig. 10). Lange and Carmichael (1996) estimated that ~25 km³ of magma erupted in the Aurora volcanic field, and that the relative volumes of the different Aurora lavas are ~2% basalt, ~36% basaltic andesite, ~16% two-pyroxene andesite, ~23% hornblende andesite, ~7% dacite and ~16% high-silica rhyolite.

A Pliocene plug and associated basaltic andesite lava flows crop out prominently at Locomotive Point ~5 km south of Masonic Mountain (LP in Fig. 3). These 3.90 Ma (M.A. Cosca, 2011, written commun.) rocks constitute a small eruptive center located well west of all other Pliocene–Pleistocene volcanic rocks in the Bodie Hills. The plug is along the trend of the Big Alkali domes, suggesting that it was emplaced along the same structure that also controlled Big Alkali dome emplacement.

Many Pliocene–Pleistocene volcanic rocks in the Bodie Hills are associated with short-wavelength, high-amplitude magnetic anomalies that are characteristic of young volcanic terranes. These anomalies are particularly well illuminated when filtered to emphasize shal-

low magnetic sources (P, PAC, PBP, PAP in Fig. 8B). Some of these anomalies correspond closely with specific volcanic edifices, notably Aurora Crater, Aurora Peak, and Beauty Peak. The negative sense of the anomaly over Aurora Peak (Fig. 8B) indicates that the bulk of the edifice formed during a time of reversed polarity. Some Aurora volcanic field volcanoes also are coincident with magnetic anomalies that indicate deeper sources, notably the deep-source magnetic anomalies coincident with Aurora Crater (PAC in Fig. 8A) and the Beauty Peak shield volcano (PBP in Fig. 8A). The latter anomaly is directly over Beauty Peak and is much more restricted laterally than the shallow-source magnetic anomalies ascribed to Beauty Peak andesite flows (PBP in Fig. 8B). The negative deep-source magnetic anomaly immediately west of Beauty Peak probably indicates rhyolitic volcanic rocks of Bald Peak beneath relatively thin andesite flows of Beauty Peak.

PETROGRAPHY OF BODIE HILLS VOLCANIC ROCKS

Most Bodie Hills volcanic field units have distinctive petrographic features (Table 3) that were useful in delineating the geologic distribution of these rocks. Essentially all contain sparse to moderately abundant phenocrysts (≥ 0.2 mm) enclosed in variably devitrified or hydrated (but locally pristine) glass. Phenocryst characteristics, including mineralogy, size, and abundance, vary widely (Table 3). The most mafic units generally contain the highest abundances of phenocrysts and mafic minerals. The groundmass typically contains variable microphenocryst assemblages, dominated by plagioclase, but also includes combinations of Fe-Ti oxide minerals, clinopyroxene, and less commonly hornblende and/or biotite. These microphenocrysts are typically 0.05–0.2 mm across (phenocryst sizes noted herein are maximum crystal dimensions). Glomerocryst aggregates as much as several millimeters in diameter are present in many samples. Some nearly aphyric rhyolite lava flow units are visibly flow laminated and phenocrysts in other units are trachytically aligned. Exotic lithic fragments or inclusions are rare. Many Bodie Hills volcanic rocks are at least weakly weathered and/or altered by late magmatic or hydrothermal processes, both of which affected the character of mafic silicates, plagioclase, and the groundmass.

Plagioclase is a nearly ubiquitous phenocryst in Bodie Hills volcanic rocks. Euhedral, albite-twinned laths (1–2 mm) are present in essentially all of these rocks. Almost all plagioclase phenocrysts are oscillatory zoned and some, especially in intermediate-composition lava flows,

are variably sieve textured. Many units contain multiple plagioclase populations defined by size and/or distinctive reaction rims and resorption textures. Plagioclase phenocrysts in the silicic trachyandesite to dacite flow dome complexes (Rough Creek, Aurora Canyon, Willow Springs, Potato Peak, and Silver Hill) are distinctly larger (5–10 mm) than in other Bodie Hills rocks.

Hornblende forms euhedral to subhedral 0.5–2 mm acicular crystals that have distinctive, variably developed black opaque reaction rims that develop during magma ascent, depressurization, and degassing (Rutherford and Hill, 1993). In weathered or altered samples hornblende is completely replaced by a black amorphous material not resolvable using light microscopy.

Pyroxene, dominantly clinopyroxene, is common in many Bodie Hills units. It forms pale tan to pale green subhedral to euhedral crystals 0.5–2 mm long. Rare orthopyroxene is colorless to rosy tan and forms euhedral to subhedral 0.5–1 mm crystals.

Biotite is subhedral, tan to deep red brown, and 0.5–2 mm across, and like hornblende, is completely oxidized in many samples.

Olivine is sparingly present in some of the most mafic Bodie Hills rocks, in the trachy-andesites of Willow Springs and West Brawley Peak, and in the trachydacite of Rough Creek, in which it forms variably altered, 0.3–1 mm subhedral phenocrysts.

Small amounts of magnetite and less abundant ilmenite are ubiquitous.

Quartz is absent in all but the most silicic units. Where present, it forms variably resorbed and embayed, rounded anhedral to subhedral 0.5 mm phenocrysts.

Alkali feldspar is less common than quartz, but forms variably and weakly perthitic Carlsbad-twinned, euhedral to subhedral 0.5–2 mm phenocrysts in several rhyolite units and rarely in the most silicic trachydacite to rhyolite units.

Accessory mineral suites include nearly ubiquitous apatite, and in several of the rhyolite units, variable combinations of titanite, zircon, and allanite.

GEOCHEMISTRY OF THE BODIE HILLS VOLCANIC FIELD

Major Oxide Data

Silica contents of Bodie Hills volcanic field units range from ~50 to almost 78 wt% (Table 4; Supplemental Table 2 [see footnote 2]). However, most samples contain between ~55 and 68 wt% SiO₂, few samples contain between 67 and 71 wt% SiO₂, and rhyolites form a distinct subset containing between 71 and 78 wt% SiO₂.

TABLE 4. AVERAGE COMPOSITIONS OF MAJOR VOLCANIC UNITS IN THE BODIE HILLS VOLCANIC FIELD

	Masonic domes (59)	Rough Creek (13)	Clark Canyon (4)	Brawley Peak (11)	Aurora Creek (4)	West Creek (1)	Del Monte Canyon (7)	Rock Springs Canyon (6)	Bridgeport Canyon (3)
SiO ₂	58.92 ± 2.60	60.68 ± 1.12	59.99 ± 2.29	62.69 ± 1.1	61.35 ± 0.65	62.38 ± 0.79	75.46 ± 2.15	72.95 ± 2.13	76.26 ± 1.45
TiO ₂	0.86 ± 0.13	0.73 ± 0.12	0.82 ± 0.14	0.64 ± 0.03	0.71 ± 0.04	0.71 ± 0.06	0.18 ± 0.09	0.26 ± 0.09	0.13 ± 0.09
Al ₂ O ₃ *	17.72 ± 0.89	17.4 ± 0.85	18.03 ± 0.88	17.40 ± 0.53	17.70 ± 0.87	17.16 ± 0.61	13.58 ± 1.05	14.08 ± 0.79	13.48 ± 0.81
FeO*	5.94 ± 0.88	5.26 ± 0.77	5.33 ± 1.08	4.51 ± 0.26	4.83 ± 0.56	4.96 ± 0.36	1.02 ± 0.38	1.91 ± 0.47	0.78 ± 0.33
MnO	0.10 ± 0.02	0.09 ± 0.03	0.09 ± 0.04	0.08 ± 0.01	0.07 ± 0.03	0.06 ± 0.02	0.04 ± 0.02	0.03 ± 0.01	0.04 ± 0.02
MgO	3.28 ± 1.16	2.92 ± 0.46	3.11 ± 1.10	2.10 ± 0.77	2.54 ± 0.86	2.48 ± 0.72	0.36 ± 0.24	0.77 ± 0.34	0.09 ± 0.02
CaO	6.13 ± 1.04	5.97 ± 0.46	5.47 ± 0.87	5.17 ± 0.56	5.63 ± 0.28	5.01 ± 0.58	1.12 ± 0.32	2.07 ± 0.38	0.75 ± 0.16
Na ₂ O	4.03 ± 0.35	4.12 ± 0.23	3.81 ± 0.36	4.36 ± 0.30	4.09 ± 0.31	4.03 ± 0.18	3.33 ± 0.26	3.36 ± 0.22	3.57 ± 0.21
K ₂ O	2.69 ± 0.72	2.55 ± 0.30	3.02 ± 0.83	2.77 ± 0.37	2.80 ± 0.15	2.95 ± 0.47	4.86 ± 0.50	4.46 ± 0.49	4.88 ± 0.07
P ₂ O ₅	0.34 ± 0.08	0.27 ± 0.04	0.33 ± 0.11	0.28 ± 0.05	0.29 ± 0.07	0.26 ± 0.08	0.04 ± 0.02	0.10 ± 0.02	0.01 ± 0.01
LOI	1.35 ± 0.84	1.30 ± 0.49	2.55 ± 0.79	1.30 ± 0.26	1.14 ± 0.18	2.73 ± 0.97	4.92 ± 1.34	1.42 ± 1.52	0.71 ± 0.24
Ba	1149 ± 287	1058 ± 104	1226 ± 291	1101 ± 89	1285 ± 111	1240 ± 198	796 ± 332	934 ± 91	650 ± 385
Cs	2.2 ± 1.8	1.8 ± 0.5	4.5 ± 4.5	2.6 ± 1.3	2.0 ± 0.8	3.5 ± 0.9	9.9 ± 1.1	6.3 ± 2.6	8.1 ± 2.6
Rb	67 ± 32	55 ± 7	83 ± 45	64 ± 16	74 ± 6	76 ± 11	187 ± 31	135 ± 18	167 ± 28
Sr	917 ± 257	916 ± 140	834 ± 274	1002 ± 114	754 ± 60	872 ± 150	139 ± 47	347 ± 40	115 ± 50
Y	17.8 ± 3.2	16.2 ± 2.3	15.8 ± 2.3	12.2 ± 1.2	18.0 ± 3.3	13.2 ± 1.8	9.7 ± 3.4	10.1 ± 3.2	19.8 ± 2.1
Zr	162 ± 40	129 ± 19	166 ± 30	126 ± 30	168 ± 33	136 ± 27	109 ± 52	106 ± 35	98 ± 36
Hf	4.6 ± 1.2	3.8 ± 0.4	4.5 ± 0.7	3.5 ± 0.8	4.8 ± 0.5	3.4 ± 1.2	3.3 ± 0.9	3.2 ± 0.8	6.3 ± 0.6
Nb	7.4 ± 2.0	6.4 ± 1.4	6.9 ± 0.9	5.3 ± 0.9	7.3 ± 1.3	5.9 ± 1.1	8.3 ± 2.4	6.8 ± 1.6	13.2 ± 2.6
Th	9.8 ± 7.3	9.0 ± 1.6	7.1 ± 3.2	9.2 ± 2.6	10.3 ± 2.6	10.4 ± 2.8	23.5 ± 3.6	18.8 ± 1.5	22.3 ± 6.1
U	3.75 ± 4.59	3.76 ± 1.22	2.39 ± 1.15	3.32 ± 0.96	3.15 ± 0.79	3.55 ± 1.06	8.68 ± 1.52	6.53 ± 0.58	8.18 ± 1.93
Ga	22 ± 2	20 ± 1	21 ± 1	21 ± 1	23 ± 2	20 ± 2	14 ± 1	15 ± 1	20 ± 1
La	34 ± 10.7	27.3 ± 5.4	28.9 ± 4.3	28.8 ± 5.8	38.6 ± 8.6	32.7 ± 7.3	31.1 ± 6.4	29.7 ± 3.4	44.3 ± 3.3
Ce	65.5 ± 19.6	52.1 ± 12.7	56.6 ± 12.3	54.4 ± 10.8	73.5 ± 16.9	59.8 ± 12.8	53.1 ± 12.8	49.7 ± 7.7	47.9 ± 5.0
Pr	8.11 ± 2.21	6.14 ± 1.17	6.84 ± 2.16	6.37 ± 1.14	8.69 ± 1.84	7.05 ± 1.49	5.22 ± 1.41	5.15 ± 1.04	4.79 ± 0.47
Nd	31.2 ± 8.0	24.1 ± 4.7	27.8 ± 10.8	24.3 ± 4.2	32.9 ± 7.1	27.4 ± 6.0	16.8 ± 5.3	17.1 ± 3.7	14.6 ± 2.1
Sm	5.6 ± 1.2	4.3 ± 0.9	5.3 ± 2.2	4.2 ± 0.8	5.8 ± 1.1	4.9 ± 1.4	2.5 ± 1	2.8 ± 0.8	2.1 ± 0.5
Eu	1.36 ± 0.25	1.13 ± 0.21	1.34 ± 0.24	1.07 ± 0.13	1.37 ± 0.23	1.28 ± 0.31	0.42 ± 0.22	0.60 ± 0.12	0.40 ± 0.14
Gd	4.45 ± 0.87	3.67 ± 0.71	3.96 ± 1.15	3.03 ± 0.40	5.01 ± 0.87	3.77 ± 0.74	1.76 ± 0.77	2.14 ± 0.55	1.71 ± 0.32
Tb	0.63 ± 0.11	0.53 ± 0.10	0.56 ± 0.15	0.43 ± 0.05	0.70 ± 0.09	0.50 ± 0.09	0.28 ± 0.11	0.31 ± 0.09	0.27 ± 0.05
Dy	3.34 ± 0.55	3.01 ± 0.83	3.17 ± 0.78	2.31 ± 0.24	3.44 ± 0.55	2.60 ± 0.38	1.56 ± 0.64	1.64 ± 0.55	1.43 ± 0.29
Ho	0.65 ± 0.11	0.60 ± 0.17	0.60 ± 0.12	0.44 ± 0.05	0.68 ± 0.12	0.48 ± 0.05	0.33 ± 0.12	0.34 ± 0.12	0.28 ± 0.05
Er	1.83 ± 0.36	1.82 ± 0.60	1.60 ± 0.27	1.21 ± 0.13	1.82 ± 0.20	1.30 ± 0.10	1.11 ± 0.34	1.18 ± 0.43	0.88 ± 0.08
Tm	0.26 ± 0.06	0.25 ± 0.08	0.22 ± 0.04	0.17 ± 0.02	0.26 ± 0.03	0.19 ± 0.02	0.17 ± 0.06	0.15 ± 0.04	0.14 ± 0.02
Yb	1.70 ± 0.37	1.70 ± 0.49	1.47 ± 0.22	1.16 ± 0.13	1.78 ± 0.22	1.19 ± 0.17	1.20 ± 0.24	1.10 ± 0.33	1.77 ± 0.21
Lu	0.29 ± 0.06	0.26 ± 0.10	0.24 ± 0.04	0.2 ± 0.04	0.29 ± 0.04	0.20 ± 0.02	0.20 ± 0.05	0.19 ± 0.05	0.28 ± 0.04
Co	20 ± 6	17 ± 2	16 ± 5	15 ± 2	15 ± 4	17 ± 2	1.1 ± 1	4 ± 1	8 ± 2
Cr	55 ± 54	57 ± 24	60 ± 29	42 ± 23	55 ± 30	53 ± 32	bdl	9 ± 3	10 ± -
Ni	38 ± 31	24 ± 4	31 ± 13	27 ± 15	31 ± 14	28 ± 10	8 ± 7	12 ± 6	16 ± -
Sc	11 ± 3	12 ± 2	8 ± 2	10 ± 3	11 ± 1	3 ± -	4 ± 1	4 ± 1	7 ± 2
V	143 ± 27	124 ± 39	129 ± 27	105 ± 15	122 ± 10	111 ± 13	8 ± 5	30 ± 16	12 ± -
Cu	48 ± 21	52 ± 26	51 ± 19	32 ± 10	38 ± 10	35 ± 9	3 ± -	8 ± 4	73 ± 11
Mo	2.7 ± 0.7	2.0 ± -	4.7 ± 0.6	3.5 ± 0.6	2.0 ± -	3.5 ± 0.7	5.3 ± 1.7	4.3 ± 2.5	29 ± 3
Pb	17 ± 6	16 ± 4	15 ± 3	17 ± 3	22 ± 3	18 ± 4	30 ± 2	25 ± 1	30 ± 4
Zn	76 ± 14	64 ± 11	72 ± 10	61 ± 8	86 ± 10	81 ± 22	38 ± 21	26 ± 11	54 ± 2
Sn	2.9 ± 3.6	1.6 ± 0.7	1.0 ± -	2.0 ± 1.4	2 ± -	bdl	1.7 ± 1.2	20 ± 1.0	2.3 ± 1.2
W	1.1 ± 0.3	1.0 ± -	1.7 ± 0.6	1.2 ± 0.4	1 ± -	1.5 ± 0.7	3.0 ± 0.8	2 ± -	2.3 ± 0.5
Ta	0.6 ± 0.1	0.6 ± 0.1	0.5 ± 0.1	0.7 ± -	0.5 ± 0.1	0.6 ± 0.2	0.8 ± 0.2	0.7 ± 0.1	0.9 ± 0.2

(continued)

Bodie Hills volcanic field

TABLE 4. AVERAGE COMPOSITIONS OF MAJOR VOLCANIC UNITS IN THE BODIE HILLS VOLCANIC FIELD (continued)

	Del Monte (18)	Aurora Canyon (21)	Bodie Creek (4)	Bodie Hills (20)	Bald Peak (3)	Mount Biederman (49)	Silver Hill (25)	Potato Peak (36)	Willow Spring (23)	Big Alkali (12)
SiO ₂	61.00 ± 3.33	63.31 ± 2.43	72.09 ± 1.22	73.99 ± 1.69	77.12 ± 0.48	58.68 ± 3.21	63.96 ± 1.69	63.04 ± 1.03	62.01 ± 1.86	69.31 ± 1.67
TiO ₂	0.82 ± 0.18	0.73 ± 0.15	0.26 ± 0.01	0.21 ± 0.08	0.11 ± 0.04	0.96 ± 0.19	0.71 ± 0.12	0.70 ± 0.07	0.80 ± 0.11	0.30 ± 0.04
Al ₂ O ₃	17.3 ± 0.73	16.89 ± 0.47	15.14 ± 0.54	14.11 ± 0.61	12.90 ± 0.36	17.47 ± 0.75	17.33 ± 0.97	17.36 ± 0.66	16.65 ± 0.61	16.51 ± 0.8
FeO*	5.04 ± 1.34	4.50 ± 0.93	1.55 ± 0.21	1.36 ± 0.45	1.05 ± 0.15	6.03 ± 1.12	4.36 ± 0.43	4.67 ± 0.37	4.81 ± 0.71	2.05 ± 0.37
MnO	0.08 ± 0.03	0.07 ± 0.01	0.04 ± 0.01	0.05 ± 0.02	0.04 ± 0.02	0.10 ± 0.03	0.08 ± 0.03	0.08 ± 0.03	0.08 ± 0.02	0.04 ± 0.01
MgO	2.69 ± 1.55	2.06 ± 0.69	0.57 ± 0.03	0.44 ± 0.21	0.12 ± 0.05	3.24 ± 1.54	1.91 ± 0.50	1.88 ± 0.49	2.88 ± 0.74	0.83 ± 0.25
CaO	5.29 ± 1.50	4.61 ± 1.01	2.12 ± 0.42	1.39 ± 0.46	0.70 ± 0.06	6.36 ± 1.15	4.25 ± 0.72	4.89 ± 0.31	5.35 ± 0.93	2.72 ± 0.53
Na ₂ O	3.76 ± 0.37	3.69 ± 0.37	3.82 ± 0.64	3.52 ± 0.37	3.80 ± 0.77	3.93 ± 0.40	3.98 ± 0.32	3.86 ± 0.33	3.79 ± 0.22	4.29 ± 0.41
K ₂ O	3.72 ± 0.81	3.85 ± 0.58	4.31 ± 0.37	4.87 ± 0.35	5.54 ± 0.56	2.80 ± 0.61	3.09 ± 0.56	3.16 ± 0.36	3.32 ± 0.39	3.69 ± 0.44
P ₂ O ₅	0.29 ± 0.05	0.28 ± 0.09	0.12 ± 0.02	0.06 ± 0.04	0.01 ± 0.01	0.44 ± 0.12	0.33 ± 0.07	0.35 ± 0.12	0.31 ± 0.06	0.26 ± 0.39
LOI	1.98 ± 0.32	1.72 ± 0.85	2.75 ± 3.22	2.18 ± 0.94	3.42 ± 2.53	1.38 ± 0.59	1.66 ± 0.79	1.44 ± 0.51	1.54 ± 0.76	1.75 ± 0.62
Ba	1323 ± 244	1184 ± 175	877 ± 159	724 ± 320	470 ± 277	1375 ± 305	1415 ± 243	1311 ± 176	1262 ± 144	1547 ± 134
Cs	8.5 ± 4.8	6.7 ± 4.2	36.5 ± 35.7	10.6 ± 3.5	62.6 ± 73.3	2.6 ± 1.5	2.6 ± 1.2	3.3 ± 1.1	4.0 ± 1.4	2.7 ± 0.8
Rb	129 ± 50	123 ± 31	196 ± 104	183 ± 23	323 ± 101	72 ± 27	87 ± 32	85 ± 10	92 ± 14	72 ± 14
Sr	658 ± 137	704 ± 156	410 ± 138	89 ± 44	1018 ± 303	958 ± 183	866 ± 133	962 ± 101	1100 ± 206	1100 ± 206
Y	18.5 ± 1.8	17.2 ± 2.4	10.1 ± 2.7	8.9 ± 1.2	8.6 ± 1.3	19.4 ± 4.3	12.7 ± 1.6	14.9 ± 2.3	16.2 ± 3.4	7.2 ± 0.8
Zr	210 ± 54	200 ± 40	139 ± 28	108 ± 23	80 ± 27	167 ± 42	120 ± 21	142 ± 25	142 ± 25	121 ± 8
Hf	5.8 ± 1.5	5.8 ± 1.4	4 ± -	3.6 ± 0.7	3.0 ± 0.7	4.3 ± 1.1	3.3 ± 0.6	4.0 ± 0.4	4.2 ± 0.6	3.5 ± 0.5
Nb	9.4 ± 2.1	9.7 ± 2.2	12 ± -	13.5 ± 1.5	14.6 ± 2.5	9.7 ± 3.3	8.7 ± 1.7	9.1 ± 0.7	9.3 ± 1.2	4.3 ± 0.5
Th	19.3 ± 6.6	21.5 ± 2.3	23.7 ± 3.7	22.7 ± 3.2	9.2 ± 4.4	8.5 ± 2.5	9.9 ± 1.8	12.5 ± 2.0	4.7 ± 1.4	1.7 ± 1.4
U	5.96 ± 2.23	6.39 ± 1.98	7.9 ± 1.76	8.46 ± 1.47	8.82 ± 1.53	3.02 ± 2.51	3.04 ± 0.71	3.43 ± 0.59	4.59 ± 0.74	1.97 ± 1.49
Ga	20 ± 1	20 ± 2	17 ± -	16 ± 1	15 ± -	21 ± 2	20 ± 1	20 ± 1	20 ± 1	19 ± 1
La	40.3 ± 6.1	40.7 ± 5.8	32.4 ± 2.0	31.3 ± 4.9	29.0 ± 6.1	43.3 ± 14.9	35.7 ± 7.1	35.2 ± 5.4	37.2 ± 3.7	21.7 ± 4.4
Ce	75.6 ± 9.6	75.4 ± 9.9	54.9 ± 0.9	50.1 ± 8.4	48.4 ± 9.4	79.8 ± 26.2	63.8 ± 11.6	64.3 ± 9.3	68.2 ± 6.9	38.9 ± 7.1
Pr	8.92 ± 1.01	8.85 ± 1.24	5.58 ± 0.23	5.1 ± 1.01	4.71 ± 1.05	10.21 ± 3.38	7.96 ± 1.91	7.66 ± 1.2	8.18 ± 0.90	4.56 ± 0.82
Nd	33.7 ± 3.2	32.9 ± 4.6	18.2 ± 0.1	16.0 ± 3.8	14.2 ± 3.9	40.7 ± 14.0	29.8 ± 7.4	29.1 ± 4.4	31.4 ± 3.8	16.5 ± 3.0
Sm	6.1 ± 0.7	5.8 ± 1.0	2.6 ± 0.1	2.3 ± 0.6	2.0 ± 0.7	6.9 ± 2.0	5.1 ± 1.1	5.1 ± 0.8	5.6 ± 0.7	2.7 ± 0.5
Eu	1.37 ± 0.18	1.31 ± 0.26	0.65 ± 0.10	0.45 ± 0.16	0.28 ± 0.11	1.68 ± 0.48	1.25 ± 0.21	1.30 ± 0.19	1.43 ± 0.16	0.66 ± 0.11
Gd	4.71 ± 0.61	4.51 ± 0.82	2.0 ± 0.38	1.66 ± 0.42	1.50 ± 0.42	5.2 ± 1.4	3.58 ± 0.61	4.11 ± 0.64	4.47 ± 0.63	1.99 ± 0.48
Tb	0.64 ± 0.07	0.62 ± 0.10	0.31 ± 0.01	0.24 ± 0.05	0.24 ± 0.05	0.69 ± 0.18	0.47 ± 0.05	0.56 ± 0.09	0.60 ± 0.09	0.27 ± 0.05
Dy	3.50 ± 0.34	3.26 ± 0.47	1.74 ± 0.52	1.39 ± 0.26	1.29 ± 0.25	3.50 ± 0.78	2.37 ± 0.29	2.88 ± 0.41	3.03 ± 0.48	1.36 ± 0.18
Ho	0.67 ± 0.06	0.61 ± 0.10	0.34 ± 0.13	0.28 ± 0.05	0.25 ± 0.06	0.66 ± 0.14	0.44 ± 0.05	0.54 ± 0.08	0.56 ± 0.10	0.26 ± 0.03
Er	1.86 ± 0.18	1.75 ± 0.21	1.06 ± 0.37	0.88 ± 0.12	0.89 ± 0.16	1.77 ± 0.40	1.15 ± 0.16	1.52 ± 0.22	1.64 ± 0.29	0.72 ± 0.07
Tm	0.27 ± 0.03	0.17 ± 0.03	0.17 ± 0.05	0.14 ± 0.02	0.14 ± 0.02	0.25 ± 0.06	0.17 ± 0.02	0.21 ± 0.03	0.22 ± 0.04	0.10 ± 0.01
Yb	1.77 ± 0.18	1.64 ± 0.21	1.20 ± 0.28	1.04 ± 0.09	1.08 ± 0.08	1.57 ± 0.38	1.07 ± 0.11	1.40 ± 0.21	1.44 ± 0.23	0.70 ± 0.08
Lu	0.27 ± 0.04	0.18 ± 0.03	0.17 ± 0.03	0.19 ± 0.02	0.27 ± 0.07	0.18 ± 0.03	0.25 ± 0.04	0.25 ± 0.04	0.25 ± 0.05	0.12 ± 0.02
Co	16 ± 7	12 ± 4	3 ± -	3 ± 1	1 ± -	19 ± 6	12 ± 3	13 ± 2	16 ± 4	5 ± 1
Cr	81 ± 58	30 ± 13	11 ± 6	10 ± 6	bdl	70 ± 90	23 ± 31	18 ± 17	81 ± 52	14 ± 5
Ni	29 ± 17	21 ± 7	8 ± 1	7 ± 2	bdl	38 ± 36	13 ± 7	22 ± 61	42 ± 35	10 ± 5
Sc	13 ± 5	10 ± 4	bdl	2 ± 1	bdl	10 ± 4	6 ± 1	7 ± 1	12 ± 4	bdl
V	117 ± 60	106 ± 27	26 ± 7	20 ± 11	bdl	133 ± 31	86 ± 31	99 ± 21	122 ± 43	32 ± 7
Cu	42 ± 20	36 ± 27	6 ± 1	8 ± 4	9 ± -	42 ± 27	27 ± 12	25 ± 11	30 ± 12	15 ± 9
Mo	3.4 ± 1.7	3.3 ± 0.7	3 ± -	2.8 ± 0.4	3.3 ± 0.6	3.3 ± 2.0	bdl	3.0 ± 1.3	3.5 ± 2.1	3.5 ± 2.1
Pb	22 ± 6	21 ± 4	23 ± 4	27 ± 4	27 ± 6	19 ± 6	21 ± 2	20 ± 2	20 ± 3	31 ± 4
Zn	69 ± 18	63 ± 10	25 ± 4	21 ± 5	30 ± 9	80 ± 14	71 ± 7	69 ± 11	65 ± 9	46 ± 13
Sn	1.9 ± 0.6	2.0 ± 0.8	2.5 ± 0.7	1.9 ± 0.8	1.4 ± 0.9	2.1 ± 1.0	1.5 ± 0.6	1.7 ± 0.6	1.8 ± 0.8	1.3 ± 0.6
W	2.1 ± 0.7	1.6 ± 0.7	4.5 ± 3.5	2.2 ± 0.8	7.0 ± 6.2	2.9 ± 6.0	1 ± -	1.3 ± 0.5	1.7 ± 0.5	1 ± -
Ta	0.7 ± 0.1	0.7 ± 0.1	0.8 ± 0.1	1.0 ± 0.2	1.1 ± 0.2	0.7 ± 0.1	0.6 ± 0.1	0.6 ± 0.1	0.7 ± 0.1	0.7 ± 0.1

Note: Major oxide data in weight percent, recalculated to 100%; volatile free. LOI—loss on ignition; i.e., sum of all volatile constituents; bdl—below detection limit. Trace element data in parts per million. Averages and standard deviations calculated for the number of analyses (in parentheses) available for each rock unit. —, following ± indicates no variation among analyzed samples.

The Bodie Hills rocks are high-K (Le Maitre, 1989) and somewhat alkaline (Fig. 10; Le Bas et al., 1986). The Na_2O contents of the Bodie Hills rocks are relatively constant, indicating that elevated total alkali contents exclusively reflect elevated K_2O abundances. The Bodie Hills rocks form three compositional groups, one composed of trachyandesite, one of silicic trachyandesite and minor dacite, and one of rhyolite, also corresponding to petrographically distinct rocks.

Geochemical characteristics of the Bodie Hills rocks are consistent with their genesis in a continental margin arc setting. Relative to standard metrics (in cited sources) they are subalkaline (Irvine and Baragar, 1971), metaluminous to weakly peraluminous (Shand, 1951), calc-alkaline (Miyashiro, 1974), and calc-alkaline (Frost et al., 2001), and follow a calc-alkaline trend (Irvine and Baragar, 1971). Abundances of TiO_2 , Al_2O_3 , FeO^* , MnO , and CaO decrease in an essentially linear and systematic fashion with increasing SiO_2 . Abundances of MgO decrease with increasing SiO_2 along a subtly concave-up trend. The P_2O_5 abundances decrease linearly at SiO_2 abundances $>\sim 60$ wt%, but vary non-systematically at lower SiO_2 contents. The Na_2O abundances display no consistent covariation with SiO_2 content, and K_2O abundances scatter to higher concentrations with increasing SiO_2 (Fig. 12). Compositions of Bodie Hills rocks form arrays or groupings on variation diagrams that are reasonably diagnostic of the mapped units and associated Bodie Hills volcanic field eruptive stages (Supplemental Figs. 1–5 in the Supplemental Figure File³).

The weakly alkaline character and elevated K_2O contents of the Bodie Hills rocks are similar to rocks elsewhere in the southern segment of the ancestral Cascades arc (du Bray et al., 2009). At any given SiO_2 content, the Bodie Hills and rocks in the Sonora Pass area of the central Sierra Nevada (exclusive of rocks of the Stanislaus Group, which mostly have distinctly elevated K_2O contents; Putirka and Busby, 2007; Busby et al., 2008) have comparable K_2O contents. In the Bodie Hills, the trachydacite of Bridgeport also has elevated K_2O contents at any given SiO_2 that are similar to those of the Stanislaus Group rocks. In contrast, compositions of rocks from the northern segment of the ancestral Cascades arc (du Bray et al., 2006) are medium K and have lower total alkali contents than the Bodie Hills rocks.

³Supplemental Figure File. PDF file of 12 supplemental figures. If you are viewing the PDF of this paper or reading it offline, please visit <http://dx.doi.org/10.1130/GES00674.S3> or the full-text article on www.gsapubs.org to view the Supplemental Figure File.

Trace Element Data

Bodie Hills volcanic rocks have elevated large ion lithophile element (LILE) abundances and low high-field-strength element abundances similar to those of convergent-margin, broadly calc-alkaline igneous rocks. Abundances of Zr, Y, and transition metals (Co, Cr, Ni, Sc, and V) decrease with increasing SiO_2 , whereas abundances of LILEs (Rb, Cs, Th, and U) increase with increasing SiO_2 . In the context of trace element tectonic classification schemes (Pearce et al., 1984), the geochemistry of the Bodie Hills rocks is consistent with their genesis in a magmatic arc environment (Supplemental Fig. 6 in the Supplemental Figure File [see footnote 3]). An arc setting is corroborated by values of incompatible trace element ratios. Wood et al. (1979) and Gill (1981) established that Ba/Ta, Ba/Nb, and La/Nb ratios for modern arc rocks are >450 , >26 , and 2–7, respectively. The Ba/Ta (735–2423, average 1974), Ba/Nb (56–229, average 140), and La/Nb (2–6, average 4) ratios for Bodie Hills rocks are consistent with ratios of modern arc volcanic rocks. The average Th/La in Bodie Hills volcanic rocks is 0.35, which is also consistent with an arc origin (Plank, 2005).

The majority of Bodie Hills rocks have relatively Sr-rich compositions that cluster near the Sr apex on a ternary K-Rb-Sr diagram (Supplemental Fig. 7 in Supplemental Figure File [see footnote 3]) and are consistent with only modest plagioclase fractionation during their petrogenetic evolution. The most silicic of the Bodie Hills rocks, including the rhyolites of Del Monte Canyon, Bodie Hills, Aurora Creek, Rock Springs Canyon, and Bald Peak, have compositions with greater K_2O and Rb abundances, relative to Sr, that are consistent with the representative magmas having undergone somewhat greater amounts of plagioclase fractionation. Similarly, Sr and Eu/Sm versus SiO_2 relations limit the extent of plagioclase fractionation in most Bodie Hills volcanic rocks (Supplemental Figs. 8–9 in the Supplemental Figure File; see footnote 3). The Sr abundances and Eu/Sm are essentially uncorrelated with those of SiO_2 in all but the rhyolitic rocks, consistent with limited plagioclase fractionation. However, among the Bodie Hills rhyolites, Sr abundances and Eu/Sm are well correlated with SiO_2 content and decrease with increasing SiO_2 , suggesting a significant role for plagioclase fractionation in the petrogenesis of these rocks.

Chondrite-normalized rare earth element (REE) patterns for the Bodie Hills rocks are typical of intermediate composition, calc-alkaline, continental margin volcanic arc rocks (e.g., Gill, 1981; Cameron and Cameron, 1985; Wark,

1991; Feeley and Davidson, 1994). REE patterns are light (L) REE enriched and have negligible to moderate negative Eu anomalies (Fig. 13); heavy (H) REE segments are flat to slightly concave up. Average REE patterns for all Bodie Hills rocks (Fig. 13) are essentially parallel (La_N/Yb_N values define a narrow range). Mafic Bodie Hills units have the highest REE contents and negligible negative Eu anomalies. Notably, REE patterns of the rhyolites have the lowest REE contents. Overall depletion of REEs, and particularly depletion of the middle REEs, may reflect equilibration of these melts with apatite in a partial melt residuum or crustal rocks with which melts interacted, or apatite fractionation in crustal reservoirs. The magnitudes of negative Eu anomalies are systematically greater among the more silicic Bodie Hills rocks, suggesting that plagioclase fractionation contributed significantly to the petrogenesis of those rocks.

The REE data for the Bodie Hills rocks form three distinct groups. The largest of these groups, which includes all of the trachyandesite and trachydacite units except the Rough Creek, West Brawley Peak, and Silver Hill units, have the greatest total REE abundances, small to negligible negative Eu anomalies, and similar total REE abundances and chondrite-normalized patterns. The REE patterns for the Rough Creek, West Brawley Peak, and Silver Hill units (the second group) are distinguished from the first group by slightly lower LREE abundances and distinctly lower HREE abundances; patterns for these three units are rotated slightly clockwise in their HREE parts relative to those of the first group. The third group includes all of the rhyolite units in the Bodie Hills. The REE abundances in these rocks are distinctly lower than in other Bodie Hills rocks and define a relatively broad compositional range; the REE patterns for these rocks have significantly larger negative Eu anomalies and distinctly concave-up HREE pattern segments.

The REE abundance variations within most basaltic to dacitic Bodie Hills units are relatively limited, although variation within most of the rhyolite units is significant. Within-unit REE abundance variations characteristically yield parallel REE patterns, which depict systematically higher or lower REE abundances, with essentially constant-magnitude negative Eu anomalies. Consequently, processes resulting in overall REE abundance variation in most Bodie Hills units involved neither relative REE fractionation nor rotation of corresponding REE patterns. Among Bodie Hills rhyolites, within-unit REE abundances vary significantly; in particular, samples within any single unit with lower REE abundances also have larger magnitude negative Eu anomalies.

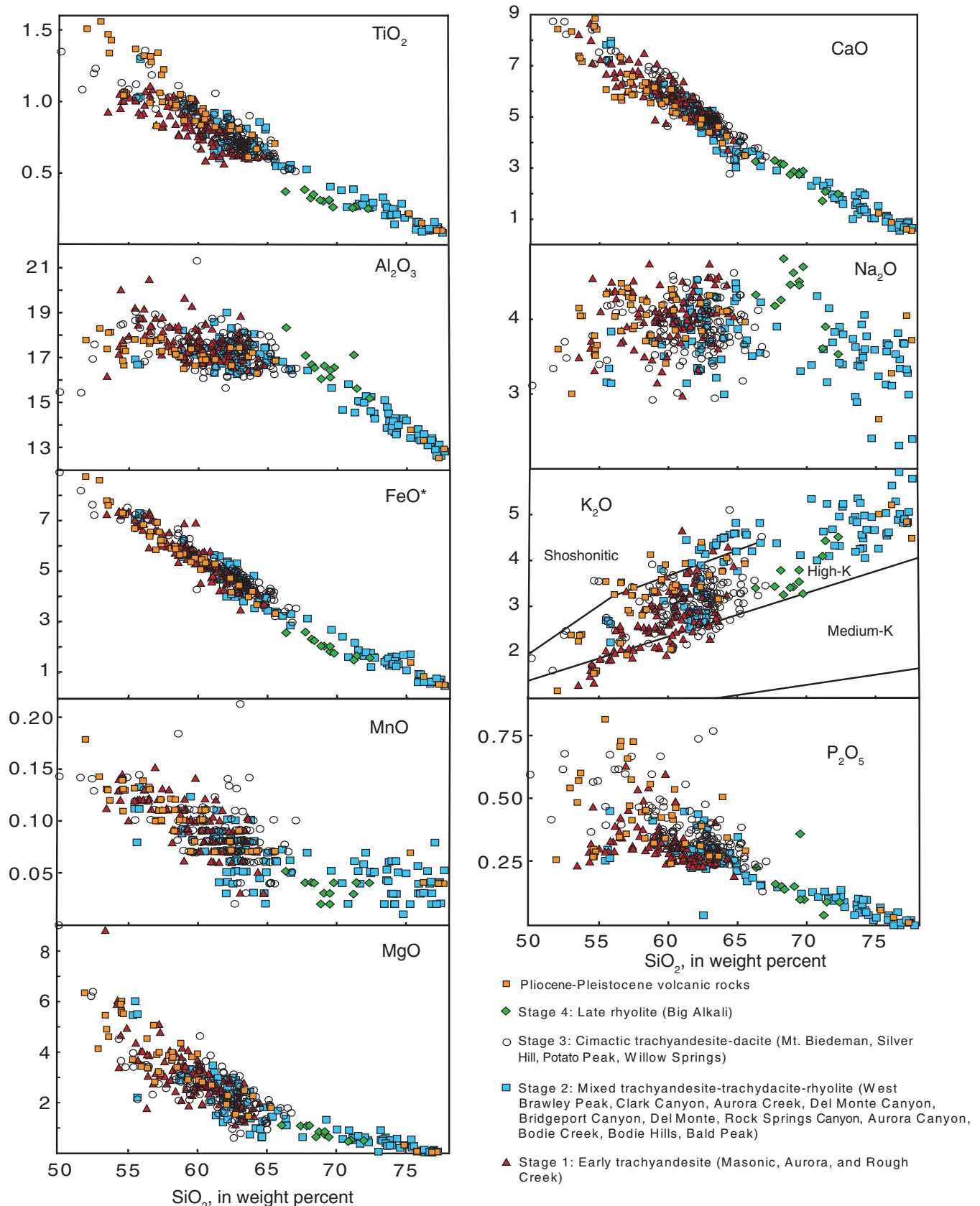


Figure 12. Variation diagrams showing abundances of major oxides (wt%) in rocks of the Bodie Hills volcanic field. On K₂O versus SiO₂ diagram, boundaries between low-K, medium-K, and high-K are from Le Maitre (1989); high-K-shoshonitic boundary is from Ewart (1982).

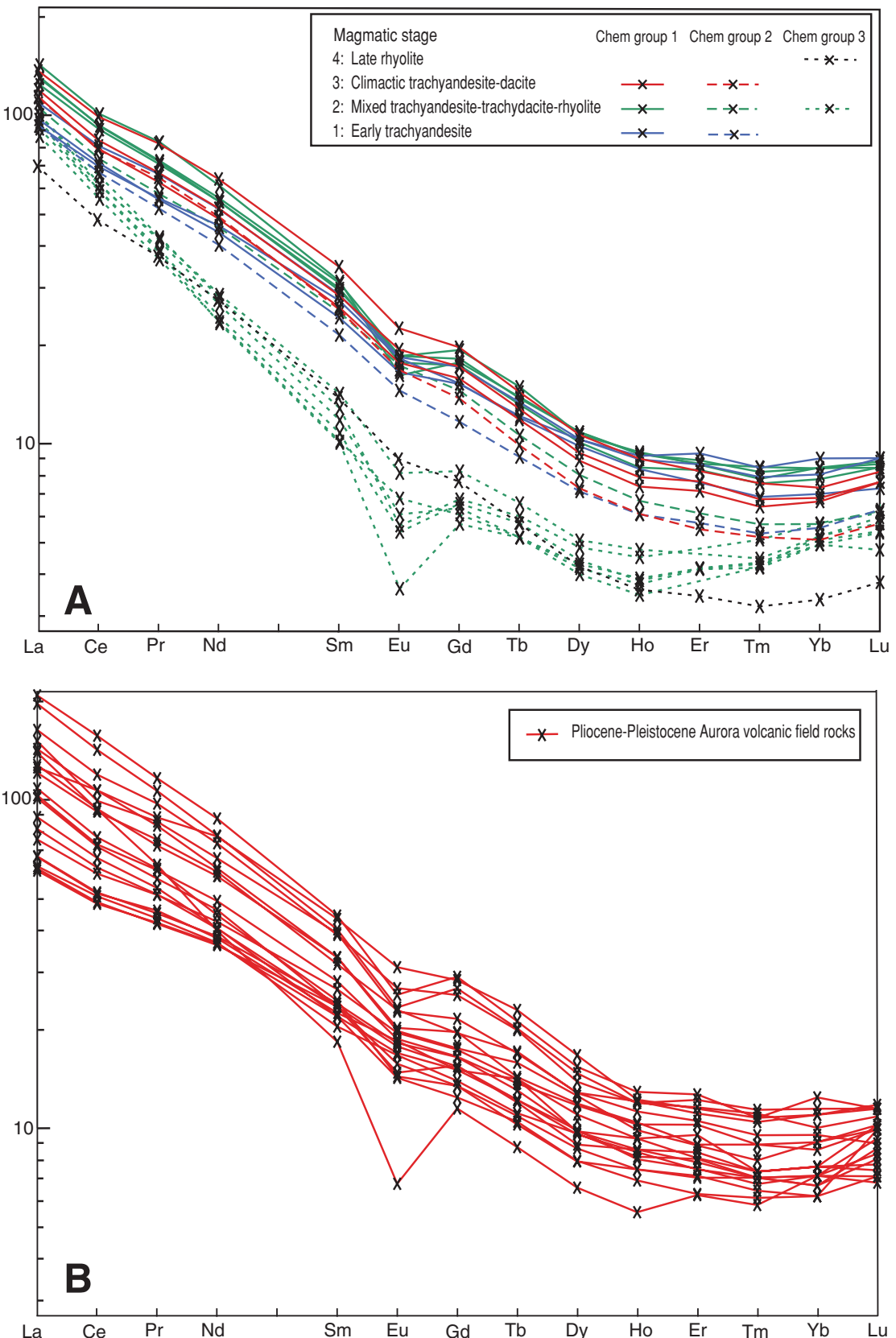


Figure 13. Average chondrite-normalized rare earth element diagrams; chondrite abundances are from Anders and Ebihara (1982). (A) Bodie Hills volcanic field. Dotted, dashed, and solid lines identify three geochemically distinct groups of Bodie Hill volcanic field units. (B) Aurora volcanic field.

Primitive mantle-normalized trace element patterns for the Bodie Hills rocks (Fig. 14) are similar to those characteristic of moderately differentiated arc magmas, such as those in the Andean, Kamchatka, and Central American arcs (GEOROC, 2007). The patterns have moderate negative slopes and all include large negative Nb-Ta and positive Pb anomalies. The negative Nb-Ta anomalies are diagnostic of subduction-related magmatism (Wood et al., 1979; Gill, 1981; Pearce et al., 1984) and suggest that volcanic rocks of the Bodie Hills represent magmatism related to the southern segment of the ancestral Cascades arc. Despite similarities to arc magmatism, and particularly to the Cascades arc, it is important to note that Bodie Hills volcanic rocks younger than ca. 10 Ma are inferred to have erupted following cessation of subduction in this area (Fig. 1; Atwater and Stock, 1998). Primitive mantle-normalized trace element patterns for the Bodie Hills rocks include variably developed negative P, Zr, and Ti anomalies, which are most well developed in the most silicic of the Bodie Hills units. These anomalies may reflect high-level fractionation processes involving accessory minerals, such as apatite, zircon, and Fe-Ti oxides, or variable retention of these minerals in a source region residuum or crustal rocks with which the Bodie Hills magmas interacted.

The three groups of Bodie Hills units identified using REE patterns form similar clusters of primitive mantle-normalized trace element patterns. The first group, represented by the trachyandesite and trachydacite units, forms a set of tightly clustered patterns best distinguished by their elevated abundances of the most compatible elements. Patterns for second group (Rough Creek, West Brawley Peak, and Silver Hill units), in addition to their REE characteristics, are distinguished by their low Th, Nb, Ta, K₂O, and Pb abundances. The final group, rhyolite units, is distinguished by elevated Rb, Th, Nb, Ta, K₂O, and Pb abundances and low to very low abundances of Ba, P, Zr, and most other compatible elements. As defined by the REEs, variations in abundances of other trace elements are limited within individual Bodie Hills units and are greatest within rhyolite units.

FAULTS, VEINS, VOLCANIC LANDFORMS, AND THE MIocene STRESS FIELD

The orientation of the regional strain field during Miocene volcanism in the Bodie Hills is defined by the orientations of mineralized structures and from the morphology of eruptive features. Because mineralization has been well dated in the Masonic (ca. 13 Ma), Aurora

(ca. 10.3 Ma), and Bodie (ca. 8.4 Ma) districts, mineralized structures in these districts define the temporal variation of the regional strain field in the Bodie Hills. However, rocks in the Bodie Hills were rotated ~10°–30° clockwise around a vertical axis after ca. 9 Ma (King et al., 2007; Carlson et al., 2010). This rotation requires that the strain field interpreted from rock structure be unrotated in a counterclockwise direction by 10°–30° to yield the absolute orientation of the Miocene stress field at the time of rock formation. This rotation postdates the mineralized structures in the Masonic and Aurora districts, but, because the timing of rotation is uncertain, it is also uncertain if veins in the Bodie district are rotated.

Mineralized structures in the Masonic district consist of northeast-trending fault breccias hosted by Mesozoic basement rocks and volcaniclastic deposits of the Masonic volcanic center. Mineralized zones are crisscrossed by hairline silica veinlets and hematite-stained fractures that form an approximately conjugate set of steeply dipping north-south and N60°E trending fractures (Figs. 11A and 15A). Slickensides and/or displaced vein segments indicate that north-south fractures have right-lateral offset and N60°E fractures have left-lateral offset. These kinematic indicators are interpreted as a conjugate strike-slip fault set consistent with N60°W extension and N30°E compression (Fig. 15B).

Quartz veins in the Aurora district strike dominantly N60°E and north-south (Figs. 11B, 11C, and 15C). Internal vein fabric indicates repeated cycles of brecciation and open-space filling. Where the north-south and N60°E vein segments intersect, each vein is cut by veinlets of both strikes, indicating they are contemporaneous. The major north-striking Prospectus fault offsets two segments of a N60°E vein set (Prospectus and Humboldt veins) with right-lateral displacement. The kinematics of slickensided walls of a subset of the veins suggest that the veins in the Aurora district constitute a conjugate fracture pair, including a right-lateral north-south set and a left-lateral N60°E set, consistent with N60°W extension and N30°E compression (Fig. 15D).

Quartz veins in the Bodie district are well banded with millimeter to centimeter scale bands and inward-facing crystal terminations, indicative of repeated tensional fracturing of the veins (Fig. 11D). Veins strike ~N10°E to N50°E, with maxima at N15°E and N45°E (Fig. 15E). Veins are wider where their strike bends from N15°E to N30°–40°E. An average of the measured vein strikes dominated by normal (extensional) faulting is N28°E (Fig. 15F).

Structures in all three mining districts reflect a maximum extensional strain axis oriented ~N60°W. Narrow veinlets in the Masonic dis-

trict and the major vein trends in the Aurora district occupy conjugate strike-slip fault sets, indicating that the maximum compressive strain axis was N30°E and horizontal, while the intermediate strain axis was vertical. Banded veins in the Bodie district occupy normal faults with vertical maximum compressive strain, and reflect a switch of the maximum compressive and intermediate strain axis directions between ca. 10 and 8.5 Ma.

Relatively few mapped faults are demonstrably coeval with magmatic activity (Fig. 3). Most faults entirely within rocks older than ca. 9.2 Ma (pre-stage 3) strike northeast or north and have moderate to steep dips. Northeast-striking normal faults flank the basement exposure at Masonic Mountain and are parallel to (and possibly coeval with) mineralized bodies in the Masonic district. The ca. 9.6 Ma Paramount basin appears to be bounded by northeast-striking faults that also offset the Eureka Valley Tuff (ca. 9.4 Ma) and possibly Potato Peak lava flows (ca. 9.0–8.8 Ma). Basin fill includes sinter terraces that appear to be vertically offset by a series of approximately north-striking faults. Aeromagnetic data filtered at both 0.2 and 1.9 km show a prominent N60°E lineament bounding the southeast side of the Masonic eruptive center and the north sides of the Potato Peak center and the Paramount basin (Fig. 8). Faults in stage 3 rocks (ca. 9.2–8.0 Ma trachyandesite and dacite domes) primarily have northwest to west-northwest and north to north-northeast strikes and steep dips.

Stage 1–3 Bodie Hills eruptive centers are dominated by subcircular composite volcanoes and large dome fields that directly overlie deeply rooted intrusions, as inferred from geophysical data. In aggregate, stage 3 trachyandesite-dacite dome complexes are elongate in an east-west direction, and the complexes decrease in age progressively to the west. In contrast, stage 4 rhyolite domes are localized in a narrow north-trending belt mostly within the western part of the stage 3 dacite field along the west flank of the Bodie Hills (Fig. 3).

Dikes, fissure-fed eruptive features, monogenetic volcanoes, and elongate grabens or rectilinear volcanotectonic depressions are notably uncommon to absent in the Miocene Bodie Hills volcanic field. The absence of these features and the faulting pattern are consistent with minimal differential horizontal stress variation during formation of the Bodie Hills volcanic field (e.g., Nakamura, 1977; Hildreth, 1981; Takada, 1994; Tosdal and Richards, 2001). In contrast, the Pliocene–Pleistocene (3.6–0.1 Ma) Aurora volcanic field in the Bodie Hills is characterized by north-northeast–elongated monogenetic volcanoes that are locally offset by north-north-

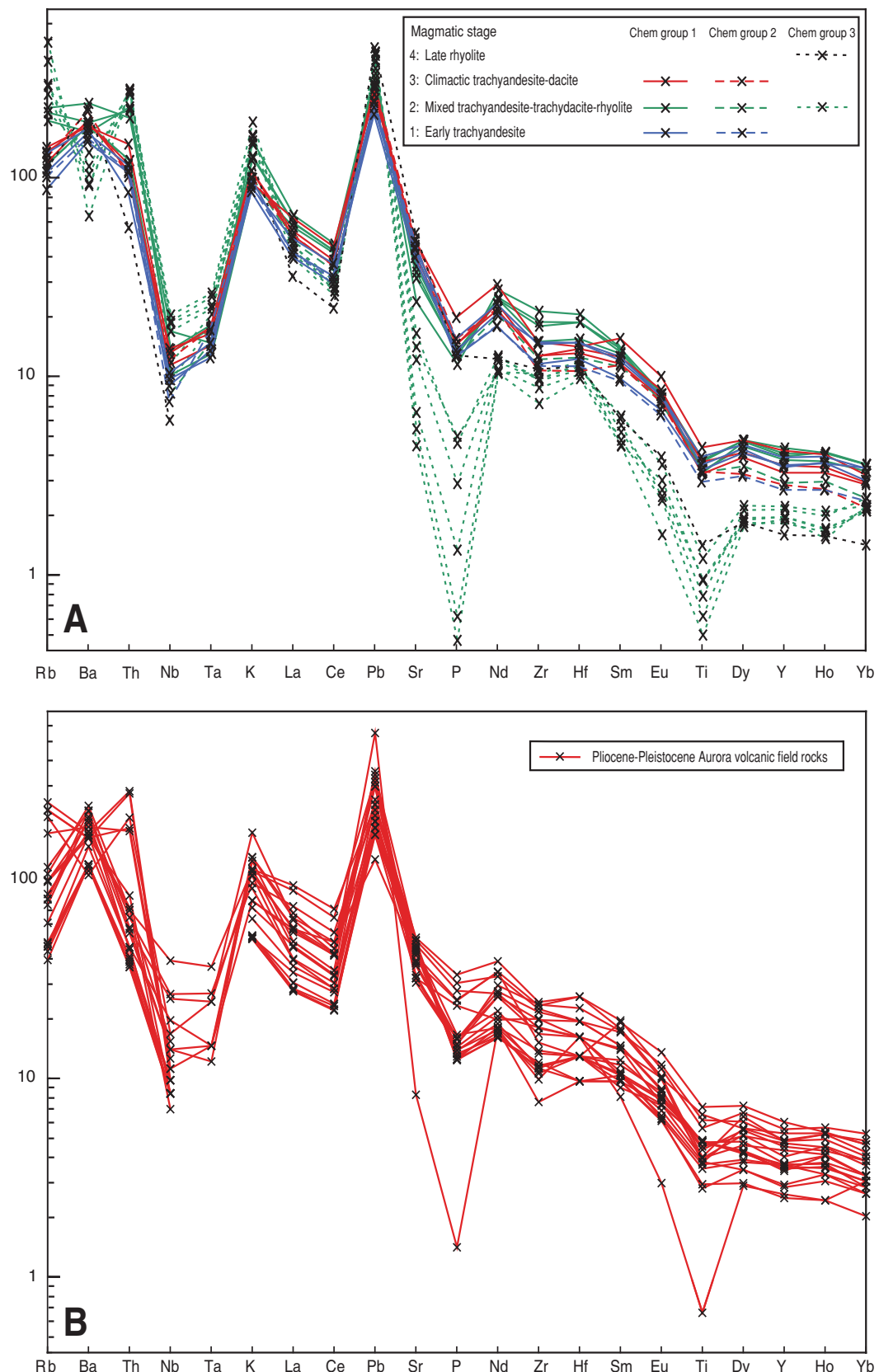
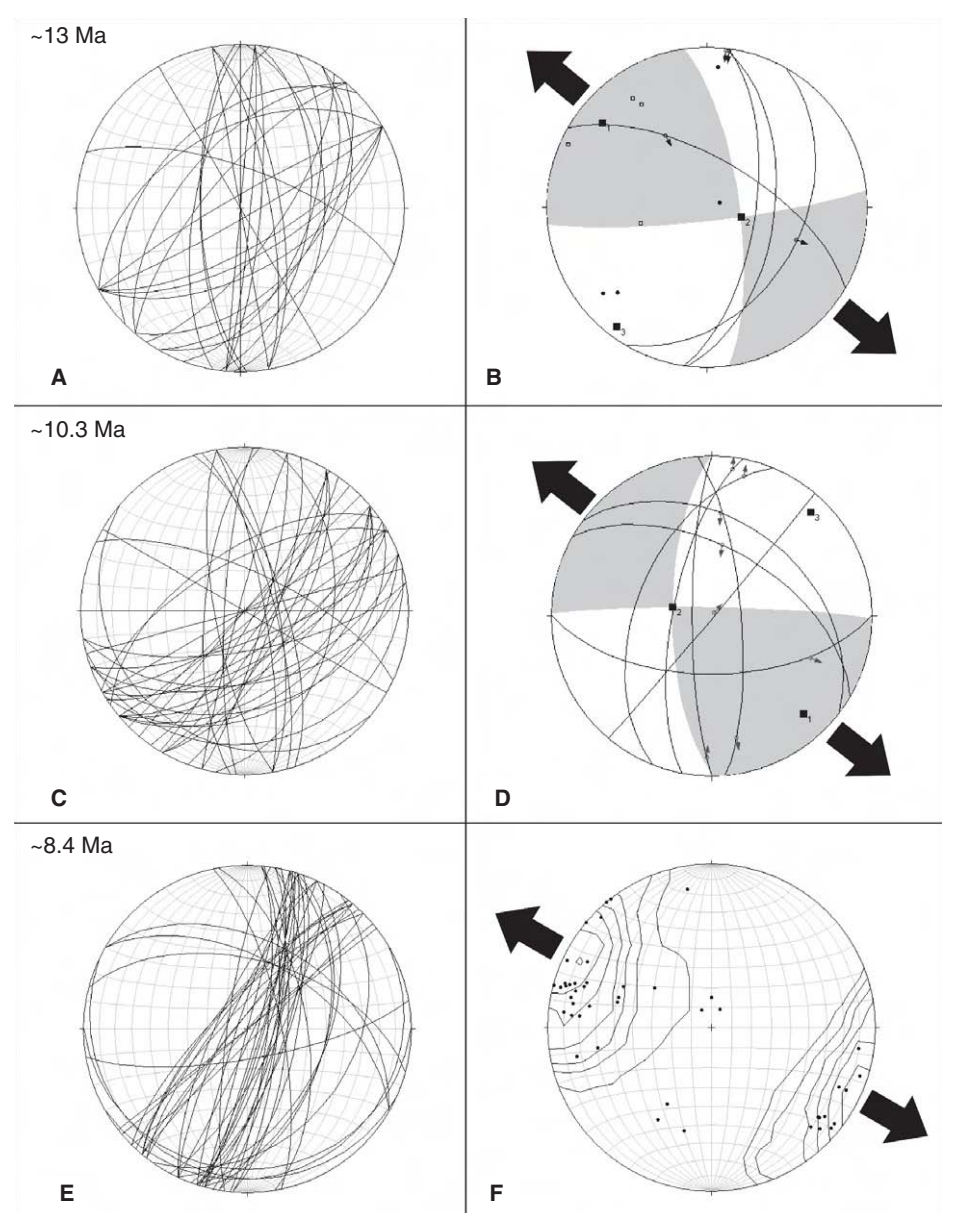


Figure 14. Average primitive mantle-normalized (Sun and McDonough, 1989) trace element diagrams for rocks of the Bodie Hills volcanic field. (A) Bodie Hills volcanic field. Dotted, dashed, and solid lines identify three geochemically distinct groups of Bodie Hills volcanic field units. (B) Aurora volcanic field.

Figure 15. Equal area lower hemisphere stereonet plots for veins and faults in the Masonic (ca. 13 Ma), Aurora (ca. 10.3 Ma), and Bodie districts (ca. 8.4 Ma). (A) Great circles showing orientations of narrow quartz microveinlets (1–3 mm thick) in the Masonic district ($n = 32$), dominated by approximately north-south and N60°E striking trends. (B) Kinematic data are from slickensided surfaces on walls of four veinlets, plotted using the Rick Allmendinger's FaultKinWin v1.2: A program for analyzing fault slip data for Windows computers (<ftp://www.geo.cornell.edu/pub/rwa/Windows/FaultKinWinFull122.zip>; for the latest version, see <http://www.geo.cornell.edu/geology/faculty/RWA/programs/faultkin-5-beta.html>). Great circles show orientation of slickensided surface with arrow showing trend and plunge of slickenline and relative movement direction of hanging wall of fault. Each fault yields unique maximum compression (P) axis (solid circle) and maximum extension (T) axis (open square); these are used to derive best-fit quadrants (orientations of nodal planes: 352°, 74°; 84°, 83°) of extension (gray) and compression (white), similar to those used to illustrate earthquake first motions. The solid, numbered squares yield the computed stress axes (eigenvectors) using linked Bingham analysis: 1 = maximum extension (309°, 17°), 2 = intermediate (106°, 72°), 3 = maximum compression (217°, 7°). The black arrows outside the stereonet illustrate the maximum extension direction. (C) Great circles showing orientations of discrete quartz veins (0.1–4 m thick) in the Aurora district ($n = 42$), dominated by approximately north-south and N60°E trends. (D) Kinematic data from slickensided surfaces on walls of eight veins plotted using methods and symbols as in B above; computed stress axes: 1 = maximum extension (137°, 17°), 2 = intermediate (282°, 70°), 3 = maximum compression (44°, 11°); nodal planes of best-fit quadrants: 179°, 70°; 271°, 86°. The black arrows outside the stereonet illustrate the maximum extension direction. (E) Great circles showing orientations of banding (0.3–1.5 cm) and vein margins of banded quartz-calcite veins (0.2–0.6 m thick) in the Bodie district ($n = 46$). (F) Poles to banded vein orientations in E above, with calculated Kamb contours (contour interval = 2) using Rick Allmendinger's contouring software, StereoWin for Windows (<ftp://www.geo.cornell.edu/pub/rwa/Windows/StereoWinFull120.zip>; for the latest version of the software, see <http://www.geo.cornell.edu/geology/faculty/RWA/programs/stereonet-7-for-windows.html>). Contour maximum (11°, 298°) is interpreted as maximum extension direction (black arrows) during veining.

east-elongate stepover grabens linked to east-northeast-striking left-lateral faults (some of which are still active; Wesnousky, 2005) along the north Mono Basin escarpment. These features suggest greater variation in differential horizontal stress during formation of the Aurora volcanic field.

Bodie Hills volcanic rocks are inferred to record a progressive change in the regional



stress field. Prior to ca. 10 Ma, low differential horizontal stresses with northward compression and westward extension (corrected for tectonic rotations) resulted in subcircular, polygenetic volcanoes with episodes of hydrothermal mineralization controlled by conjugate sets of strike-slip faults. After ca. 10–9 Ma, the maximum compressive stress axis became vertical, and extension-related veins accompanied a progres-

sive westward migration of stage 3 dacitic to trachyandesitic magmatism. The change in stress field is approximately coincident with northward migration of the Mendocino triple junction and the inferred cessation of subduction beneath the Bodie Hills. Following a 2 Ma hiatus, a narrow, north-trending belt of rhyolitic magmatism in the western part of the Bodie Hills may have been localized ca. 6 Ma by normal faults reflective of

more west-directed extension. Pliocene–Pleistocene magmatism was even more strongly controlled by north-striking extensional faults, which formed stepover grabens in a system of northeast-striking left-lateral faults.

MIOCENE MINERAL DEPOSITS AND ALTERATION ZONES

Significant magmatic-hydrothermal mineral deposits and large areas of hydrothermally altered rock in the Bodie Hills are intimately associated with the evolution of the Bodie Hills volcanic field (Figs. 4 and 16; Table 5). The most important deposits are gold-silver veins at Bodie and Aurora and a stratiform sulfur resource in Cinnabar Canyon. Other Miocene mineral resources include Au-Ag-Cu fault breccia and replacement deposits at Masonic and four small mercury replacement, vein, and sinter deposits on the northwest side of Potato Peak (Alta Plana mine), in Cinnabar Canyon (Calmono-Old Timer mine), near the headwaters of Rough Creek (Paramount mine), and near Spring Peak (Fig. 16; Table 5). The sulfur resource and the first three mercury deposits are within aerially extensive alteration zones.

Reported production from veins in the Bodie district is 1.46×10^6 troy oz (i.e., 45,411,076 g) Au and 7.3×10^6 troy oz (227,055,382 g) Ag recovered from ~ 1.5 Mt of ore (Long et al., 1998). Veins formed at 8.4–8.2 Ma (Table 2; Berger et al., 1999) are hosted by flows, domes, and breccias of the ca. 9 Ma Silver Hill dacite complex. Reported production from veins in the Aurora district is 1.91×10^6 troy oz (59,407,641 g) Au and 20.6×10^6 troy oz (640,731,626 g) Ag recovered from ~ 3.9 Mt of ore (Long et al., 1998). Veins in the Aurora district formed ca. 10.3 Ma (Breit, 2000). Most veins are hosted in ca. 13 Ma trachyandesite of Aurora, although some occur in the 11.2 Ma rhyolite of Aurora Creek. Veins in both districts strike north to northeast, dip east and west at high to moderate angles, and can be traced for tens to hundreds of meters (Fig. 11B). The most productive veins are tabular, banded, and <1 m thick (Fig. 11D); ore was largely mined within several hundred meters below the surface. Veins consist mostly of quartz and adularia, with lesser pyrite, K-mica, calcite, silver minerals, and electrum. In both districts, veins formed 0.5–1 Ma after emplacement of their host domes. Exposed parts of veins are inferred to have formed at depths ranging from essentially the paleosurface (north end of Bodie) to several hundred meters below the paleosurface (main part of Bodie and Aurora) (Herrera et al., 1991; Osborne, 1991).

Reported production from tabular fault breccias and replacement deposits at Masonic is

0.06×10^6 troy oz (1,866,209 g) Au and 0.04×10^6 troy oz (1,244,139 g) Ag recovered from 0.08 Mt of ore (Long et al., 1998). Ore-bearing structures are 1–2-m-wide breccia zones and centimeter-wide veins in a series of en echelon north- and northeast-striking curvilinear faults in Mesozoic granitic and metamorphic rocks and in ca. 14.7–14.0 Ma trachyandesite flows and volcaniclastic strata of the Masonic eruptive center (Fig. 11A). Fault breccia matrices and veins consist of quartz, alunite, kaolinite-dickite, enargite and other Cu-As-Sb-S minerals, and barite (Vikre and Henry, 2011). Finely bedded hydrothermal sediments locally fill cavities in breccias in Mesozoic rocks in the Sarita and Lakeview mines (Fig. 11F) and suggest formation near the paleosurface. Because these mines are near the inferred center of the Masonic volcano along fault contacts between unaltered Mesozoic basement rocks and strongly altered Miocene volcanic rocks, the presence of the near-surface sediments indicates that there has been significant uplift of basement rocks and erosion of the Masonic stratovolcano.

The unexposed sulfur resource in Cinnabar Canyon (Cinnabar Canyon sulfur deposit, ~ 2.9 Mt sulfur; Ward, 1992) is hosted by a sequence of volcaniclastic rocks and andesite lavas probably derived from the ca. 9 Ma Mount Biederman stratovolcano. Permeable volcaniclastic rocks were pervasively leached and replaced ca. 8.7 Ma by quartz-alunite-kaolinite-pyrite-sulfur assemblages (Table 5; Cinnabar Canyon alteration zone; Vikre and Henry, 2011), possibly in response to degassing of magma represented by the stage 3 trachy-andesite domes. In the Cinnabar Canyon sulfur deposit, sulfur fills leached phenocryst and clast sites and fractures in volcaniclastic strata immediately northwest of Cinnabar Hill. The small Calmono-Old Timer Hg mine is in leached and clay-altered volcaniclastic strata and flows at the south base of Cinnabar Hill (Table 5). Altered volcaniclastic rocks extend ~ 8 km from Cinnabar Canyon northwest to U.S. Highway 395, but alunite from near U.S. Highway 395 is somewhat younger, ca. 8.2 Ma (Table 2).

Large (~ 25 – 30 km 2) alteration zones extend from the west side of Bald Peak to the Paramount Hg mine (Paramount–Bald Peak alteration zone; Fig. 15; Table 5), and from the East Walker River to Fletcher Valley (Red Wash alteration zone). The stratiform Paramount–Bald Peak alteration zone is mostly hosted in ca. 9.6 Ma and older volcaniclastic deposits (tuff of Paramount) deposited in the northeast-elongated Paramount basin (the basal part of the Eureka Valley Tuff, the ca. 9.7 Ma Tollhouse Flat Member(?), is locally altered). It includes sinter at the Paramount Hg mine (Fig. 11E; Holmes, 1965),

sinter and silicified clay-altered sandstone and conglomerate south and north of the Paramount mine, and sinter, silicified clay-altered tuff, and tuff breccia with chalcedonic silica veins between Atastral Creek and Bald Peak. The stratiform and largely stratabound, east-west-oriented Red Wash alteration zone formed in coarse volcaniclastic strata that are part of the ca. 14.7–14.0 Ma Masonic stratovolcano. The permeable volcaniclastic rocks were pervasively replaced by quartz, alunite, kaolinite, pyrite, and other clay minerals ca. 13.3 Ma, but contain no identified mineral resources. Smaller quartz-alunite-dominant alteration zones are present on the northwest side of Potato Peak (Potato Peak alteration zone), in Aurora Canyon (Aurora Canyon alteration zone), on East Brawley Peak (East Brawley Peak alteration zone) and 1 km west of Aurora (Sawtooth Ridge alteration zone). A small area of silicified hydrothermal eruption breccia (Four Corners) is in distal volcaniclastic deposits associated with the Masonic center. Sinter overlying Mesozoic rocks (Spring Peak sinter; Table 5) contains small Hg prospects.

DISCUSSION

Magmatic Evolution of the Bodie Hills Volcanic Field

Middle Miocene Bodie Hills volcanic field rocks were erupted onto an erosional surface developed on Late Cretaceous and older basement rocks. Paleosols are locally preserved, but Tertiary sedimentary rocks are not exposed beneath the Miocene volcanic rocks. Unlike other areas in the western Great Basin, west-draining Eocene to Early Miocene paleochannels apparently did not cross the 40 km north-south width of the Bodie Hills.

Eruptive activity in the >700 km 2 Bodie Hills volcanic field spanned ~ 9 Ma and produced four trachyandesitic stratovolcanoes with associated debris flow aprons near the margins of the field, and numerous silicic trachyandesite to rhyolite flow dome complexes were emplaced generally more centrally within the field (Figs. 3 and 17). Volcanism waxed and waned during development of the Bodie Hills volcanic field but was distinctly more voluminous between ca. 14.7–12.9 Ma and 9.2–8.0 Ma (Fig. 4). The large Masonic (erupted volume >150 – 200 km 3) and Aurora stratovolcanoes formed early during evolution of the field and produced its most mafic rocks. The composite Silver Hill–Potato Peak–Willow Springs dome complexes (erupted volume ≥ 100 km 3) formed late in its development. Stratovolcanoes were active for hundreds of thousands of years, and late in their evolution,

Bodie Hills volcanic field

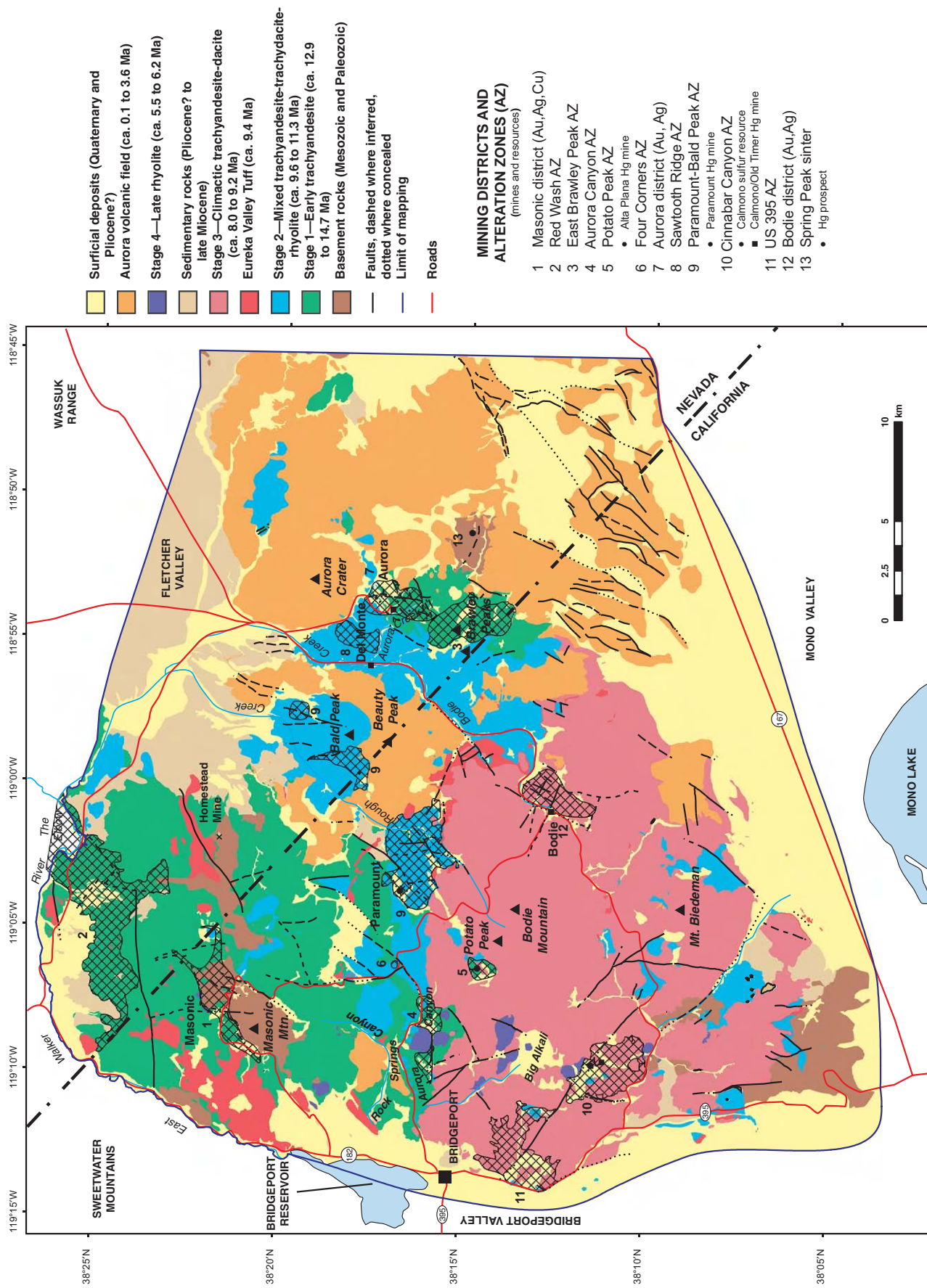


Figure 16. Generalized geologic map (from Fig. 3) showing mining districts, prospects, and alteration zones.

TABLE 5. CHARACTERISTICS OF TERTIARY MINING DISTRICTS, DEPOSITS, RESOURCES, AND ALTERATION ZONES IN THE BODIE HILLS, CALIFORNIA-NEVADA

Number (Fig. 16)	Name (AZ, alteration zone)	Age (Ma)*	Production and/or resources†	Type of deposit or alteration	Host rocks	Dimensions of mineralized and altered rocks
1	Masonic district	13.4 to 13.0 (Ar-Ar alunite)	55,000 oz Au, 39,000 oz Ag, 900 lbs Cu	High-sulfidation Au-Ag	Mesozoic metamorphic and granitic rocks, volcaniclastic rocks and lava flows of Masonic center	Northeast-trending altered zone to 1 km wide and 7.5 km long
2	Red Wash AZ	13.3 to 13.4 (Ar-Ar alunite)	None	Quartz-alunite alteration	Volcaniclastic rocks of Masonic center	East-to-east-northeast-elongate zone (~30 km ² total area)
3	East Brawley Peak AZ	12.5 to 12.0 (Ar-Ar alunite)	None	Quartz-alunite alteration	Trachyanadesite lavas and breccias of Aurora center	Elliptical zone ~4 km north-northwest by ~2 km west-east (~7 km ² total area)
4	Aurora Canyon AZ	10.8 (Ar-Ar alunite)	None	Quartz-alunite alteration	Trachyanadesite lavas and breccias of Masonic center	Irregular zone ~4.5 km east-west by 0.5- 1.0 km north-south (~3 km ² total area)
5	Potato Peak AZ	10.8 (Ar-Ar alunite)	Small Hg production (Alta Plana mine) None	Replacement	Volcaniclastic rocks of Masonic center(?)	Circular zone ~1.3 km in diameter (~1.3 km ² total exposed area)
6	Four Corners AZ	Undated; <14. >10.4		Silicified hydrothermal breccia	Trachyanadesite of Masonic center	Two outcrops ~60 m wide forming arc ~300 m long
7	Aurora district	10.6 to 10.1 (adularia)	1.91 Moz Au, 20.62 Moz Ag	Low-sulfidation epithermal Au-Ag vein	Aurora center trachyanadesite and Aurora Creek center rhyolite	Area containing quartz veins ~1-2 km east- west by 3.5 km north-south; contiguous with older East Brawley Peak AZ to south
8	Sawtooth Ridge AZ	Undated; <11 Ma	None	Quartz-alunite alteration	Rhyolite flow domes of the Aurora Creek center	Rectangular ~1 km east-west by 2 km north-south (2 km ²)
9	Paramount basin-Bald Peak AZ	Undated; ca. 9.5 based on stratigraphy	Small Hg production (Paramount mine)	Stratiform hot-spring alteration	Rhyolitic tuffs and volcaniclastic rocks deposited in Paramount basin	Elongated zone, ~8 km northeast by 2-3 km northwest (~16 km ² total exposed area)
10	Cinnabar Canyon AZ	8.7 (Ar-Ar alunite)	Calimno: 16.8 Mt @ 17.9% S ⁰ (resource, 1982); Small Hg production (Calmono- Old Timer mine)	Stratiform sulfur	Volcaniclastic flow sequence of Mount Biederman center	Elliptical zone ~5.5 km northwest-southeast by 3 km northeast-southwest (~13 km ² total area); concealed sulfur deposit covers ~0.12 km ²
11	US 395 AZ	8.2 (Ar-Ar alunite)	None	Quartz-alunite alteration	Volcaniclastic flow sequence of Mount Biederman center	Circular zone ~4.5 km in diameter (~16 km ² total area)
12	Bodie district	8.4 to 8.2 (Ar-Ar adularia)	1.458 Moz Au, 7.28 Moz Ag, 75 Mt @ 0.037 oz/t Au (1995)	Low sulfidation epithermal Au-Ag vein	Flow domes, breccias, and volcaniclastic rocks of the Silver Hill center	North-northeast-elongated alteration zone ~1.2 km east-west by 3.5 km north-nor- east-south-southwest (total area ~6 km ²)
13	Spring Peak	Undated		Sinter	None	5-m-thick sinter covering ~0.04 km ²
Number (Fig. 16)		Style and controls of alteration and mineralization		Ore mineral associations	Other features	References
1	Narrow veins and breccias along north- and northeast-striking faults	Residual quartz, alunite, kaolinite-dickite, pyrophyllite, pyrite	Enargite, ilzonite, tennantite, sphalerite, electrum, barite, sulfur	Finely laminated beds of quartz-enargite sediment fill voids in volcaniclastic rocks in Sarita and Lakeview mines	Vikre and Henry, 2011	
2	Permeable volcaniclastic rocks	Quartz, alunite, kaolinite, dickite, pyrophyllite, pyrite	None	Partly covered by colluvium	Vikre and Henry, 2011	
3	Replacement zones along north-northwest- and west-southwest-striking faults	Quartz, alunite, kaolinite, dickite, pyrite	None		Breit, 2000; Vikre and Henry, 2011; this study	
4	East-west-elongate replacement zones	Quartz, alunite, clay minerals, pyrite	None		Vikre and Henry, 2011	
5	Permeable volcaniclastic rocks	Quartz, alunite, kaolinite, pyrite	Cinnabar		Holmes, 1965; Vikre and Henry, 2011	
6	Silicified bedded breccia	Quartz, hematite, kaolinite, montmorillonite	None		This study	
7	Quartz veins along northeast- and north-striking faults; most production from northeast veins	Quartz, carbonate, adularia, illite, chloride, pyrite	Electrum, Ag sulfides, Ag selenides, chalcocite, galena, arsenopyrite, fluorite, barite		Osborne, 1991; Kleinhampl et al., 1975; Breit, 2000	
8	Replacement zones in permeable tuffs and breccias related to domes	Silica minerals, kaolinite, dickite, alunite	None		Rockwell, 2010; this study	
9	Replacement zones in permeable tuffs and volcaniclastic rocks	Quartz, chalcedony, opaline silica, kaolinite, alunite, illite, montmorillonite, pyrite	Cinnabar		This study	
10	Permeable tuffs and volcaniclastic rocks	Quartz, chalcedony, opaline silica, kaolinite, montmorillonite and/or illite, pyrite	Cinnabar		Holmes, 1965; Ward, 1992; Vikre and Henry, 2011	
11	Replacement of shallow dipping volcaniclastic rocks	Silica minerals, kaolinite, dickite, alunite, illite and/or montmorillonite, pyrite	None		Vikre and Henry, 2011; this study	
12	Quartz veins along north- to north-northeast- striking faults	Quartz, adularia, illite, calcite, pyrite montmorillonite, chlorite, pyrite	Electrum, Ag sulfides and sulfosulfates, galena, sphalerite, chalcopyrite, tetrahedrite		Chesterman et al., 1986; Herrera et al., 1991, 1993; Berger et al., 1999	
13	Sinter terrace	Opaline and chaledonic silica, minor illite and/or montmorillonite, pyrite	Cinnabar		This study	

*See Table 2 for $^{40}\text{Ar}/^{39}\text{Ar}$ ages of alteration minerals.

†Production data from Long et al. (1998).

Bodie Hills volcanic field

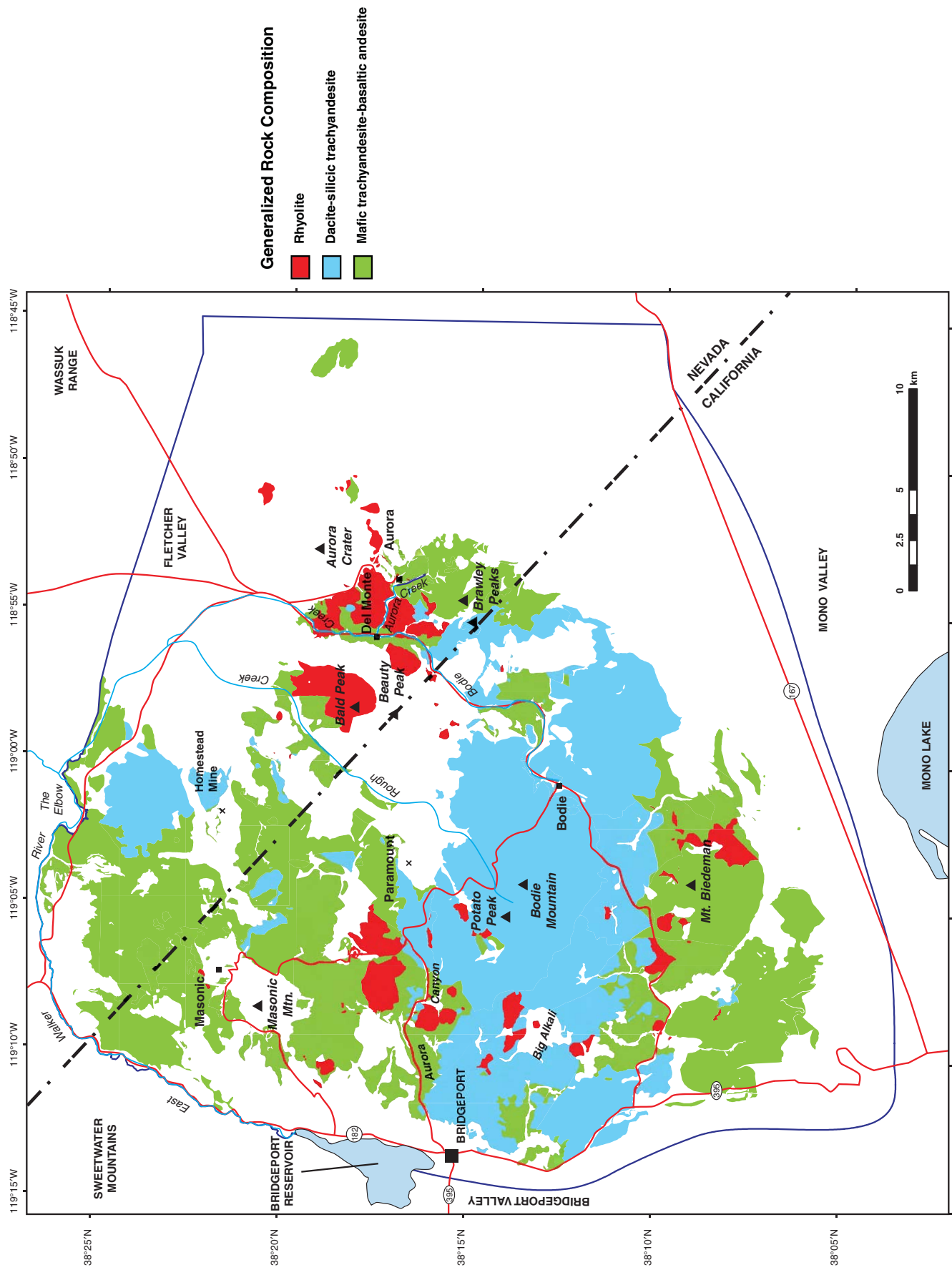


Figure 17. Geologic map of the Bodie Hills volcanic field showing generalized bulk compositions of major eruptive units. Eruptive units are separated into groups based on SiO₂ contents: basaltic andesite-mafic trachyandesite (<61% SiO₂), silicic trachyandesite-trachydacite (61%–68% SiO₂), and rhyolite (>68% SiO₂).

magmatic-hydrothermal systems developed in the Masonic and Aurora mining districts and in the Red Wash alteration zone. Northeast- and north-striking faults active late during this volcanism (after 14 to ca. 12.8 Ma) probably exposed Mesozoic basement rocks within the Masonic stratovolcano and possibly exposed Mesozoic basement near Aurora.

An apparent 1.5 Ma hiatus in volcanism between ca. 12.9 and 11.3 Ma followed late-stage dome emplacement in the Masonic center, formation of the Aurora volcano, and Rough Creek dome complex emplacement. Volcanism resumed ca. 11.3 Ma with formation of the West Brawley Peak stratovolcano and eruption of lavas from the poorly defined Rancheria volcano and emplacement of small intrusions in Aurora Canyon, and lasted nearly continuously until 8.0 Ma. A short gap in volcanic activity between ca. 9.6 and 9.2 Ma may separate magmatism represented by the Bodie Hills and Bald Peak rhyolite dome complexes from that of the Mount Biedeman volcano. Epithermal Au-Ag vein deposits in the Aurora and Bodie districts formed ca. 10.3 and 8.4 Ma, respectively, shortly after emplacement of their host rhyolite and dacite domes. The large Paramount–Bald Peak alteration zone formed ca. 9.5 Ma and probably is related to the magmatism that formed the Bald Peak rhyolite dome. Large volume volcanism in the Bodie Hills volcanic field ended at 8.0 Ma but was followed by a small-volume episode of silicic dome emplacement between 6.2 and 5.5 Ma.

Petrogenetic Implications of Bodie Hills Volcanic Field Geochemistry

Bodie Hills volcanic rocks are subalkaline and calc-alkalic, consistent with genesis in a subduction-related continental magmatic arc setting. Trace element characteristics also indicate a subduction-related origin. Each of the Bodie Hills units is characterized by well-developed negative Nb-Ta anomalies and ratios of Ba, Ta, La, Th, and Nb well within the ranges typical of arc magmas. One of the most distinctive features of the Bodie Hills volcanic field rocks is elevated K₂O content. Volcanic rocks in other volcanic fields of the southern segment of the ancestral Cascades arc also display elevated K₂O abundances (Fig. 18; Putirka and Busby, 2007; Cousens et al., 2008). MASH (melting, assimilation, storage, and homogenization) zone processes that foster assimilation of K-rich continental crust by subduction-related, mantle-derived partial melts (Hildreth and Moorbath, 1988) probably contributed to the high-K signature characteristic of the Bodie Hills volcanic rocks. Elevated K₂O abundances have

been attributed to increased hybridization of arc magmas that transit thick continental crust (Feeley and Davidson, 1994). In particular, most samples of the third REE geochemical group (which includes most of the rhyolitic rocks in the Bodie Hills) have distinctive Ce/Pb, Th/La, and K/P indicative of significant granitoid wall-rock assimilation (Supplemental Figs. 10–12 in Supplemental Figure File [see footnote 3]). However, Putirka and Busby (2007) argued convincingly that elevated K₂O abundances characteristic of ancestral Cascades arc rocks in central Sierra Nevada result from varying degrees of mantle partial melting and subsequent fractional crystallization. Such a model does not require unusual enrichment and/or depletion processes to have affected mantle sources. Elevated K₂O abundances characteristic of the Bodie Hills rocks probably reflect a complex combination of these processes.

Each of the Bodie Hills volcanic field rock units has relatively distinctive geochemical features. Geochemical variation within most of these units is minimal, which suggests that fractionation in their source reservoirs was limited. In particular, within-unit REE abundance variations are minor, constituent patterns are parallel, and small negative Eu anomalies are of fixed magnitude. Consequently, intraunit compositional variation is consistent with varying small amounts of interstitial liquid loss among samples of any given unit.

The existence of three distinct groups of REE abundances among the Bodie Hills volcanic field rocks suggests at least as many reservoirs for these rocks. These distinct reservoirs suggest that multiple sources and/or various assimilation and/or homogenization pathways are responsible for magmas represented by the Bodie Hills units. Small amounts of accessory mineral fractionation or equilibration with crustal rocks containing such accessory minerals may have contributed to the trace element signatures characteristic of individual rock units. Ongoing research targets establishing more definitively the fine-scale petrogenesis of these rocks.

Crustal Controls on Localization and Emplacement of the Bodie Hills Volcanic Field

The Bodie Hills are associated with a region of low gravity bounded on the north, south, and east by northeast- and west-northwest-striking gravity gradients (Fig. 6A, white dashed lines). The bulk of Bodie Hills magmatism was centrally localized within laterally restricted exposures of pre-Tertiary rocks east of Masonic Mountain, south of Aurora, and west of Mt. Biedeman (Fig. 3), and a broad gravity low

also is focused between these three pre-Tertiary exposures. We observe local gravity highs that generally coincide with the exposed pre-Tertiary rocks, notably the gravity high immediately south of Aurora (Fig. 6A). On the basis of this correlation, we interpret large positive anomalies to the north, south, and east of the Bodie Hills as originating from pre-Tertiary basement at or near the topographic surface, and the bounding linear gradients (Fig. 6A, white dashed lines) as contacts between relatively low density rocks beneath the Bodie Hills and relatively high density, pre-Tertiary metamorphic basement.

The broad gravity low is likely caused by one or a combination of two lithologies: low-density volcanic rocks of the Bodie Hills, and/or low-density silicic intrusive rocks that underlie the Bodie Hills. We favor the latter interpretation because topography and gravity anomalies are not spatially correlated, indicating that the gravity lows are related to lithologies below the volcanic edifices. The interpreted silicic intrusive rocks are completely concealed beneath the Bodie Hills and Aurora volcanic fields and are probably either an eastward protrusion of the Mesozoic Sierra Nevada batholith, which causes broad gravity lows to the west (Fig. 5), or late Cenozoic felsic intrusive rocks related to Bodie Hills volcanism. We cannot distinguish between these two ages of plutonic rocks from gravity anomalies alone, but the association of the Bodie Hills gravity low with Bodie Hills volcanic rocks strongly supports the latter interpretation. Specifically, the latter interpretation is consistent with our geologic mapping (Fig. 17), which portrays siliceous (lower density) rocks in the center of the Bodie Hills volcanic field, where gravity is lowest, and more mafic (higher density) rocks on the periphery of the field.

The Masonic volcano is along the most prominent west-northwest-striking gravity lineament (Fig. 6A). Low gravity on the southwest side of the lineament may correspond with the intrusive roots of the Masonic volcano, whereas gravity highs on the northeast side of the lineament are presumably caused by concealed pre-Tertiary basement. Similarly, the Mount Biedeman stratovolcano is coincident with another prominent northwest-striking lineament at the southern margin of the gravity low. Other gravity gradients (white dotted lines in Fig. 6A) with similar west-northwest and northeast orientations are within the rhomboid-shaped gravity low. We tentatively interpret these gravity gradients to indicate crustal boundaries (possibly faults) within the underlying pre-Tertiary basement that localized emplacement of intrusions associated with the Bodie Hills volcanic field.

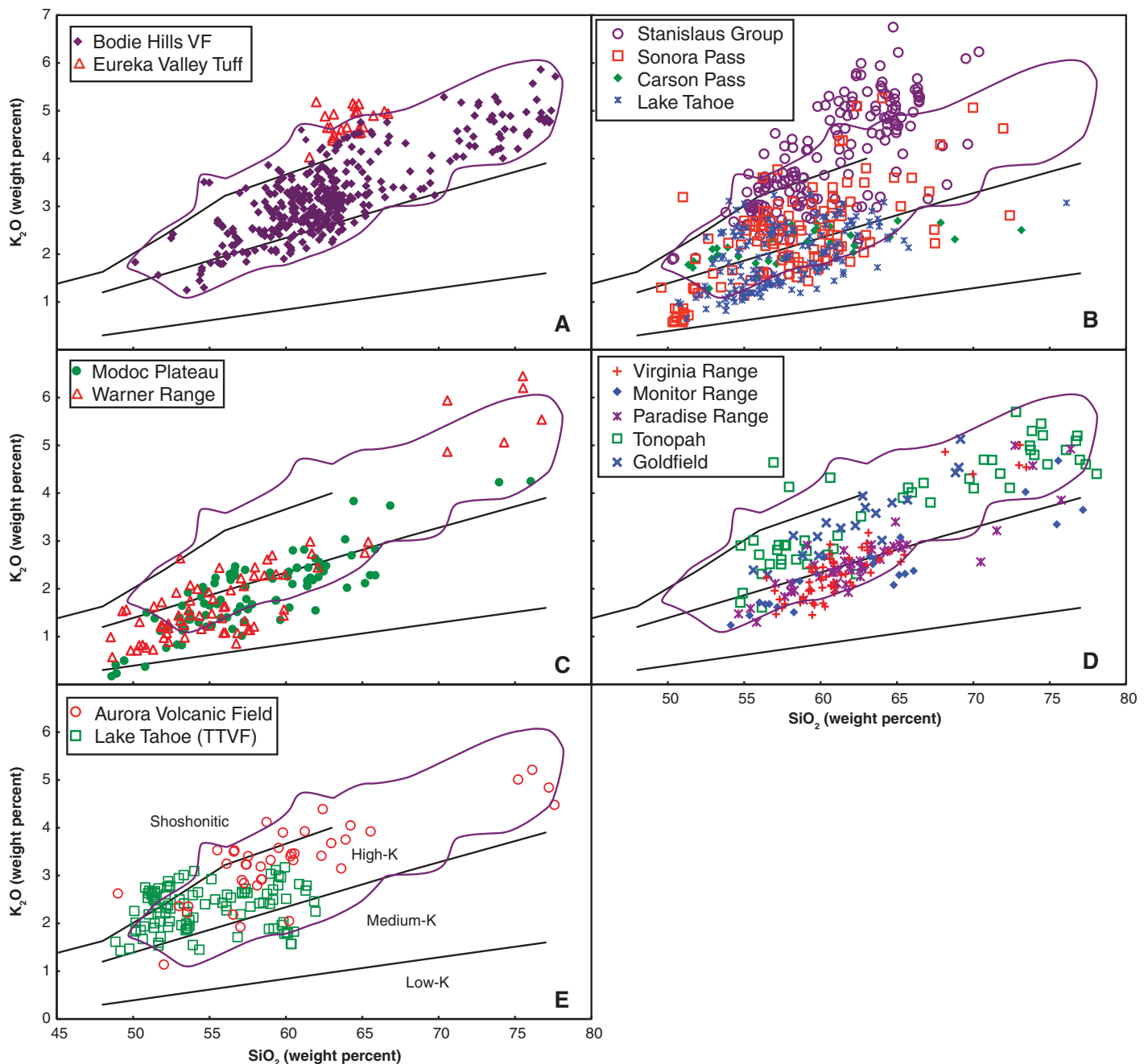


Figure 18. K_2O - SiO_2 diagrams for ancestral arc rocks and postsubduction rocks in northeastern California and northwestern Nevada. (A) Bodie Hills volcanic field and Eureka Valley Tuff in the Bodie Hills. (B) Central Sierra Nevada (Sonora Pass, Carson Pass, and Lake Tahoe) and Stanislaus Group in the central Sierra Nevada, which is composed of the Table Mountain Latite, Eureka Valley Tuff, and Dardanelles Formation. (C) Warner Range and Modoc Plateau between the Warner Range and Lassen Peak. (D) Monitor Range and west-central Nevada. (E) Pliocene–Pleistocene postsubduction rocks in the Bodie Hills (Aurora volcanic field) and the Lake Tahoe area (Tahoe-Truckee volcanic field, TTVF). Purple line encloses data for the Bodie Hills volcanic field. Data are from du Bray et al. (2009), C.D. Henry (2010, written commun.), Cousens et al. (2011), Colgan et al. (2011), and our data for the Monitor Range and southwest Paradise Range. Field boundaries on K_2O versus SiO_2 diagram are from Le Maitre (1989); high K-shoshonitic dividing line is from Ewart (1982). All major oxide analyses normalized to 100% volatile-free prior to plotting.

Several positive magnetic anomalies (Fig. 8A) suggest magnetic intrusions at depths of ~2 km below the present topographic surface. Magnetic data, filtered in order to emphasize magnetic sources at 1.9 km depth (Fig. 8A), include positive anomalies associated with known volcanic edifices. Potato Peak, Bodie Mountain, and West Brawley Peak are essentially coincident with pronounced positive magnetic anomalies (Fig. 8A). Thus, the negative gravity anomalies probably indicate deep silicic plutonic rocks, emplaced either before or during Bodie Hills magmatism. These inferred deep plutonic rocks are beneath shallow magnetic intrusions coincident with positive magnetic anomalies that are directly associated with some of the Bodie Hills volcanic centers.

Magnetic anomalies indicate that most of the volcanic centers are approximately circular in shape, which suggest that magma emplacement was localized in a relatively uniform horizontal stress field rather than along linear zones that would result from a differential horizontal stress field. In contrast, a particularly prominent magnetic lineament strikes northeast and separates the Masonic volcano from the Potato Peak, Bald Peak, Beauty Peak, and other volcanic centers (Fig. 8, black dashed line). This time-transgressive alignment of volcanic centers corresponds to the northwest side of the Paramount basin and may indicate a crustal fault of regional extent.

Localization of the Bodie Hills Volcanic Field

Miocene Bodie Hills magmatism was focused by complex interactions between the Walker Lane, a northwest-striking zone of right-lateral faults accommodating dextral shear between the Pacific and North American plates, and the Mina deflection, a broad east-west zone of faults of various types that accommodates a 60 km right step in the Walker Lane (Stewart, 1988, 1992; Oldow, 2003; Faulds and Henry, 2008). The Bodie Hills are situated between the right-lateral Walker Lane and the little deformed Sierra Nevada block, northwest of the Mina deflection (Fig. 2). Miocene volcanism in the Bodie Hills began between 15 and 14 Ma, synchronous with the onset of large-magnitude east-west extension ~50 km to the north near Yerington (Dilles and Gans, 1995; Stockli et al., 2002; Surpless et al., 2002). Extensional faulting progressively stepped westward from Yerington to the modern Sierran front along the Genoa fault east of Lake Tahoe by 3 Ma (Fig. 2). However, neither large-magnitude 15–14 Ma extension nor the Pliocene and younger range-bounding faults continue southward from the latitude of Yerington into the Bodie Hills. These features appear to end

north of a series of northeast-striking, down-to-the-southeast normal faults 5–10 km northwest of the Bodie Hills (Fig. 2). These northeast-striking faults displace the 9.4 Ma Eureka Valley Tuff, and the northeasternmost of these faults bounds the Coal Valley basin, which contains strata at least as old as 11.7 Ma (Gilbert and Reynolds, 1973). These northeast-striking faults approximately parallel the left-lateral faults of the Mina deflection farther south. The initiation of movement on faults of the Mina deflection is poorly constrained, and is considered to be post-10 Ma (Stockli et al., 2003), 6–8 Ma (Oldow et al., 2008), or even 3 Ma (Tincher and Stockli, 2009), all much younger than the 15–14 Ma initiation of Bodie Hills volcanism. Thus, although modern fault systems and extensional zones may have affected later phases of Bodie Hills magmatism, they appear to be too young to have influenced its onset. However, the Mina deflection may have been localized by pre-Tertiary structures, notably the margin of the Neoproterozoic craton (Figs. 1 and 2; Wetterauer, 1977; Stewart, 1988; Tosdal et al., 2000; Faulds and Henry, 2008). Interaction of these older east-west structures with large-scale east-west extension to the north of the Bodie Hills may also have helped focus the early episodes of Bodie Hills magmatism.

Tectonic Implications of the Distribution of Eureka Valley Tuff

The distribution of Eureka Valley Tuff suggests that several of its outflow lobes were channeled around and across the Bodie Hills (Fig. 7E). The tuff is thought to have erupted from the Little Walker center ~20 km west of the Bodie Hills (Fig. 2; Noble et al., 1974; King et al., 2007; Pluhar et al., 2009), and to have flowed away from its source down the paleotopography. The widespread distribution of the tuff both west and east of the Little Walker center, especially its presence in the Bodie Hills, indicates that since 9.4 Ma there has not been significant strike-slip displacement between the Little Walker center and the Bodie Hills and that the Little Walker center must have been at a higher elevation than the Bodie Hills at 9.4 Ma. This latter relationship suggests either the presence of a significant volcanic edifice when the tuff erupted or, more likely, that uplift of the Little Walker center (and possibly the central Sierra Nevada) relative to the Bodie Hills began prior to eruption of the Eureka Valley Tuff. Busby et al. (2008), Busby and Putirka (2009), and C.J. Busby (2011, written commun.) showed that Basin and Range faulting began in the central Sierra Nevada ca. 11 Ma and was coincident with development of the Little Walker center.

The fault-bounded Coal Valley and Fletcher basin strata on the northeast side of the Bodie Hills contain tephra dated as 11.7 Ma (Gilbert and Reynolds, 1973), which also suggests that Basin and Range faulting began in the area prior to eruption of the Eureka Valley Tuff. Elsewhere in the western Basin and Range, rapid extension began ca. 15–14 Ma in the Yerington area–central Wassuk Range, 40–50 km north of the Bodie Hills (Fig. 2; Dilles and Gans, 1995; Stockli et al., 2002; Surpless et al., 2002), while uplift and tilting began ca. 12 Ma in the White Mountains, 70 km southeast of the Bodie Hills (Fig. 2; Stockli et al., 2003). These relations suggest that Basin and Range faulting began and the Bodie Hills were downfaulted relative to the Little Walker center prior to eruption of the Eureka Valley Tuff ca. 9.4 Ma.

In the central part of the Bodie Hills, the present-day elevation at the base of the Eureka Valley Tuff progressively increases from ~1800 m at Bridgeport Reservoir to 2800 m on the north side of Potato Peak and then decreases eastward to <2500 m in Rough and Bodie Creeks, forming an asymmetric domal pattern encompassing the topographic Bodie Hills, centered on Potato Peak, and indicating significant deformation of the distribution of the tuff following its deposition. This pattern may record structural doming of the central Bodie Hills following eruption of the Eureka Valley Tuff, possibly due to emplacement of a shallow magma chamber or chambers, which sourced the Silver Hill, Potato Peak, and Willow Springs dome complexes. Gravity data discussed herein suggest that silicic plutons may underlie these complexes in the center of the Bodie Hills. Alternatively, this pattern might indicate rollover in the upper plate of the arcuate set of normal faults dipping beneath the northwest side of the Bodie Hills (continuation of the Coal Valley fault mentioned above) or other unrecognized faults.

Regional Style and Composition of Southern Ancestral Cascades Arc Magmatism

The Bodie Hills volcanic field is similar to other large, long-lived volcanic fields in the southern part of the ancestral Cascades arc, including those in the Virginia Range near Virginia City (Hudson et al., 2009), the Monitor Range (eastern part of Ebbets Pass–Markleeville volcanic field) (John et al., 1981; Vikre and Henry, 2011), and on the east side of the Walker Lane, including the Gabbs Valley Range–southwest Paradise Range (Ekren et al., 1980; John, 1992), at Tonopah (Bonham and Garside, 1979), and at Goldfield (Ashley, 1974). Typical eruptive sequences in these fields include early,

more mafic (andesite and/or basaltic andesite) lavas and debris flows that are overlain and intruded by more silicic flow dome complexes (dacite and rhyolite). Stratovolcanoes have been identified in several fields (Bodie Hills, Virginia Range, Monitor Range) but are not recognized in fields farther east, where small cones and dome fields are more common. Most volcanic centers are relatively equidimensional and lack sheeted dike swarms and other elongated features, which suggest they formed during periods of low differential horizontal stress. Most ancestral arc volcanic fields hosted large cogenetic hydrothermal systems, and significant epithermal Au-Ag deposits are associated with the Bodie Hills, Virginia Range, Tonopah, Goldfield, and Paradise Range centers. The Bodie Hills volcanic field is exceptional for its long duration and complexity, which includes multiple periods of andesitic stratovolcanoes, silicic dome magmatism, and numerous hydrothermal systems (Fig. 4).

The style and composition of ancestral arc volcanism in the Bodie Hills and other large volcanic fields in the Walker Lane contrast with ancestral arc volcanism in the central Sierra Nevada and northeastern California. Mafic rocks with SiO_2 contents <55% are distinctly uncommon in fields within the Walker Lane, where andesite and dacite dominate (Figs. 19 and 20). Although intermediate to felsic compositions, especially andesite, are abundant, basalts and basaltic andesites are much more common in the northwestern parts of the ancestral arc, especially north of Lake Tahoe, than in its eastern and southern parts. Though stratovolcanoes have been recognized in the Ebbetts Pass area of the central Sierra Nevada and on the north side of Lake Tahoe (Cousens et al., 2008; Busby and Putirka, 2010), lava domes with associated block and ash flows and debris flows are the dominant types of eruptive features in the central Sierra Nevada (Busby et al., 2008). Mafic shield volcanoes and coalescing lava dome fields dominate Miocene volcanism in northeastern California (Grose, 2000; Colgan et al., 2011).

The scarcity of basalts in the southeastern centers and in the Sonora Pass to Carson Pass area of the central Sierra Nevada may be due to thicker crust there than in areas farther north. Putirka and Busby (2007) suggested that thick (~35 km), low-density crust underlying the central Sierra Nevada filtered mafic magmas. In the absence of a strongly extensional stress field conducive to rapid ascent of deeply sourced magma, dry basaltic melts lack sufficient buoyancy to ascend to the surface and erupt. Magmas of this type may have stalled in the lower or middle crust, where they crystallized, differentiated, and interacted

with the crust to form MASH zones (Hildreth and Moorbath, 1988) capable of producing more silicic residual magma compositions characteristic of the central California ancestral arc segment. In northeastern California, crust underlying the northern Sierra Nevada and Modoc Plateau is much thinner (Mavko and Thompson, 1983; Zucca et al., 1986; Heimgartner et al., 2006; Putirka and Busby, 2007; Lerch et al., 2007), and deeply sourced basalt melts ascended directly to the surface and erupted. Enhanced crustal thickness similarly may have controlled eruptibility of mafic magmas in the southeastern part of the ancestral arc, resulting in the dominance of intermediate compositions in centers within the Walker Lane.

Changes in Volcanism and Tectonics as the Mendocino Triple Junction Migrated North and Subduction Ended Beneath the Bodie Hills

During the middle of Bodie Hills volcanic field development, ca. 10 Ma, the Mendocino triple junction passed north of the Bodie Hills and subduction beneath the volcanic field is inferred to have ceased (Fig. 1; Atwater and Stock, 1998). However, magmatism in the Bodie Hills continued nearly unabated with a second peak in eruptive activity between ca. 9 and 8 Ma that took place 1–2 Ma following the inferred end of subduction (Fig. 4) at ca. 10 Ma. Both the mafic trachyandesite Mount Biederman stratovolcano and numerous silicic trachyandesite, trachydacite, and rhyolite domes were emplaced after 10 Ma and are similar in composition and eruption style to earlier erupted parts of the volcanic field (Figs. 10, 12, 13, and 14). A lag of several million years between subduction ending and cessation of subduction-related magmatism is common elsewhere in the southwestern part of the ancestral Cascade arc (Cousens et al., 2008, 2011; Busby and Putirka, 2009). Continuation of magmatism for several million years following cessation of subduction beneath the Lake Tahoe area likely involved several factors, including the presence of lithospheric-scale faults that provided conduits for ascent of mantle-derived magmas (Cousens et al., 2008). In the Bodie Hills, lithospheric-scale faults also likely localized the Bodie Hills volcanic field and perpetuated long-lived volcanism.

In the Bodie Hills, a change in the regional strain pattern is also coincident with the inferred end of subduction. Between ca. 10 and 8.5 Ma, the maximum and intermediate compressive strain axes switched and maximum compression became vertical, resulting in a change from transtensional to mildly extensional deformation. The strain field became more strongly transtensional

during Pliocene to Pleistocene Aurora volcanic field magmatism, and volcanism was localized by extensional stepovers on left-lateral faults of the Mina deflection.

The Late Miocene strain pattern and style of volcanic activity in the Bodie Hills contrast sharply with the strain pattern and style of volcanism in the nearby Little Walker center–Sonora Pass area described by Putirka and Busby (2007), Busby et al. (2008), C.J. Busby (2011, written commun.), and Busby and Putirka (2010), who proposed a significant change in the strain field occurred in this area between ca. 11 and 9 Ma, and related this change to the “birth” of a Sierra Nevada microplate. They suggested that the Little Walker center is localized in a releasing stepover on right-lateral transtensional faults along the western edge of the Walker Lane. In the Sonora Pass area, this transtensional deformation resulted in very active north-northwest-striking and lesser northeast-striking faults, which allowed eruption of deeply sourced, high-K “flood lavas” (trachyandesites and basaltic trachyandesites) from 6–8-km-long fissures along north-northwest-striking microplate boundary faults. These lavas and unusually large volume volcano collapse deposits ponded in north-northwest-elongate grabens and rectilinear volcano-tectonic subsidence structures formed along the boundary faults.

Geological and Geochemical Comparison of Miocene Subduction-Related Ancestral Arc Rocks to Postsubduction Pliocene–Pleistocene Aurora Volcanic Center Rocks

Miocene, subduction-related volcanic rocks of the Bodie Hills volcanic field erupted in a structural setting different from that prevailing during eruption of postsubduction Pliocene–Pleistocene rocks of the Aurora volcanic field. The change in tectonic setting was accompanied by changes in eruptive style, volcano morphology, and petrographic characteristics of volcanic rocks erupted in the two fields. Miocene volcanic rocks of the Bodie Hills volcanic field are associated with long-lived, large-volume polygenetic stratovolcanoes and composite dome fields. These rocks include complex mixtures of lava flows, block and ash flows, flow breccias, debris flow deposits including extensive lahars, dome collapse breccias, and small exogenous domes. Most Miocene volcanic rocks are coarsely and abundantly porphyritic, biotite is a common phenocryst phase in all but the most mafic units, and Fe-Ti oxide minerals are common (Table 3). In contrast, most Aurora volcanic field rocks are lava flows related to small shield volcanoes, monogenetic cones, and small domes with associated flow breccias.

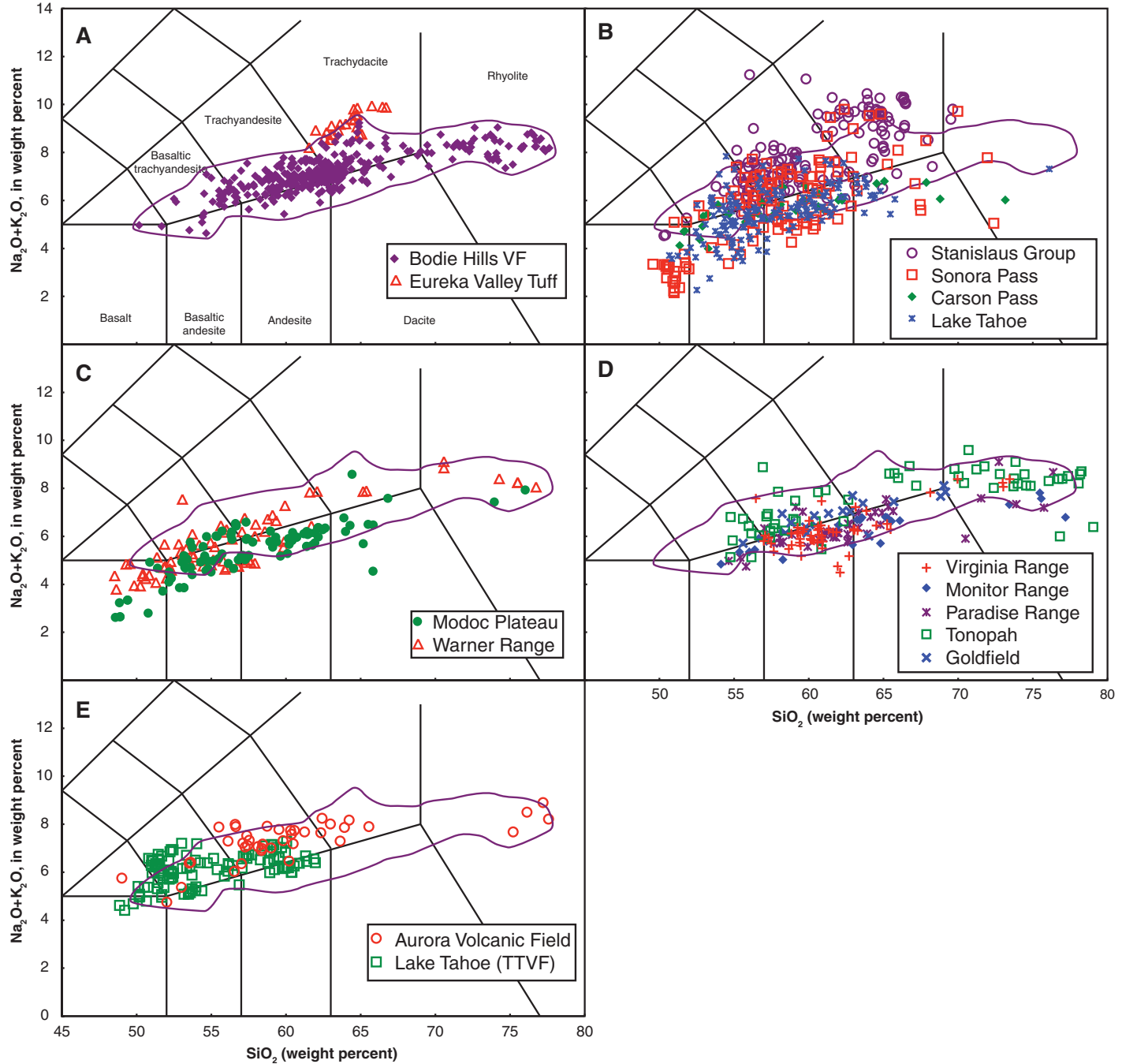
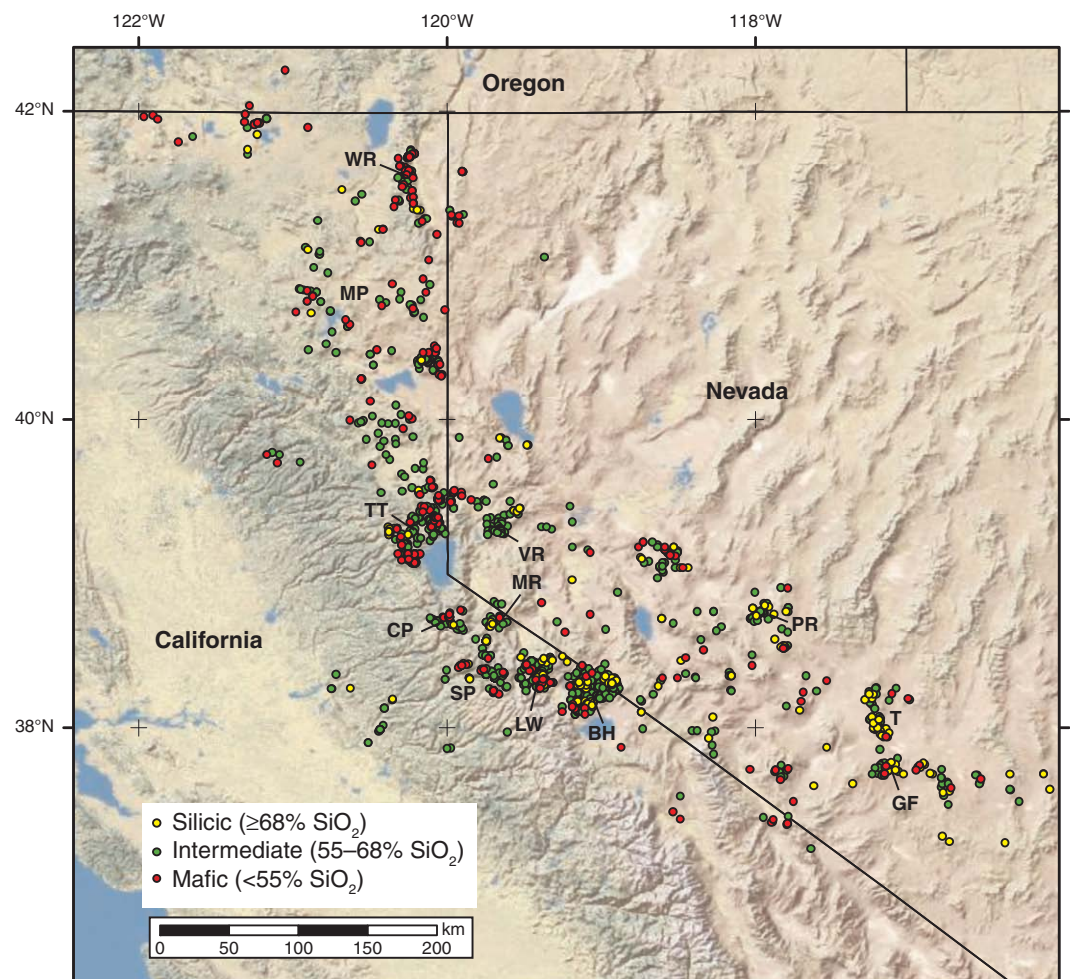


Figure 19. Total alkali-silica diagrams for ancestral arc rocks and postsubduction rocks in northeastern California and northwestern Nevada. (A) Bodie Hills volcanic field and Eureka Valley Tuff in the Bodie Hills. (B) Central Sierra Nevada (Sonora Pass, Carson Pass, and Lake Tahoe) and Stanislaus Group in the central Sierra Nevada, which is composed of the Table Mountain Latite, Eureka Valley Tuff, and Dardanelles Formation. (C) Warner Range and Modoc Plateau between the Warner Range and Lassen Peak. (D) Monitor Range and west-central Nevada. (E) Pliocene–Pleistocene postsubduction rocks in the Bodie Hills (Aurora volcanic field) and the Lake Tahoe area (Tahoe-Truckee volcanic field, TTVF). Purple line encloses data for the Bodie Hills volcanic field. Data are from du Bray et al. (2009), C.D. Henry (2010, written commun.), Cousens et al. (2011), Colgan et al. (2011), and our data for the Monitor Range and southwest Paradise Range. Field boundaries are from Le Bas et al. (1986); alkaline-subalkaline boundary is from Irvine and Baragar (1971). All major oxide analyses normalized to 100% volatile-free prior to plotting.

Figure 20. Map showing rock compositions for the southern segment of the ancestral arc in California and Nevada. Rocks are separated into mafic (<55% SiO₂), intermediate (55%–68% SiO₂), and silicic (>68% SiO₂) compositions. Data are from this study, du Bray et al. (2009), and C.D. Henry (2010, written commun.). Samples of the Lousetown Formation and Pyramid Sequence northeast of the Virginia Range that are of uncertain tectonic affinity are excluded. BH—Bodie Hills; CP—Carson Pass; GF—Goldfield; TT—Tahoe-Truckee; LW—Little Walker center; MP—Modoc Plateau; MR—Monitor Range; PR—Paradise Range; SP—Sonora Pass; T—Tonopah; VR—Virginia Range; WR—Warner Range.



Localization of eruptive centers more closely reflects structural control than for the Miocene eruptive centers. Rocks of the Aurora volcanic field are mostly sparsely porphyritic, biotite phenocrysts are uncommon, and Fe-Ti oxide phenocrysts are absent (Lange and Carmichael, 1996).

The geochemistry of volcanic rocks erupted from the two fields also is subtly different. The Aurora volcanic field rocks form a high-K to shoshonitic, calc-alkaline series (Figs. 18 and 19) with trace element contents, such as Ba/Nb > 50, characteristic of subduction-related magmas (Lange and Carmichael, 1996). These rocks are significantly enriched in REEs, especially LREEs, relative to subduction-related volcanic rocks of the Bodie Hills (Fig. 13). Negative P, Zr, and Ti anomalies (Fig. 14) are less pronounced than in the older subduction-related rocks, probably a consequence of either less source region retention of accessory minerals, such as apatite, zircon, or ilmenite and/or titanite, or limited fractionation of these minerals in their preeruptive magma chambers. Negative Nb-Ta anomalies of the Aurora volcanic field rocks tend to

be smaller than those of the Bodie Hills rocks. However, the Aurora magmas were relatively oxidized (magmatic oxygen fugacities within –0.4 to +2.4 log units of Ni-NiO oxygen buffer) and water rich (1.5–6 wt% H₂O) (Lange and Carmichael, 1996), both characteristics of subduction-related magmas.

Lange and Carmichael (1996) proposed that the Aurora volcanic field magmas formed at the crust-mantle interface by partial melting of underplated basalt, and suggested that repeated partial melting of recently crystallized basalt and rapid ascent of small volumes of magma are consistent with the relatively low average eruption rate of the Aurora volcanic field, their low phenocryst contents, and their major and trace element geochemistry. The extensional environment operative during formation of the volcanic field seems to have facilitated rapid magma ascent. The K- and H₂O-rich nature of the Aurora volcanic field rocks is also consistent with small degrees of partial melting of lithospheric basalt, as suggested by Putirka and Busby (2007) for the high-K rocks of the central Sierra Nevada.

The average eruption rate for the Bodie Hills volcanic field is difficult to accurately estimate due to extensive erosion and incomplete exposure, but a conservative estimate of 500 km³ of magma erupted during ~7 Ma (15–8 Ma) in the >700 km² volcanic field yields an average eruption rate ~5 times greater than that estimated for the Aurora volcanic field by Lange and Carmichael (1996). The trace element compositions of rocks in both fields reflect a strong influence by subduction zone processes. Higher eruption rates, more phenocryst-rich lavas, and the inferred presence of large plutons beneath the volcanic field, however, suggest that the Bodie Hills volcanic field was the product of substantially different processes than those responsible for the Aurora volcanic field.

Hydrothermal Systems and the Bodie Hills Volcanic Field

Numerous hydrothermal systems were active during protracted development of the Bodie Hills volcanic field and illustrate several important

points regarding formation of mineral deposits in the southern part of the ancestral arc. (1) Although large alteration zones are related to the Aurora and Masonic volcanoes, no significant mineral deposits are temporally related to these or other Bodie Hills trachyandesite stratovolcanoes. The large Au-Ag deposits at Bodie and Aurora are more closely related temporally to more silicic (dacite to rhyolite) dome complexes. Important epithermal Au-Ag deposits elsewhere in the southern part of the ancestral arc, including the Comstock Lode (Virginia Range), Goldfield, Tonopah, and Paradise Peak deposits, are associated temporally with similar intermediate composition dome fields. (2) Permeability and focused fluid flow are important factors in the development of economic metal concentrations. The high permeability of volcaniclastic rocks and interbedded tuffs in the Paramount basin and on the north side of the Masonic volcano (Red Wash alteration zone) resulted in unfocused fluid flow and very large areas of hydrothermally altered rock (as much as 30 km²), but very dispersed and low-grade mineralization. In contrast, areas of economically significant hydrothermally altered rock are much smaller in the Bodie and Aurora districts, where fluid flow was focused into narrow zones that concentrated ore fluids. (3) Rock lithology has a strong effect on fracturing and formation of veins. Lava flow and flow dome units have greater tensional and shear strengths, which promote brittle fracturing and maintenance of open fractures that can channelize vein-forming hydrothermal fluids. In contrast, the volcaniclastic and sedimentary rocks in the Bodie Hills did not maintain open fractures unless they were previously hydrothermally altered, and hydrothermal fluids that interacted with these rocks were dispersed through large volumes of highly permeable rock.

SUMMARY AND CONCLUSIONS

The Miocene Bodie Hills volcanic field is a large, long-lived locus of eruptive activity in the southern part of the ancestral Cascade arc that has many similarities to other large volcanic fields of the southern ancestral arc. The >700 km² Bodie Hills volcanic field was assembled from ca. 14.7 to 5.5 Ma and its products erupted directly onto a Tertiary erosional highland developed on Paleozoic and Mesozoic metamorphic and granitic rocks. The volcanic field is near the west side of the Walker Lane and just northwest of the west end of the Mina deflection, both zones of lithosphere-scale structures. The location and long duration of the Bodie Hills volcanism are probably related to these lithospheric-scale structures, which provided conduits for mantle-

derived magmas to ascend into and transit the crust. Gravity data indicate that the Bodie Hills volcanic field is underlain by low-density rocks that are an eastern prong of the Mesozoic Sierra Nevada batholith or, more likely, Miocene plutons related to the volcanic field. Aeromagnetic data filtered for ~2 km depths suggest that significant magnetic bodies underlie inferred vents for several large Miocene volcanoes and that the volcanic field may be underlain by large Miocene plutons.

The Bodie Hills volcanic field is composed of trachyandesite stratovolcanoes emplaced on the margins of the field and silicic trachyandesite to rhyolite flow dome complexes mostly emplaced into the center of the field. Volcanism waxed and waned during its long history, and includes two peak periods of eruptive activity that correspond to an early period of mafic stratovolcano formation and a period 4–5 Ma later during which large overlapping silicic trachyandesite-dacite dome fields were constructed. A final period of volumetrically minor silicic dome emplacement followed ~2 Ma later. Following an ~2 Ma hiatus in magmatic activity, bimodal volcanic rocks of the ca. 3.6–0.1 Ma Aurora volcanic field were unconformably deposited on rocks of the Bodie Hills volcanic field. Bodie Hills volcanic field rocks have compositions that vary continuously from ~50 to 78 wt% SiO₂, although few contain <55 wt% SiO₂. The rocks define three main compositional groups, (1) silicic basaltic trachyandesite-trachyandesite, (2) silicic trachyandesite-trachydacite, and (3) rhyolite, which correspond to different eruptive units and volcanoes. Rock compositions form a high-K calc-alkaline series with pronounced negative Ti-P-Nb-Ta anomalies and high Ba/Nb, Ba/Ta, La/Nb, and Th/La ratios typical of subduction-related continental margin arcs.

Bodie Hills volcanic rocks and mineral deposits record progressive changes in regional strain patterns. Prior to ca. 10 Ma, low differential horizontal stresses resulted in subcircular, polygenetic volcanoes and associated episodes of hydrothermal mineralization controlled by conjugate sets of strike-slip faults. After ca. 10–9 Ma, the maximum compressive stress axis became vertical, and extension-related faults and veins accompanied a progressive westward migration of trachydacitic magmatism. The change is approximately temporally coincident with northward migration of the Mendocino triple junction and inferred cessation of subduction beneath the Bodie Hills. A narrow north-south trending belt of rhyolitic magmatism in the western part of the Bodie Hills may have been localized ca. 6 Ma by normal faults reflective of stronger westward extensional stresses. Pliocene–Pleistocene magmatism was

even more strongly controlled by north-striking extensional faults linked as stepover grabens to northeast-striking left-lateral faults.

Rock compositions and volcanic center landforms are broadly similar throughout the southern part of the ancestral arc south of Lake Tahoe (~39°–39.5°N); dome fields among less abundant stratovolcanoes are common, intermediate compositions are abundant, and mafic compositions are scarce. The scarcity of mafic volcanic rocks is likely a consequence of thick crust that prevented ascent of mantle-derived basalt magmas; instead, mafic magmas stalled in the crust and formed MASH zones that fostered development of more silicic compositions. Farther north along the Middle to Late Miocene arc between Lake Tahoe and the Warner Range, the crust was much thinner, basalt melts rose directly to the surface, and ancestral arc eruptions formed mafic shield volcanoes. In contrast, distinctly K₂O-rich Stanislaus Group rocks of the Little Walker center may represent magmas derived from small degrees of partial melting of the upper mantle, which ascended rapidly along transtensional faults related to development of the Sierra microplate (Putirka and Busby, 2007; Busby et al., 2008).

ACKNOWLEDGMENTS

We thank Jim Rytuba, Barnaby Rockwell, Ed Mankinen, and Luc Farmer for help in the field, Bill Silberman for access to his unpublished maps, Chris Henry for providing unpublished chemical analyses, Larry Snee and Mike Cosca for unpublished ⁴⁰Ar/³⁹Ar ages, Barney Berger and Amir Smailbegovic for lively discussions, and Chad Carlson, Jonathan Glen, and Chris Pluhar for discussions concerning paleomagnetic data and their regional tectonic implications. This work was funded by the U.S. Geological Survey Mineral Resources Program. Reviews by Joe Colgan, Mike Sawlan, Keith Putirka, and Cathy Busby helped sharpen considerably our presentation and interpretations.

REFERENCES CITED

- Al-Rawi, Y.T., 1969, Cenozoic history of the northern part of Mono Basin, California and Nevada [Ph.D. thesis]: Berkeley, University of California, 163 p.
- Anders, E., and Ebihara, M., 1982, Solar-system abundances of the elements: *Geochimica et Cosmochimica Acta*, v. 46, p. 2362–2380, doi: 10.1016/0016-7037(82)90208-3.
- Armstrong, R.L., and Ward, P., 1991, Evolving geographic patterns of Cenozoic magmatism in the North American Cordillera: The temporal and spatial association of magmatism and metamorphic core complexes: *Journal of Geophysical Research*, v. 96, p. 13,201–13,224, doi: 10.1029/91JB00412.
- Ashley, R.P., 1974, Goldfield mining district, in Bonham, H.F., et al., eds., *Guidebook to the geology of four Tertiary volcanic centers in central Nevada*: Nevada Bureau of Mines and Geology Report 19, p. 49–66.
- Atwater, T., 1970, Implications of plate tectonics for the Cenozoic tectonic evolution of western North America: *Geological Society of America Bulletin*, v. 81, p. 3513–3535, doi: 10.1130/0016-7606(1970)81[3513:IOPTFT]2.0.CO;2.
- Atwater, T., and Stock, J., 1998, Pacific–North America plate tectonics of the Neogene southwestern United

Bodie Hills volcanic field

- States—An update: International Geology Review, v. 40, p. 375–402, doi: 10.1080/00206819809465216.
- Berger, B.R., Snee, L.W., and Tingley, J.W., 1999, Implications of new structural and $^{40}\text{Ar}/^{39}\text{Ar}$ data on hydraulic evolution of epithermal veins and ore formation, Aurora and Bodie mining districts, Nevada-California: Geological Society of America Abstracts with Programs, v. 31, no. 7, p. 94.
- Best, M.G., Christiansen, E.H., Deino, A.L., Grommé, C.S., McKee, E.H., and Noble, D.C., 1989, Excursion 3A: Eocene through Miocene volcanism in the Great Basin of the western United States, in Chapin, C.E., and Zidek, J., eds., 1989, Field excursions to volcanic terranes in the western United States Volume II—Cascades and Intermountain West: New Mexico Bureau of Mines and Mineral Resources Memoir 47, p. 91–133.
- Blakely, R.J., 1995, Potential theory in gravity and magnetic applications: Cambridge, UK, Cambridge University Press, 441 p.
- Blakely, R.J., and Jachens, R.C., 1991, Regional study of mineral resources in Nevada: Insights from three-dimensional analysis of gravity and magnetic anomalies: Geological Society of America Bulletin, v. 103, p. 795–803, doi: 10.1130/0016-7606(1991)103<0795:RSOMRI>2.3.CO;2.
- Bonham, H.F., Jr., and Garside, L.J., 1979, Geology of the Tonopah, Lone Mountain, Klondike, and northern Mud Spring Lake quadrangles, Nevada: Nevada Bureau of Mines and Geology Bulletin 92, 136 p.
- Breit, F.J., Jr., 2000, Structural and temporal relationships and geochemical characteristics of the East Brawley Peak acid-sulfate prospect and the adjacent Aurora adularia-sericite system [M.S. thesis]: Reno, University of Nevada, 215 p.
- Busby, C.J., and Putirka, K., 2009, Miocene evolution of the western edge of the Nevadaplano in the central and northern Sierra Nevada: Palaeocanyons, magmatism, and structure: International Geology Review, v. 51, p. 670–701, doi: 10.1080/00206810902978265.
- Busby, C.J., and Putirka, K., 2010, Geologic signals of the initiation of continental rifting within the ancestral Cascades arc: Geological Society of America Abstracts with Programs, v. 42, no. 5, p. 345.
- Busby, C.J., Hagan, J.C., Putirka, K., Pluhar, C.J., Gans, P.B., Wagner, D.L., Rood, D., DeOreo, S.B., Skilling, I., and Wagner, D.L., 2008, The ancestral Cascades arc—Cenozoic evolution of the central Sierra Nevada (California) and the birth of the new plate boundary, in Wright, J.E., and Shervais, J.W., eds., Ophiolites, arcs, and batholiths—A tribute to Cliff Hopson: Geological Society of America Special Paper 438, p. 331–378.
- Cameron, K.L., and Cameron, M., 1985, Rare earth element, $^{87}\text{Sr}/^{86}\text{Sr}$, and $^{143}\text{Nd}/^{144}\text{Nd}$ compositions of Cenozoic orogenic dacites from Baja California, northwestern Mexico, and adjacent west Texas: evidence for the predominance of a subcrustal component: Contributions to Mineralogy and Petrology, v. 91, p. 1–11, doi: 10.1007/BF00429422.
- Carlson, C.W., Pluhar, C.J., and Glen, J.M., 2010, Tectonic tales: Changes in central Walker Lane strain accommodation near Bridgeport, California; as told by the Stanislaus Group: American Geophysical Union, Fall Meeting 2010, abs. GP11A-0746.
- Chesterman, C.W., 1968, Volcanic geology of the Bodie Hills, Mono County, California, in Coats, R.R., et al., eds., Studies in volcanology: Geological Society of America Memoir 116, p. 45–68.
- Chesterman, C.W., and Gray, C.H., Jr., 1975, Geology of the Bodie 15-minute quadrangle, Mono County, California: California Division of Mines and Geology Map Sheet 21, scale 1:48,000.
- Chesterman, C.W., Chapman, R.H., and Gray, C.H., Jr., 1986, Geology and ore deposits of the Bodie mining district, Mono County, California: California Division of Mines and Geology Bulletin 206, 35 p.
- Christiansen, R.L., and Yeats, R.S., 1992, Post-Laramide geology of the U.S. Cordilleran region, in Burchfiel, B.C., et al., eds., The Cordilleran orogen—Conterminous U.S.: Boulder, Colorado, Geological Society of America, Geology of North America, v. G-3, p. 261–406.
- Colgan, J.P., Egger, A.E., John, D.A., Cousens, B., Fleck, R.J., and Henry, C.D., 2011, Oligocene and Miocene arc volcanism in northeastern California: Evidence for post-Eocene segmentation of the subducting Farallon plate: Geosphere, v. 7, p. 733–755, doi: 10.1130/GES00650.1.
- Cousens, B.L., Prytulak, J., Henry, C.D., Alcazar, A., and Brownrigg, T., 2008, Geology, geochronology, and geochemistry of the Miocene–Pliocene ancestral Cascades arc, northern Sierra Nevada, California and Nevada: The roles of the upper mantle, subducting slab, and the Sierra Nevada lithosphere: Geosphere, v. 4, p. 814–828, doi: 10.1130/ges00166.1.
- Cousens, B.L., Henry, C.D., Harvey, B.J., Brownrigg, T., Prytulak, J., and Allan, J.E., 2011, Secular variations in magmatism during a continental arc to post-arc transition: Plio-Pleistocene volcanism in the Lake Tahoe/Truckee area, Northern Sierra Nevada, California: Lithos, v. 123, p. 225–242, doi: 10.1016/j.lithos.2010.09.009.
- Craftord, A.E.J., 2007, Geologic map of Nevada: U.S. Geological Survey Data Series 249, CD-ROM, 46 p.
- Dickinson, W.R., 1997, Tectonic implications of Cenozoic volcanism in coastal California: Geological Society of America Bulletin, v. 109, p. 936–954, doi: 10.1130/0016-7606(1997)109<0936:OTIOCV>2.3.CO;2.
- Dickinson, W.R., 2006, Geotectonic evolution of the Great Basin: Geosphere, v. 2, p. 353–368, doi: 10.1130/GES00054.1.
- Dilles, J.H., and Gans, P.B., 1995, The chronology of Cenozoic volcanism and deformation in the Yerington area, western Basin and Range and Walker Lane: Geological Society of America Bulletin, v. 107, p. 474–486, doi: 10.1130/0016-7606(1995)107<0474:TCOCVA>2.3.CO;2.
- Dohrenwend, J.C., 1981, Reconnaissance surficial geologic map of the Trench Canyon quadrangle, California and Nevada: U.S. Geological Survey Open-File Report 81-1155, scale 1:62,500.
- Dohrenwend, J.C., 1982, Reconnaissance surficial geologic map of the Aurora quadrangle, California and Nevada: U.S. Geological Survey Miscellaneous Field Studies Map MF-1373, scale 1:62,500.
- Dohrenwend, J.C., and Brem, G.F., 1982, Reconnaissance surficial geologic map of the Bridgeport quadrangle, California and Nevada: U.S. Geological Survey Miscellaneous Field Studies Map MF-1371, scale 1:62,500.
- du Bray, E.A., and John, D.A., 2011, Petrologic, tectonic, and metallogenetic evolution of the ancestral Cascades magmatic arc, Washington, Oregon, and northern California: Geosphere, v. 7, p. 1102–1133, doi: 10.1130/GES00669.1.
- du Bray, E.A., John, D.A., Sherrod, D.R., Evarts, R.C., Conrey, R.M., and Lexa, J., 2006, Geochemical database for volcanic rocks of the western Cascades, Washington, Oregon, and California: U.S. Geological Survey Data Series 155, 49 p.
- du Bray, E.A., John, D.A., Putirka, K., and Cousens, B.L., 2009, Geochemical database for igneous rocks of the ancestral Cascades arc—Southern segment, California and Nevada: U.S. Geological Survey Digital Data Series 439, 1 CD-ROM.
- Eaton, G.P., Wahl, R.R., Prostka, H.J., Mabey, D.R., and Kleinkopf, M.D., 1978, Regional gravity and tectonic patterns: Their relation to late Cenozoic epeirogeny and lateral spreading in the western Cordillera, in Smith, R.B., and Eaton, G.P., eds., Cenozoic tectonics and regional geophysics of the Western Cordillera: Geological Society of America Memoir 152, p. 51–91.
- Ekren, E.B., Byers, F.M., Jr., Hardyman, R.F., Marvin, R.F., and Silberman, M.L., 1980, Stratigraphy, preliminary petrology, and some structural features of Tertiary volcanic rocks in the Gabbs Valley and Gillis Ranges, Nevada: U.S. Geological Survey Bulletin 1464, 54 p.
- Ewart, A., 1982, The mineralogy and petrology of Tertiary Recent orogenic volcanic rocks with special reference to the andesitic–basaltic compositional range, in Thorpe, R.S., ed., Andesites: New York, John Wiley and Sons, p. 25–87.
- Faulds, J.E., and Henry, C.D., 2008, Tectonic influences on the spatial and temporal evolution of the Walker Lane: An incipient transform fault along the evolving Pacific–North American plate boundary, in Spencer, J.E., and Titley, S.R., eds., Ores and orogenesis: Circum-Pacific tectonics, geologic evolution, and ore deposits: Arizona Geological Society Digest 22, p. 437–470.
- Feeley, T.C., and Davidson, J.P., 1994, Petrology of calc-alkaline lavas at Volcan Ollaguee and the origin of compositional diversity at central Andean stratovolcanoes: Journal of Petrology, v. 35, p. 1295–1340, doi: 10.1093/petrology/35.5.1295.
- Fleck, R.J., Sutter, J.H., and Elliott, D.H., 1977, Interpretation of discordant $^{40}\text{Ar}/^{39}\text{Ar}$ age-spectra of Mesozoic tholeites from Antarctica: Geochimica et Cosmochimica Acta, v. 41, p. 15–32, doi: 10.1016/0016-7037(77)90184-3.
- Frost, B.R., Barnes, C.G., Collins, W.J., Arculus, R.J., Ellis, D.J., and Frost, C.D., 2001, A geochemical classification for granitic rocks: Journal of Petrology, v. 42, p. 2033–2048, doi: 10.1093/petrology/42.11.2033.
- GEOROC, 2007, GEOROC, Geochemistry of rocks of the oceans and continents database: Max-Planck-Institut für Chemie, <http://georoc.mpcn-mainz.gwdg.de/georoc/>.
- Gilbert, C.M., and Reynolds, M.W., 1973, Character and chronology of basin development, western margin of the Basin and Range Province: Geological Society of America Bulletin, v. 84, p. 2489–2510, doi: 10.1130/0016-7606(1973)84<2489:CACOBD>2.0.CO;2.
- Gilbert, C.M., Christiansen, M.N., Al-Rawi, Y., and Lajoie, K.R., 1968, Structural and volcanic history of Mono Basin, California-Nevada, in Coats, R.R., et al., eds., Studies in volcanology: Geological Society of America Memoir 116, p. 275–329.
- Gill, J., 1981, Orogenic andesites and plate tectonics: New York, Springer-Verlag, 390 p.
- Glazner, A.F., and Farmer, G.L., 2008, Ancestral Cascades = modern Cascades: Geological Society of America Abstracts with Programs, v. 40, no. 1, p. 98.
- Grose, T.L., 2000, Volcanoes in the Susanville region, Lassen, Modoc, and Plumas counties, northeastern California: California Geology, v. 53, p. 4–23.
- Gutierrez, C., Bryant, W., Saucedo, G., and Wills, C., 2010, Geologic map of California (original compilation by Jennings, C.W., 1977): California Geologic Data Map Series Map 2, scale 1:750,000.
- Hagan, J.C., Busby, C.J., Putirka, K., and Renne, P.R., 2009, Cenozoic paleocanyon evolution, ancestral Cascades arc volcanism, and structure of the Hope Valley–Carson Pass region, Sierra Nevada, California: International Geology Review, v. 51, p. 777–823, doi: 10.1080/00206810903028102.
- Heimgartner, M., Louie, J.N., Scott, J.B., Thelen, W., Lopez, C.T., and Coolbaugh, M., 2006, The crustal thickness of the Great Basin: Using seismic refraction to assess regional geothermal potential: Geothermal Research Council Transactions, v. 30, p. 83–86.
- Henry, C.D., 2008, Ash-flow tuffs and paleovalleys in northeastern Nevada: Implications for Eocene paleogeography and extension in the Sevier hinterland, northern Great Basin: Geosphere, v. 4, p. 1–35, doi: 10.1130/GES00122.1.
- Henry, C.D., and Faulds, J.E., 2010, Ash-flow tuffs in the Nine Hill Tuff paleovalley and implications for tectonism and volcanism of the western Great Basin, USA: Geosphere, v. 6, p. 339–369, doi: 10.1130/GES00548.1.
- Henry, C.D., Cousens, B., John, D.A., and Colgan, J.P., 2009, Reestablishment of the ancestral Cascades arc in western Nevada and eastern California by rollback of the shallow Farallon slab: Eos (Transactions, American Geophysical Union), v. 90, no. 52, abs. V41B-2175.
- Herrera, P.A., Silberman, M.L., and Closs, L.G., 1991, Alteration mineral assemblage and trace element zoning at Bodie Bluff, northern part of the Bodie mining district, Mono County, California, in Raines, G.L., et al., eds., Geology and ore deposits of the Great Basin: Reno, Geological Society of Nevada Symposium Proceedings, p. 1189–1193.
- Herrera, P.A., Closs, L.G., and Silberman, M.L., 1993, Alteration and geochemical zoning in Bodie Bluff, Bodie mining district, California: Journal of Geochemical Exploration, v. 48, p. 259–275, doi: 10.1016/0375-6742(93)90007-9.

- Hildreth, W., 1981, Gradients in silicic magma chambers: Implications for lithospheric magmatism: *Journal of Geophysical Research*, v. 86, p. 10,153–10,192, doi: 10.1029/JB086iB11p10153.
- Hildreth, W., and Moorbath, S., 1988, Crustal contributions to arc magmatism in the Andes of central Chile: Contributions to Mineralogy and Petrology, v. 98, p. 455–489, doi: 10.1007/BF00372365.
- Hill, J.M., 1915, Some mining districts in northeastern California and northwestern Nevada: U.S. Geological Survey Bulletin 594, 200 p.
- Holmes, G.H., 1965, Mercury in California, in *Mercury potential of the United States*: U.S. Bureau of Mines Information Circular 8252, p. 87–206.
- Hudson, D.M., Castor, S.B., Garside, L.J., and Henry, C.D., 2009, Geologic map of the Virginia City quadrangle, Washoe, Storey, and Lyon Counties and Carson City, Nevada: Nevada Bureau of Mines and Geology Map 165, scale 1:24,000, 37 p.
- Humphreys, E.D., 1995, Post-Laramide removal of the Farallon slab, western United States: *Geology*, v. 23, p. 987–990, doi: 10.1130/0091-7613(1995)023<0987:PLROTF>2.3.CO;2.
- Irvine, T.N., and Baragar, W.R.A., 1971, A guide to the chemical classification of the common volcanic rocks: *Canadian Journal of Earth Sciences*, v. 8, p. 523–548, doi: 10.1139/e71-055.
- John, D.A., 1992, Stratigraphy, regional distribution, and reconnaissance geochemistry of Oligocene and Miocene volcanic rocks in the Paradise Range and northern Pactolus Hills, Nye County, Nevada: U.S. Geological Survey Bulletin 1974, 67 p.
- John, D.A., 2001, Miocene and early Pliocene epithermal gold-silver deposits in the northern Great Basin, western USA: Characteristics, distribution, and relationship to magmatism: *Economic Geology and the Bulletin of the Society of Economic Geologists*, v. 96, p. 1827–1853, doi: 10.2113/96.8.1827.
- John, D.A., Giusto, J., Moore, W.J., and Armin, R.A., 1981, Reconnaissance geologic map of the Topaz Lake 15° quadrangle, California-Nevada, with Quaternary geology by J.C. Dohrenwend: U.S. Geological Survey Open-File Report 81-273, scale 1:62,500.
- Johnson, M.A., 1951, Geology of the Masonic mining district, Mono County, California [M.S. thesis]: Berkeley, University of California, 51 p.
- King, N.M., Hillhouse, J.W., Gromme, S., Hausback, B.P., and Pluhar, C.J., 2007, Stratigraphy, paleomagnetism, and anisotropy of magnetic susceptibility of the Miocene Stanislaus Group, central Sierra Nevada and Sweetwater Mountains, California and Nevada: *Geosphere*, v. 3, p. 646–666, doi: 10.1130/ges00132.1.
- Kistler, R.W., 1990, Two different lithosphere types in the Sierra Nevada, California, in Anderson, J.L., ed., The nature and origin of Cordilleran metamorphism: *Geological Society of America Memoir* 174, p. 271–281.
- Kistler, R.W., and Peterman, Z.E., 1978, Reconstruction of crustal blocks of California on the basis of initial strontium isotopic compositions of Mesozoic granite rocks: U.S. Geological Survey Professional Paper 1071, 17 p.
- Kleinhampl, F.J., Davis, W.E., Silberman, M.L., Chesterman, C.W., Chapman, R.H., and Gray, C.H., Jr., 1975, Aeromagnetic and limited gravity studies and generalized geology of the Bodie Hills region, Nevada and California: U.S. Geological Survey Bulletin 1384, 38 p.
- Lange, R.A., and Carmichael, I.S.E., 1996, The Aurora volcanic field, California-Nevada: Oxygen fugacity constraints on the development of andesitic magma: Contributions to Mineralogy and Petrology, v. 125, p. 167–185, doi: 10.1007/s004100050214.
- Lange, R.A., Carmichael, I.S.E., and Renne, P., 1993, Potassic volcanism near Mono Basin, California: Evidence for high water and oxygen fugacities inherited from subduction: *Geology*, v. 21, p. 949–952, doi: 10.1130/0091-7613(1993)021<0949:PVNMBC>2.3.CO;2.
- Le Bas, M.J., Le Maitre, R.W., Streckeisen, A., Zanettin, B.A., and IUGS Subcommission on the Systematics of Igneous Rocks, 1986, Chemical classification of volcanic rocks based on the total alkali-silica diagram: *Journal of Petrology*, v. 27, p. 745–750, doi: 10.1093/petrology/27.3.745.
- Le Maitre, R.W., 1989, A classification of igneous rocks and glossary of terms: Oxford, UK, Blackwell Scientific, 193 p.
- Leach, D.W., Klemperer, S.L., Glen, J.M.G., Ponce, D.A., Miller, E.L., and Colgan, J.P., 2007, Crustal structure of the northwestern Basin and Range Province and its transition to unextended volcanic plateaus: *Geochemistry Geophysics Geosystems*, v. 8, Q02011, doi: 10.1029/2006GC001429.
- Long, K.R., DeYoung, J.H., Jr., and Ludington, S.D., 1998, Database of significant deposits of gold, silver, copper, lead, and zinc in the United States: U.S. Geological Survey Open-File Report 98-206A, 33 p.
- Ludington, S., Cox, D.P., Moring, B.C., and Leonard, K.W., 1996, Cenozoic volcanic geology of Nevada: Nevada Bureau of Mines and Geology Open-File Report 96-2, p. 5–1–5–10.
- Ludington, S., Moring, B.C., Miller, R.J., Stone, P.A., Bookstrom, A.A., Bedford, D.R., Evans, J.G., Haxel, G.A., Nutt, C.J., Flynn, K.S., and Hopkins, M.J., 2005, Preliminary integrated geologic map databases for the United States: U.S. Geological Survey Open-File Report 2005-1305, <http://pubs.usgs.gov/of/2005/1305/>.
- Mavko, B.B., and Thompson, G.A., 1983, Crustal and upper mantle structure of the northern and central Sierra Nevada: *Journal of Geophysical Research*, v. 88, p. 5874–5892, doi: 10.1029/JB088iB07p05874.
- McBirney, A.R., 1978, Volcanic evolution of the Cascades Range: *Earth and Planetary Science Annual Reviews*, v. 6, p. 437–456, doi: 10.1146/annurev.ea.06.050178.002253.
- Miyashiro, A., 1974, Volcanic rock series in island arcs and active continental margins: *American Journal of Science*, v. 274, p. 321–355, doi: 10.2475/ajs.274.4.321.
- Nakamura, K., 1977, Volcanoes as possible indicators of tectonic stress orientation—Principal and proposal: *Journal of Volcanology and Geothermal Research*, v. 2, p. 1–16, doi: 10.1016/0377-0273(77)90012-9.
- Noble, D.C., 1972, Some observations on the Cenozoic volcano-tectonic evolution of the Great Basin, western United States: *Earth and Planetary Science Letters*, v. 17, p. 142–150, doi: 10.1016/0012-821X(72)90269-5.
- Noble, D.C., Slemmons, D.B., Korringa, M.K., and Dickinson, W.R., Al-Rawi, Y., and McKee, E.H., 1974, Eureka Valley Tuff, east-central California and adjacent Nevada: *Geology*, v. 2, p. 139–142, doi: 10.1130/0091-7613(1974)<2:139:EVTECA>2.0.CO;2.
- Oldow, J.S., 1992, Late Cenozoic displacement partitioning in the northwestern Great Basin, in Craig, S.D., ed., Structure, tectonics, and mineralization of the Walker Lane; Walker Lane Symposium, proceedings volume: Reno, Nevada, Geological Society of Nevada, p. 17–52.
- Oldow, J.S., 2003, Active transtensional boundary zone between the western Great Basin and Sierra Nevada block, western U.S. Cordillera: *Geology*, v. 31, p. 1033–1036, doi: 10.1130/G19838.1.
- Oldow, J.S., Geissman, J.W., and Stockli, D.F., 2008, Evolution and strain reorganization within Late Neogene structural stepovers linking the central Walker Lane and northern Eastern California Shear Zone, western Great Basin: *International Geology Review*, v. 50, p. 270–290, doi: 10.2747/0020-6814.50.3.270.
- Osborne, M.A., 1991, Epithermal mineralization at Aurora, Nevada, in Raines, G.L., et al., eds., *Geology and ore deposits of the Great Basin: Reno, Geological Society of Nevada Symposium Proceedings*, p. 1097–1110.
- Pearce, J.A., Harris, N.B.W., and Tindle, A.G., 1984, Trace element discrimination diagrams for the tectonic interpretation of granitic rocks: *Journal of Petrology*, v. 25, p. 956–983, doi: 10.1093/petrology/25.4.956.
- Phillips, J.D., 2007, Geosoft eXecutables (GX's) developed by the U.S. Geological Survey, version 2.0, with notes on GX development from Fortran code: U.S. Geological Survey Open-File Report 2007-1355, 111 p.
- Phillips, J.D., Hansen, R.O., and Blakely, R.J., 2007, The use of curvature in potential-field interpretation: *Exploration Geophysics*, v. 38, p. 111–119, doi: 10.1071/EG07014.
- Plank, T., 2005, Constraints from thorium/lanthanum on sediment recycling at subduction zones and the evolution of the continents: *Journal of Petrology*, v. 46, p. 921–944, doi: 10.1093/petrology/egi005.
- Pluhar, C.J., Deino, A.L., King, N.M., Busby, C., Huasback, B.P., Wright, T., and Fischer, C., 2009, Lithostratigraphy, magnetostratigraphy and radio-isotopic dating of the Stanislaus Group, CA, and the age of the Little Walker caldera: *International Geology Review*, v. 51, p. 873–899, doi: 10.1080/00206810902945017.
- Priest, G.R., 1979, Geology and geochemistry of the Little Walker volcanic center, Mono County, California [Ph.D. thesis]: Corvallis, Oregon State University, 315 p.
- Priest, G.R., 1990, Volcanic and tectonic evolution of the Cascades volcanic arc, central Oregon: *Journal of Geophysical Research*, v. 95, no. B12, p. 19,583–19,599, doi: 10.1029/JB095iB12p19583.
- Putirka, K., and Busby, C.J., 2007, The tectonic significance of high-K₂O volcanism in the Sierra Nevada, California: *Geology*, v. 35, p. 923–926, doi: 10.1130/G23914A.1.
- Renne, P.R., Swisher, C.C., Deino, A.L., Karner, D.B., Owens, T.L., and DePaolo, D.J., 1998, Intercalibration of standards, absolute ages and uncertainties in ⁴⁰Ar/³⁹Ar dating: *Chemical Geology*, v. 145, p. 117–152, doi: 10.1016/S0009-2541(97)00159-9.
- Robinson, A.C., and Kistler, R.W., 1986, Maps showing isotopic dating in the Walker Lake 1° by 2° quadrangle, California and Nevada: U.S. Geological Survey Miscellaneous Field Studies Map MF-1382-N, scale 1:250,000.
- Rockwell, B.W., 2010, Mineral and vegetation maps of the Bodie Hills, Brawley Peaks, Sweetwater Mountains, and Wassuk Range, California/Nevada, generated from ASTER satellite data: U.S. Geological Survey Scientific Investigations Map 3104, scale 1:62,000, 5 p., <http://pubs.usgs.gov/sim/3104/>.
- Rutherford, M.J., and Hill, P.M., 1993, Magma ascent rates from amphibole breakdown: An experimental study applied to the 1980–1986 Mount St. Helens eruptions: *Journal of Geophysical Research*, v. 98, p. 19,667–19,685, doi: 10.1029/93JB01613.
- Saltus, R.W., and Jachens, R.C., 1995, Gravity and basin-depth maps of the Basin and Range province, western United States: U.S. Geological Survey Geophysical Investigations Map GP-1012, 1 sheet.
- Shand, S.J., 1951, *Eruptive rocks*: New York, John Wiley, 488 p.
- Sherrod, D.R., and Smith, J.G., 2000, Geologic map of upper Eocene to Holocene volcanic and related rocks of the Cascades Range, Oregon: U.S. Geological Survey Miscellaneous Investigations Series Map I-2569, scale 1:500,000, 17 p.
- Silberman, M.L., and Chesterman, C.W., 1972, K-Ar age of volcanism and mineralization, Bodie mining district and Bodie Hills volcanic field, Mono county, California: Isochron-West, no. 3, p. 13–22.
- Silberman, M.L., and Chesterman, C.W., 1991, A description of the Bodie Hills and Bodie mining district, Mono county, California with annotated road log from Bridgeport to Bodie, in Buffa, R.H., and Cooner, A.R., eds., *Geology and ore deposits of the Great Basin: Field Trip Guidebook Compendium, Volume 2*: Reno, Geological Society of Nevada, p. 601–618.
- Silberman, M.L., and McKee, E.H., 1972, A summary of radiometric age determinations on Tertiary volcanic rocks from Nevada and eastern California: part II, western Nevada: Isochron-West, no. 4, p. 7–28.
- Simpson, R.W., Jachens, R.C., Blakely, R.J., and Saltus, R.W., 1986, A new isostatic residual gravity map of the conterminous United States, with a discussion on the significance of isostatic residual anomalies: *Journal of Geophysical Research*, v. 91, p. 8348–8372, doi: 10.1029/JB091iB08p08348.
- Smailbegovic, A., 2002, Structural and lithologic constraints to mineralization in Aurora, NV and Bodie, CA mining districts, observed and interpreted with aerospace geophysical data [Ph.D. thesis]: Reno, University of Nevada, 261 p.
- Smith, J.G., 1993, Geologic map of upper Eocene to Holocene volcanic and related rocks in the Cascades Range, Washington: U.S. Geological Survey Miscellaneous Investigations Series Map I-2005, scale 1:500,000, 19 p.
- Stanford Geological Survey, 1961, Geologic map of Swauger Creek–Masonic Mountain area, Mono County, California.

Bodie Hills volcanic field

- fornia: Stanford, California, Stanford University, scale 1:31,680, <http://www-sul.stanford.edu/depts;branner/images/maps/JamesGsmith-BIG.jpg>.
- Steiger, R.H., and Jäger, E., 1977, Subcommission on geo-chronology: Convention on the use of decay constants in geo- and cosmochronology: *Earth and Planetary Science Letters*, v. 36, p. 359–362, doi: 10.1016/0012-821X(77)90060-7.
- Stewart, J.H., 1988, Tectonics of the Walker Lane belt, western Great Basin: Mesozoic and Cenozoic deformation in a zone of shear, in Ernst, W.G., ed., Metamorphism and crustal evolution of the western United States: Englewood Cliffs, New Jersey, Prentice Hall, p. 681–713.
- Stewart, J.H., 1992, Paleogeography and tectonic setting of Miocene continental strata in the northern part of the Walker Lane belt, in Craig, S.D., ed., Structure, tectonics, and mineralization of the Walker Lane; Walker Lane Symposium, proceedings volume: Reno, Geological Society of Nevada, p. 53–61.
- Stewart, J.H., Carlson, J.E., and Johannsen, D.C., 1982, Geologic map of the Walker Lake $1^{\circ} \times 2^{\circ}$ quadrangle, California and Nevada: U.S. Geological Survey Miscellaneous Field Studies Map MF-1382-A, scale 1:250,000.
- Stockli, D.F., Surpless, B.E., Dumitru, T.A., and Farley, K.A., 2002, Thermochronological constraints on the timing and magnitude of Miocene and Pliocene extension in the central Wassuk Range, western Nevada: *Tectonics*, v. 21, 1028, doi: 10.1029/2001TC001295.
- Stockli, D.F., Dumitru, T.A., McWilliams, M.O., and Farley, K.A., 2003, Cenozoic tectonic evolution of the White Mountains, California and Nevada: *Geological Society of America Bulletin*, v. 115, p. 788–816, doi: 10.1130/0016-7606(2003)115<0788:CTEOTW>2.0.CO;2.
- Sun, S.-S., and McDonough, W.F., 1989, Chemical and isotopic systematics of oceanic basalts; implications for mantle composition and processes, in Saunders, A.D., and Norry, M.J., eds., Magmatism in the ocean basins: Geological Society of London Special Publication 42, p. 313–345, doi: 10.1144/GSL.SP.1989.042.01.19.
- Surpless, B.E., Stockli, D.F., Dumitru, T.A., and Miller, E.L., 2002, Two-phase westward encroachment of Basin and Range extension into the northern Sierra Nevada: *Tectonics*, v. 21, 1002, doi: 10.1029/2000TC001257.
- Syberg, F.J.R., 1972, A Fourier method for the regional-residual problem of potential fields: *Geophysical Prospecting*, v. 20, p. 47–75, doi: 10.1111/j.1365-2478.1972.tb00619.x.
- Taggart, J.E., Jr., 2002, Analytical methods for chemical analysis of geologic and other materials: U.S. Geological Survey Open-File Report 02-223, <http://pubs.usgs.gov/of/2002/ofr-02-0223/OFR-02-0223.pdf>.
- Takada, A., 1994, The influence of regional stress and magmatic input on styles of monogenetic and polygenetic volcanism: *Journal of Geophysical Research*, v. 99, p. 13,563–13,573, doi: 10.1029/94JB00494.
- Taylor, J.R., 1982, An introduction to error analysis: The study of uncertainties in physical measurements: Mill Valley, California, University Science Books, 270 p.
- Tincher, C.R., and Stockli, D.F., 2009, Cenozoic volcanism and tectonics in the Queen Valley area, Esmeralda County, western Nevada, in Oldow, J.S., and Cashman, P.H., eds., Late Cenozoic structure and evolution of the Great Basin-Sierra Nevada transition: *Geological Society of America Special Paper* 447, p. 255–274, doi: 10.1130/2009.2447(13).
- Tosdal, R.M., and Richards, J.P., 2001, Magmatic and structural controls on the development of porphyry Cu/Mo/Au deposits, in Tosdal, R.M., and Richards, J.P., eds., Structural controls on ore genesis: *Reviews in Economic Geology*, v. 14, p. 157–181.
- Tosdal, R.M., Wooden, J.L., and Kistler, R.W., 2000, Inheritance of Nevadan mineral belts from Neoproterozoic continental breakup, in Cluer, J.K., et al., eds., *Geology and ore deposits 2000: The Great Basin and beyond: Geological Society of Nevada Symposium Proceedings*, May 15–18, 2000, p. 451–466.
- U.S. Geological Survey, 2001, Six aeromagnetic surveys in Nevada and California: A web site for distribution of data: U.S. Geological Survey Open-File Report 01-0145, <http://pubs.usgs.gov/of/2001/ofr-01-0145>, last accessed December 2010.
- Vikre, P.G., and Henry, C.D., 2011, Quartz-alunite alteration cells in the ancestral southern Cascade magmatic arc, in Steininger, R., and Pennell, B., eds., *Great Basin evolution and metallogeny: Reno, Geological Society of Nevada, 2010 Symposium proceedings*, p. 701–745.
- Ward, J.M., 1992, The Cinnabar Canyon sulfur deposit, in Wessel, G.R., and Wimberly, B.H., eds., *Native sulfur developments in geology and exploration*: Littleton, Colorado, Society for Mining, Metallurgy, and Exploration, p. 159–164.
- Wark, D.A., 1991, Oligocene ash flow volcanism, northern Sierra Madre Occidental; role of mafic and intermediate-composition magmas in rhyolite genesis: *Journal of Geophysical Research*, v. 96, p. 13,389–13,411, doi: 10.1029/90JB02666.
- Wesnousky, S.G., 2005, Active faulting in the Walker Lane: *Tectonics*, v. 24, TC3009, doi: 10.1029/2004TC001645.
- Wetterauer, R.H., 1977, The Mina deflection—A new interpretation based on the history of the Lower Jurassic Dunlap Formation, western Nevada [Ph.D. thesis]: Evanston, Illinois, Northwestern University, 155 p.
- Whitney, D.L., and Evans, B.W., 2010, Abbreviations for names of rock-forming mineral: *American Mineralogist*, v. 95, p. 185–187.
- Wood, D.A., Joron, J.L., and Treuil, M., 1979, A re-appraisal of the use of trace elements to classify and discriminate between magma series erupted in different tectonic settings: *Earth and Planetary Science Letters*, v. 45, p. 326–336, doi: 10.1016/0012-821X(79)90133-X.
- Zucca, J., Fuis, G., Milkereit, B., Mooney, W., and Catchings, R., 1986, Crustal structure of northeastern California: *Journal of Geophysical Research*, v. 91, p. 7359–7382, doi: 10.1029/JB091iB07p07359.

MANUSCRIPT RECEIVED 11 FEBRUARY 2011
REVISED MANUSCRIPT RECEIVED 4 AUGUST 2011
MANUSCRIPT ACCEPTED 7 SEPTEMBER 2011